Abstract of Dissertation Presented to the Graduate School
of the University of Florida in Partial Fulfillment of the
Requirements for the Degree of Doctor of Philosophy

EFFECT OF POROUS MEDIA AND FLUID PROPERTIES ON DENSE NON-
AQUEOUS PHASE LIQUID MIGRATION AND DILUTION MASS FLUX

By

Christian T. Totten

August 2005

Chair: Michael D. Annable
Cochair: Joeseph J. Delfino
Major Department: Environmental Engineering Sciences

The influence of porous media and fluid properties on Non Aqueous Phase Liquid

(NAPL) residual geometry and associated contaminant mass flux characteristics was

investigated. Contaminant mass flux is a function of the source zone cross sectional area

exposed to groundwater flow. Porous media and fluid properties affect source zone

morphology leading to cross sectional area development. Media grain size and NAPL

wettability were varied for relative comparisons. Fluid properties including density

differential and interfacial tension between NAPL and water were varied for relative

comparisons. The percent mass flux of perchloroethylene was measured and the

relationship between mass flux and mass loading was developed for different systems.

Results indicated wettability conditions of the media as well as density differential

between fluids had the greatest influence on contaminant flux values from the NAPL

source zone. The results showed that as density differential decreased and the media

20050614 034

became more hydrophobic, the relationship between relative mass flux and percent mass value changed from a non-linear to a linear relationship. Varying grain size had little effect on the magnitude of mass flux values but showed correlation with the mass flux and mass load relationship. The results indicated that interfacial tension between fluids had minimal effect on mass flux values and a consistent logarithmic relationship between mass flux and mass load was observed.

Dissolution experiments using trichloroethylene were completed to determine the relationship between flux values produced during mass loading and flux values produced during mass reduction. The flux development during loading appears to be hysteretic with flux development during mass reduction of dissolution.

REPORT DOCUMENTATION PAGE	Form Approved OMB No. 0704-0188

Public reporting burden for this collection of information is estimated to average 1 hour per response, including the time for reviewing instructions, searching existing data sources, gathering and maintaining the data needed, and completing and reviewing the collection of information. Send comments regarding this burden estimate or any other aspect of this collection of information, including suggestions for reducing this burden, to Washington Headquarters Services, Directorate for Information Operations and Reports, 1215 Jefferson Davis Highway, Suite 1204, Arlington, VA 22202-4302, and to the Office of Management and Budget, Paperwork Reduction Project (0704-0188), Washington, DC 20503.

1. AGENCY USE ONLY (Leave blank)	2. REPORT DATE 8.Jun.05	3. REPORT TYPE AND DATES COVERED DISSERTATION

4. TITLE AND SUBTITLE
EFFECT OF POROUS MEDIA AND FLUID PROPERTIES ON DENSE
NON-AQUEOUS PHASE LIQUID MIGRATION AND DILUTION MASS FLUX.

5. FUNDING NUMBERS

6. AUTHOR(S)
MAJ TOTTEN CHRISTIAN T

7. PERFORMING ORGANIZATION NAME(S) AND ADDRESS(ES)
UNIVERSITY OF FLORIDA

8. PERFORMING ORGANIZATION REPORT NUMBER

CI04-1111

9. SPONSORING/MONITORING AGENCY NAME(S) AND ADDRESS(ES)
THE DEPARTMENT OF THE AIR FORCE
AFIT/CIA, BLDG 125
2950 P STREET
WPAFB OH 45433

10. SPONSORING/MONITORING AGENCY REPORT NUMBER

11. SUPPLEMENTARY NOTES

12a. DISTRIBUTION AVAILABILITY STATEMENT
Unlimited distribution
In Accordance With AFI 35-205/AFIT Sup 1

DISTRIBUTION STATEMENT A
Approved for Public Release
Distribution Unlimited

12b. DISTRIBUTION CODE

13. ABSTRACT (Maximum 200 words)

14. SUBJECT TERMS

15. NUMBER OF PAGES
141

16. PRICE CODE

17. SECURITY CLASSIFICATION OF REPORT	18. SECURITY CLASSIFICATION OF THIS PAGE	19. SECURITY CLASSIFICATION OF ABSTRACT	20. LIMITATION OF ABSTRACT

Standard Form 298 (Rev. 2-89) (EG)
Prescribed by ANSI Std. 239.18
Designed using Perform Pro, WHS/DIOR, Oct 94

EFFECT OF POROUS MEDIA AND FLUID PROPERTIES ON DENSE NON-
AQUEOUS PHASE LIQUID MIGRATION AND
DILUTION MASS FLUX

By

CHRISTIAN T. TOTTEN

A DISSERTATION PRESENTED TO THE GRADUATE SCHOOL
OF THE UNIVERSITY OF FLORIDA IN PARTIAL FULFILLMENT
OF THE REQUIREMENTS FOR THE DEGREE OF
DOCTOR OF PHILOSOPHY

UNIVERSITY OF FLORIDA

2005

ACKNOWLEDGMENTS

Lastly, I must thank my wife, ██████, and children, ███████████ for their support and willingness to follow me to wherever the Air Force decides to send us. They have been great in letting me pursue my goals and doing whatever it takes to get there.

TABLE OF CONTENTS

LIST OF TABLES

LIST OF FIGURES

University of Florida Graduate School
Electronic Thesis and Dissertation (ETD) Signature Page

Student's Name: Christian T. Totten

This document has been reviewed and accepted by the student's supervisory committee.

Professor's name & title including department   Professor's signature
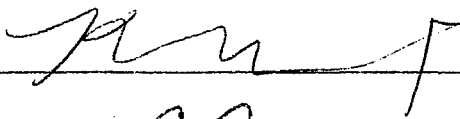
Michael D. Annable   Chair

Professor of Environmental Engineering
Sciences
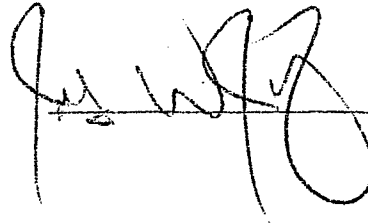
Joseph J. Delfino   Cochair

Professor of Environmental Engineering
Sciences

Kirk Hatfield

Associate Professor of Civil and Coastal
Engineering

James W. Jawitz

Assistant Professor of Soil and Water
Sciences

Month and Year of Graduation: Aug 2005

College Dean:
(when required by college)

Graduate Dean:

CHAPTER 1
INTRODUCTION

Background

Non-aqueous phase liquids (NAPLs) are chemicals that have limited solubility in water. That is, they exist as a separate phase from water. There are two broad categories of NAPLs. NAPLs that are less dense than water are called light non-aqueous phase liquids (LNAPLs), and those that are denser than water are called dense non-aqueous phase liquids (DNAPLs). Their densities relative to water cause each type of NAPL to behave differently when released into an aquifer. LNAPLs will "float" to the top of the water table. This characteristic allows easier remediation relative to its DNAPL cousin, which tends to sink.

A DNAPL will "sink" through an aquifer until it reaches an impermeable layer where it will collect and reside as a pooled separate phase. They are commonly referred to as "sinkers" and "toxic blobs" (Gordon, 1996). If fractures or breaks exist in the impermeable layer, the DNAPL could migrate deeper making access for remediation more difficult. Most DNAPLs undergo only limited degradation in the subsurface and can persist for many years while slowly releasing, through dissolution, soluble organic constituents into the groundwater (Newell and Ross, 1992). Their persistence in groundwater, combined with their low solubility, poses great challenges for DNAPL remediation.

Chlorinated solvents are chemicals used for their dissolving capabilities. Perchloroethylene (PCE) and trichloroethylene (TCE) are two of the most commonly

manufactured and used chlorinated solvents. DNAPLs such as perchloroethylene are one of the most common groundwater contaminants found because of their extensive use as industrial degreasers as well as a variety of other uses. They are of concern because of the health hazards posed to humans (Environmental Protection Agency [EPA], 2003a&b; Office of Pollution Prevention and Toxics [OPPT], 1994). Many are also dangerous because of the chemical byproducts produced during degradation. For example, trichloroethylene (TCE), used as an industrial degreaser, may degrade into vinyl chloride which is a known carcinogen (EPA, 2003c; NJDHSS, 2002). Perchloroethylene is a colorless organic liquid with a mild chloroform-like odor and has an absolute solubility in water of 150 mg/l (25 °C) and a density of 1.626 g/cm^3 (20 °C) (Verschueren, 1983) and has a Henry's constant of 0.0153 atm-m^3/mol. Trichloroethylene is a colorless or blue organic liquid and also has a chloroform-like odor similar to that of PCE. Trichloroethylene has an aqueous solubility of 1100 mg/l (25 °C) and a density of 1.46 g/cm^3 (20 °C) (Verschueren, 1983) and has a Henry's constant of 0.0103 atm-m^3/mol.

Although DNAPLs have been used for several decades, only recently have they gained attention for causing significant environmental and human health problems. As recently as 1993, the EPA reported that over 60% of sites with organic contamination are likely caused by DNAPLs and that 70% of all superfund sites with groundwater contamination have NAPLs present (Gordon, 1996). For example, the EPA has determined that more than 1 million pounds of PCE were released to land and water between 1987 and 1993 (EPA, 2003a). Considering that production and usage of PCE predates this time period, one could assume that more PCE was released before, as well

as since this time period. These assumptions make it apparent that DNAPLs such as PCE are suspected to contaminate a large number of sites.

Because of their apparent ubiquity and persistence in the environment and risk to human health, management of DNAPL contamination in groundwater sources is critical for providing the public with safe, reliable sources of drinking water. An understanding of how DNAPLs behave in groundwater systems is critical to both management and remediation of DNAPL sources. Many studies have been completed to demonstrate that source zone remediation techniques can remove a large portion of the contaminant mass present (Brooks et al. 2002; Falta et al., 1997; Fiorenza 2000;Fountain et al., 1995; Fountain et al., 1996; Jawitz et al., 1998b; Jawitz et al., 2000; Lowe et al., 1999; Martel et al., 1998; Meinardus et al., 2002; Rao et al., 1997). Additionally, a common performance metric for source zone removal has been total mass fraction or volume fraction of contaminant removed (Fiorenza, 2000; Jawitz et al., 1998b; Jawitz et al., 2000; Lowe et al., 1999; Martel et al., 1998; McCray and Brusseau, 1998; Meinardus et al., 2002; Rao et al., 1997). This performance metric may only provide partial assessment of remediation effectiveness. Contaminant flux $[M]/[L^2][T]$ is a metric that is becoming more widely used to characterize contaminant source zones (Figure 1.1) (Einarson and Mackay, 2001). The relationship between mass flux and the mass of contaminant is not clear (Parker and Park, 2004; Rao and Jawitz, 2003). It is assumed that source longevity is more directly related to mass and volume values; however flux is more a function of how the mass/volume is distributed.

How the mass/volume of the DNAPL is distributed is considered the source zone geometry. How the source zone geometry is oriented with respect to the flow field

creates a transverse area of exposure. Contaminant flux is a function of this transverse area of the source zone exposed to flow.
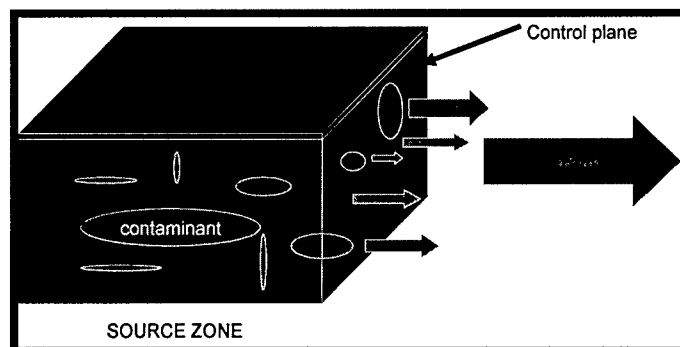
Figure 1.1. Source zone and associated flux across a control plane

Figure 1.2 displays hypothetical source zones of similar mass but oriented very differently with respect to the flow field. The distributions shown on the top of Figure 1.2 display a source zone profile with resultant fluxes annotated with J_1 and J_2. Each contour represents a discrete and equal mass loading event. The initial loading represented by the inner contour event produces geometries of equal area and hence will produce similar flux values. However, each subsequent loading event would result in each source zone producing different flux values with J_2 ultimately being greater than J_1. The lower distributions shown in Figure 1.2 provide a planar view with resultant fluxes annotated with J_3 and J_4. Again, each contour represents a discrete and equal mass loading event. The initial geometry represented by the inner contour hypothetically provides the same transverse area, although they are dissimilar in shape, resulting in similar flux values. However, each subsequent loading event shows the transverse areas with respect to flow increase more for the geometry represented by J_4 than J_3. This results in J_4 being ultimately greater than J_3. This is an example of how similar mass introduction can result in vastly different transverse areas. The resulting dissolution mass

flux values per loading event may look like those displayed in Figure 1.3. This exposed transverse area is determined by the orientation of the source zone to the aqueous flow field.
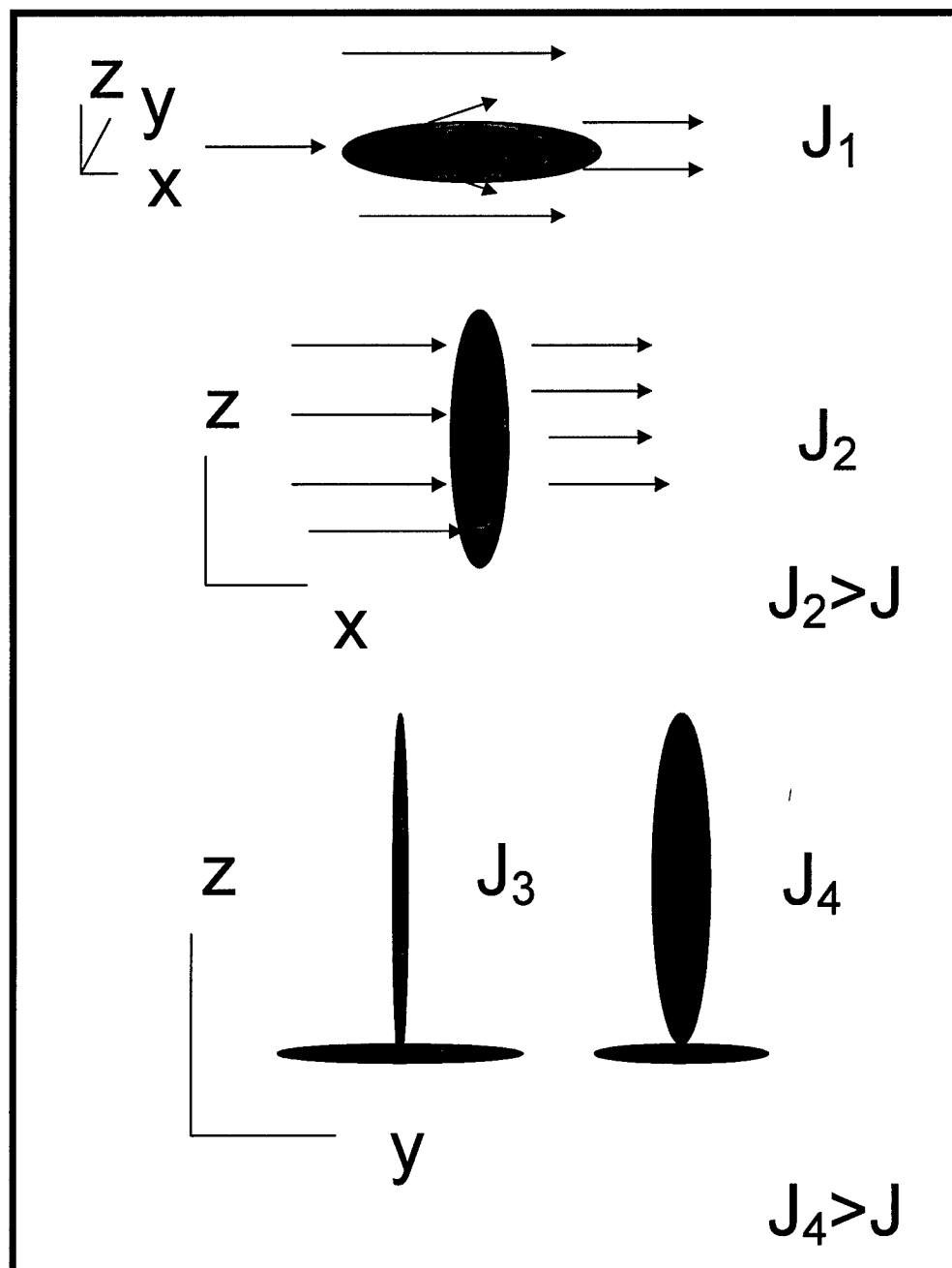
Figure 1.2. Hypothetical source zones of equal mass and their relative mass flux values
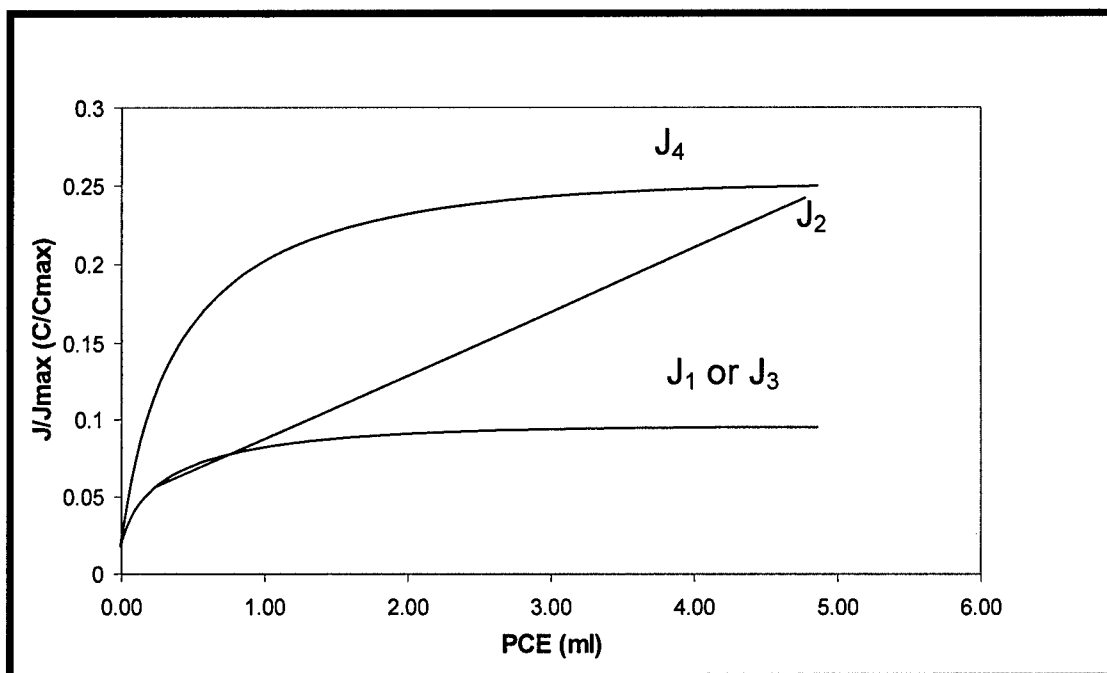
Figure 1.3. Hypothetical flux values per unit mass/volume of contaminant

Geometry and Orientation to Flow

Here, "geometry" refers to the shape of the entire NAPL source zone and

"orientation" is how the source zone is placed with respect to the groundwater flow

direction. To better characterize orientation and geometry, NAPL source zones are

divided into two sections that will contribute to mass transfer from the non-aqueous to the

aqueous phase. The first section is the residual DNAPL suspended in the soil matrix by

capillary forces and the second is the pooled section where DNAPL collects on top of a

less permeable or impermeable layer (Sale and McWhorter, 2001). This separation

identifies the potential difference in DNAPL saturation percentages between each section

as well as the potential difference in exposed contaminant surface to cross sectional flow.

Illangasekare et al. (1995) demonstrated that in general, DNAPL saturation of the

contaminant suspended as residual increases as a function of depth until pooling above a

less permeable layer. Hofstee et al. (1998) demonstrated that PCE in a two-dimensional

heterogeneous porous medium consisted of water-entrapped PCE and PCE existing as a continuous pool on top of the coarse-fine sand interface. Pooling will continue until the oil entry pressure is reached to allow the DNAPL to displace the water in the finer lower permeability sand (Corey, 2003).

Sale and McWhorter (2001) stated that mass transfer occurs primarily at the leading edges of contaminant subzones or geometrically separated sources of NAPL and that mass transfer through the remainder of the source will be inhibited by upstream interferences. Additionally, if local equilibrium is assumed, the part of the NAPL source providing the largest leading edge with respect to aqueous flow would be the largest contributor to contaminant mass flux. It may be that the residual NAPL provides the larger leading edge exposure when compared to the pooled portion, and is thus the likely larger contributor to contaminant flux.

Pooled DNAPL

Pooled DNAPL is that portion of the contaminant mass that collects on top of an impermeable or low permeability layer in an aquifer (Pankow and Cherry, 1996; Sale and McWhorter, 2001). The pooled portion of a contaminant source will typically have a larger NAPL saturation compared to the portion of DNAPL trapped as residual. The pooled portion typically will spread out horizontally along the boundary of the impermeable or low permeable layer. The pooling and horizontal spreading create a thin geometry and an orientation resulting in small leading edge exposure with respect to groundwater flow. Because of the larger volume compared to the trapped residual and the small mass transfer area, pooled sources are likely to produce low flux but persist for long periods of time (Johnson and Pankow, 1992).

Residual DNAPL

Extensive work has been focused on studies of media and fluid property interaction and their effect on DNAPL mobilization, pooling and entrapment (Abrams, 1975; Bradford and Leij, 1995; Hofstee et al., 1998; Illangaskare et al., 1995; Mayer and Miller, 1990; Moore and Slobod, 1956; Morrow et al., 1988; Ng et al., 1978; Patel and Greaves, 1987; Pennell et al., 1996; Ryan and Dhir, 1993). Capillary forces and their ratio to viscous and buoyancy forces play a significant role in DNAPL behavior in the sub-surface (Dawson and Roberts, 1997). Granular porous media are typically water wet and because of this quality, water will be drawn into the media by capillary forces. In a water wet environment, the capillary forces can be orders of magnitude larger than viscous forces, resulting in capillarity being the dominant force. Capillary forces will draw water into smaller pores, leaving oil in the larger pore spaces. The residual oil exists as isolated globules in the larger pore spaces (Moore and Slobad, 1956). The shapes of these isolated globules depend on soil homogeneity/heterogeneity which dictates the pore body to pore neck ratio or aspect ratio. Homogeneous packs of uniformly sized media have a low aspect ratio wherein NAPL blobs are spherically shaped, single pore bodies. Heterogeneous packs have a high aspect ratio and are irregularly shaped and can be connected by multiple pores (Chatzis et al., 1983; Cho, 2001; Morrow and Heller, 1985).

Residual DNAPL is important because of its ability to produce relatively high contaminant fluxes for a given mass when compared to pooled sources. The contaminant fluxes are a function of residual geometry and orientation to flow. Geometry and orientation of residual DNAPL are determined by migration and entrapment processes.

Migration process

The residual NAPL can take on a variety of geometries and orientations to flow as it migrates through the porous media. It can move vertically or horizontally through the saturated zone. The vertical and lateral migration of DNAPL is of more interest because it is usually oriented 90° to water flow, providing the leading edges and largest area for contaminant flux production. Vertical movement of DNAPLs is described by the following equation (Fetter, 1999):

$$Ho = \frac{2\sigma \cos\theta(1/r_t - 1/r_p)}{g(\rho_w - \rho_o)} \tag{1-1}$$

where H_o is the critical height or head required to displace water in a pore, σ is the interfacial tension between liquids, θ is wetting angle, r_t pore is throat radius, r_p is pore radius, g is acceleration due to gravity, ρ_w is water density and ρ_o is DNAPL density. The properties related to media characteristics are r_p, r_t and θ. The pore throat and pore radii are approximated as functions of media diameter (d) as follows (Fetter, 1999):

$$r_p = 0.212d \tag{1-2a}$$

$$r_t = 0.077d \tag{1-2b}$$

Horizontal movement of DNAPL in the saturated zone becomes important if the pressure gradient causing horizontal movement can overcome gravitation influences. Horizontal flow is given as follows (Fetter, 1999):

$$\frac{dP}{dx} = \frac{2\sigma}{L_o(1/r_t - 1/r_p)} \tag{1-3}$$

where L_o is the length of the continuous DNAPL phase in the direction of flow.

In general, DNAPLs can migrate two ways. The first is a "finger" type geometry that will trickle down through the porous media as a thin line producing discontinuous

blobs retained as residual. Contaminant fingering occurs when a uniformly infiltrating front is split into "stringers" due to instability from pore scale permeability variations (Fetter, 1999). Various studies have been conducted to gain a better understanding of fingering causes and behavior (Brewster et al., 1995; Held and Illangasekare, 1995-a; Held and Illangasekare, 1995-b; Hofstee et al., 1998; Illangasekare et al., 1995; Peters and Flock, 1981; Wang and Feyen, 1998). The second migration pathway involves a more uniform geometry where the NAPL is initially distributed into the pores producing a uniform advancing front and distribution of trapped NAPL. This might be the result of more rapid infiltration or displacement by a viscous NAPL. This type of displacement may be more likley in oil-wet media. Each of these geometries provides large differences in interfacial and overall contact area between the aqueous and non-aqueous phases.

Entrapment process

As mentioned above, NAPL entrapment is directly related to capillary forces and their ratio to viscous and buoyancy (gravitational) forces. The Capillary Number is defined as the ratio of viscous to capillary forces and the Bond Number is the ratio of buoyancy forces to capillary forces (Perry and Chilton, 1973).

Capillary Number $$N_{ca} = \frac{v_w \mu_w}{\gamma_{ow} \cos\theta} \qquad (1\text{-}4)$$

Bond Number $$N_{Bo} = \frac{\Delta\rho(k/n)}{\gamma_{ow} \cos\theta} \qquad (1\text{-}5)$$

where v_w [L/T] is the pore velocity, μ_w [FT/L$_2$]is the water viscosity, γ_{ow} [F/L] is the interfacial tension between NAPL and water, $\Delta\rho$ [M/L^3] is the density difference between immiscible fluids, k [L^2] is intrinsic permeability and n [L^{3}L^{-3}] is porosity of the porous medium. Pennell et al. (1996) combined the Capillary and Bond numbers into a Total

Trapping Number (N_T) used to develop PCE desaturation curves in a one-dimensional chamber. The N_T was developed to combine viscous and buoyancy forces with capillary forces into a single, comprehensive value. The N_T combines force relationships into a single equation and numerical value to allow for simple mobility and saturation characterization. It is important to note that the mobility referred to in relation to trapping number is the ability to mobilize entrapped residual DNAPL and not migration. The N_T identifies those media and fluid properties important to entrapped NAPL residual and entrapped residual mobility. The N_T for a vertical flow system is as follows:

$$N_T = |N_{Ca} + N_{Bo}| \qquad (1\text{-}6)$$

In the horizontal flow case, it is calculated as follows:

$$N_T = \sqrt{N^2_{Ca} + N^2_{Bo}} \qquad (1\text{-}7)$$

Theoretically, changing any of the elements in the Capillary or Bond number could change the overall N_T, possibly resulting in different entrapment characteristics for a given NAPL. Pennell et al. (1996) performed surfactant flooding where PCE-water interfacial tension was reduced. The result was increased mobility and reduced saturation of entrapped PCE. Additionally, different combinations of element values will result in the same Capillary and Bond Number and hence, the same overall N_T value.

The elements of The Capillary and Bond numbers related to media properties are intrinsic permeability, wettability, and porosity. For homogenous media of equal size spheres, porosity is a fairly consistent characteristic. However, intrinsic permeability and wettability can be varied greatly by grain size diameter changes and contact angle modification respectively.

Relating Media Property Characteristics to the Contaminant Mass Flux

Binary model

The dissolution mass flux generated by a particular source zone as a function of geometry and orientation can be described using a Binary Model (Jawitz et al., 2003). The model treats the multidimensional flow field as a collection of non-interacting stream tubes with each tube being either contaminated or clean. The collection of stream-tubes would be the entire domain such as an aquifer. The fraction (*f*) of the stream-tubes contaminated would be the source zone and the remaining fraction (1-*f*) would be the clean portion of the domain. The contaminated fraction (*f*) is directly related to source zone geometry and orientation to flow. In general, media and fluid properties dictate migration and entrapment processes. If media or fluid modifications affect source zone geometry, contaminant mass flux values could be affected as a result of changing *f* values.

Fractional mass flux versus fractional mass loading and total mass flux

The hypothetical dissolution mass flux and mass loading relationships displayed in Figure 1.3 provide absolute flux and mass values for a given system and how they relate to each other. Another interesting characteristic of these curves is their shape. The shape of the curve gives insight into how flux values are achieved during the mass loading process. The shape of these curves could be fit using the following simple empirical model:

$$Y = X^\beta \tag{1-8}$$

where Y represents fractional source strength, X is fractional mass increase and β is system efficiency. This is similar to the model approach proposed by Rao et al. (2001) for mass depletion, flux reduction relationships. This model is a retrospective look at the

flux and mass relationships of a given system because they are normalized to each

system's maximum mass and flux values. This allows curve shape non-linearity

comparison from one system to another. Figure 1.4 displays hypothetical source zones of

similar mass or volume and their related β values. Figure 1.5 displays the range of curves

that could be encountered for any given system with β determining the shape of the

curve.
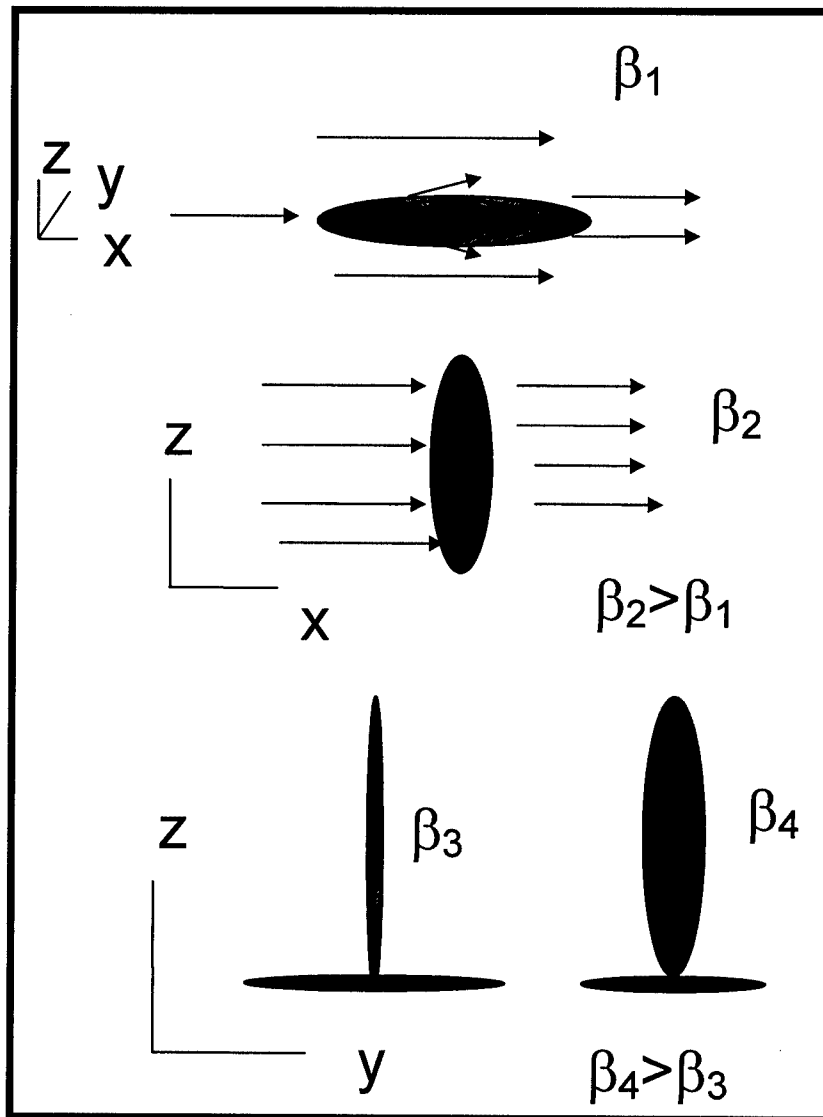
Figure 1.4. Hypothetical source zones of equal mass and their relative β values

Example β Curves

Fractional mass/volume increase (x-axis, 0 to 1)

fractional flux increase (y-axis, 0 to 1)

β < 1

β = 1

β > 1
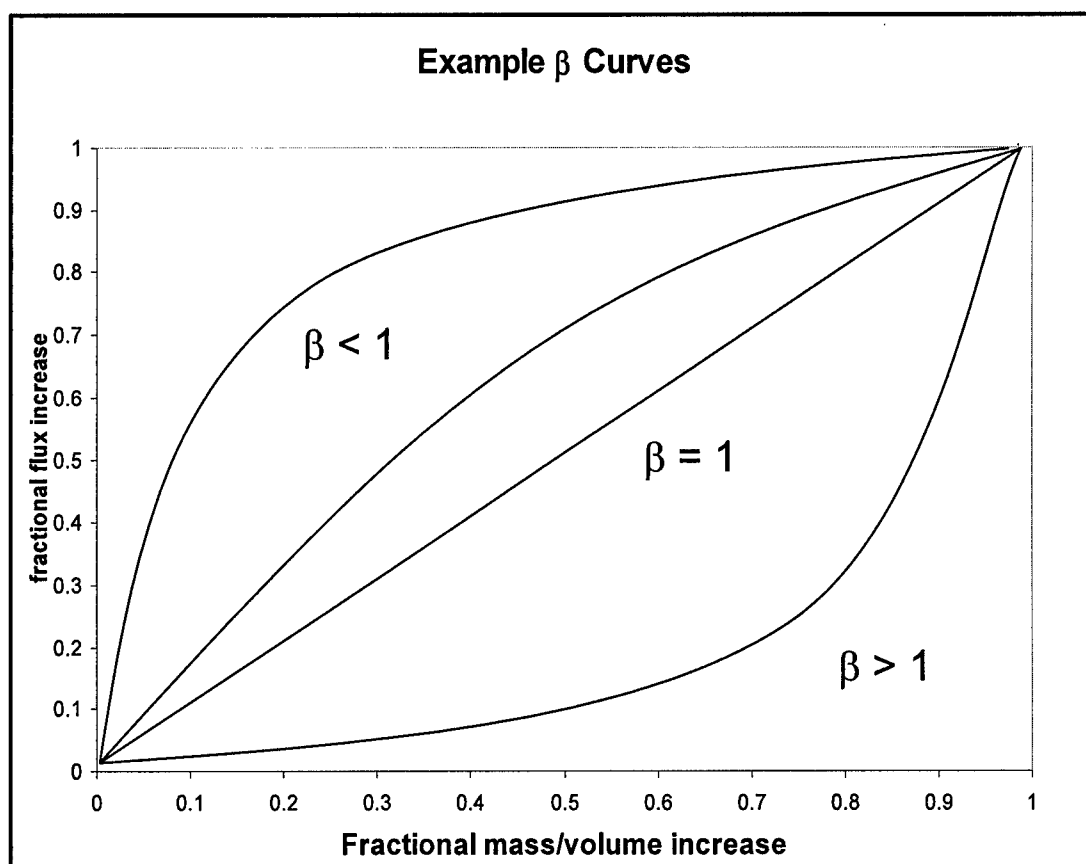
Figure 1.5. Example β value curves

A linear relationship or β value of approximately one (1.0) would indicate a one-to-one relationship between fractional mass increase and fractional flux increase. As the β value decreases below 1.0, the curves become logarithmic, indicating higher relative flux increase per fractional mass at lower fractional mass values. As the fractional mass continues to increase, the increase in fractional flux slows. The lower the β value, the more pronounced this loading behavior becomes. The opposite occurs for β values greater than one and the curves become exponential in shape, requiring greater mass to generate most of its fractional flux. It would occur in a system where flux production is delayed during mass loading. One such system would be a heterogeneous system where the DNAPL source would gather on a low permeability lens until breakthrough or

spilling occurred producing a larger residual cross section to produce higher flux values. It could be argued that β is an all inclusive value capturing a wide range of media and fluid characteristics that affect dissolution efficiency.

Study Objectives

Based on the background provided above, the following objectives of this research were to:

1. Determine the relationship between hydrophobic media content and water, air and oil entry pressure and related contact angle values. Water wet, oil wet, and intermediate wet systems were investigated to determine water entry pressure, air entry pressure, and oil entry pressure trends.

2. **Determine the relationship between porous media properties and contaminant mass flux.** Two media properties, grain size and wettability, were studied to determine their influence on geometry and contaminant mass flux properties in a two dimensional flow chamber. A reduction in grain size may affect migration and entrapment characteristics and ultimately DNAPL geometry. DNAPL distributions in an oil wet media may influence geometry of a source zone, possibly affecting contaminant mass flux properties. Absolute mass and flux value relationships as well as values were determined for these media systems.

3. **Determine the relationship between fluid properties contaminant and mass flux.** DNAPL migration in saturated porous media is influenced in part by the density differential between the aqueous and non-aqueous phase. Changing this differential while keeping other characteristics constant could change DNAPL migration. This study assessed the influence of reducing the density differential between immiscible fluids and

the effect that differential reduction has on DNAPL migration and associated contaminant mass flux properties.

Interfacial tension is an important physical property that can influence migration of DNAPLs such as PCE. Lowering interfacial tension of PCE may increase migration, thereby influencing source zone geometry, and ultimately contaminant mass flux properties. Absolute mass and flux value relationships as well as β values were determined for these fluid systems.

4. Determine the mass loading and dissolution behavior of TCE. Contaminant mass flux curves generated through mass loading were compared to those resulting from mass reduction. This provided insight into the relationship between mass loading and mass dissolution processes.

General Methodology

The following general overall design was implemented as part of the experimental portion of this research. Various parameters were held constant while a single parameter was varied.

The following general set up was used for each experiment. A series of experiments was conducted in a two-dimensional simulated aquifer experiments in systems as shown in Figure 1.6. The design shown in Figure 1.6 is just an example to show that one characteristic can be varied while others are held constant and is not an indication of the exact variations of this research. The two dimensional flow chamber employed was similar in design to those used by Jawitz et al. (1998a) and Conrad et al. (2002), and reviewed by Chevalier and Petersen (1999).
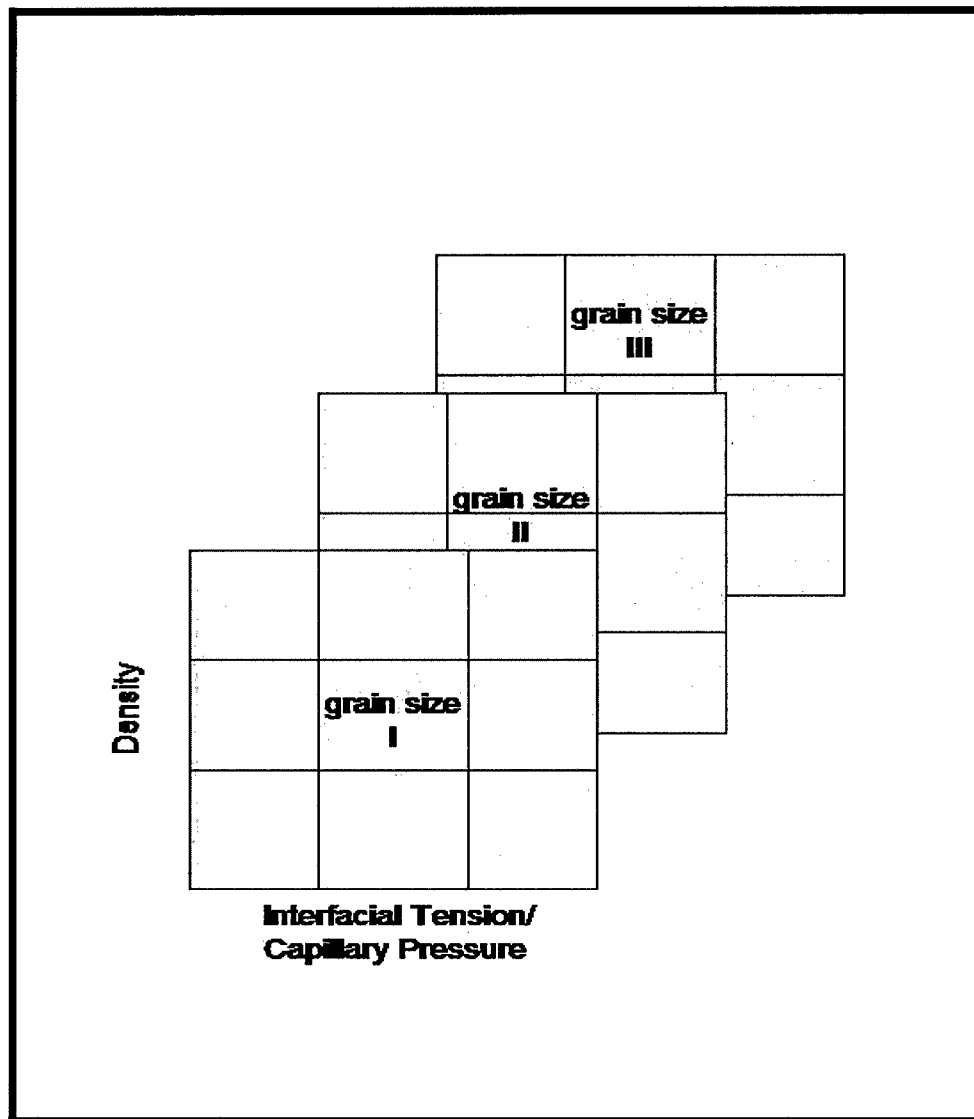
Figure 1.6. Experimental Design

The chamber design is shown in Figure 1.7. The "simulated wells" on each end of

the column had slots at intervals of 4 slots per cm and served as the influent and effluent

wells. Injection of PCE took place in the center of the chamber as shown in Figure 1.7.

PCE injection was made through the wall of the column using a needle securely fixed

with epoxy into the glass wall. PCE was injected through the needle using a gas tight

syringe placed on a syringe pump.
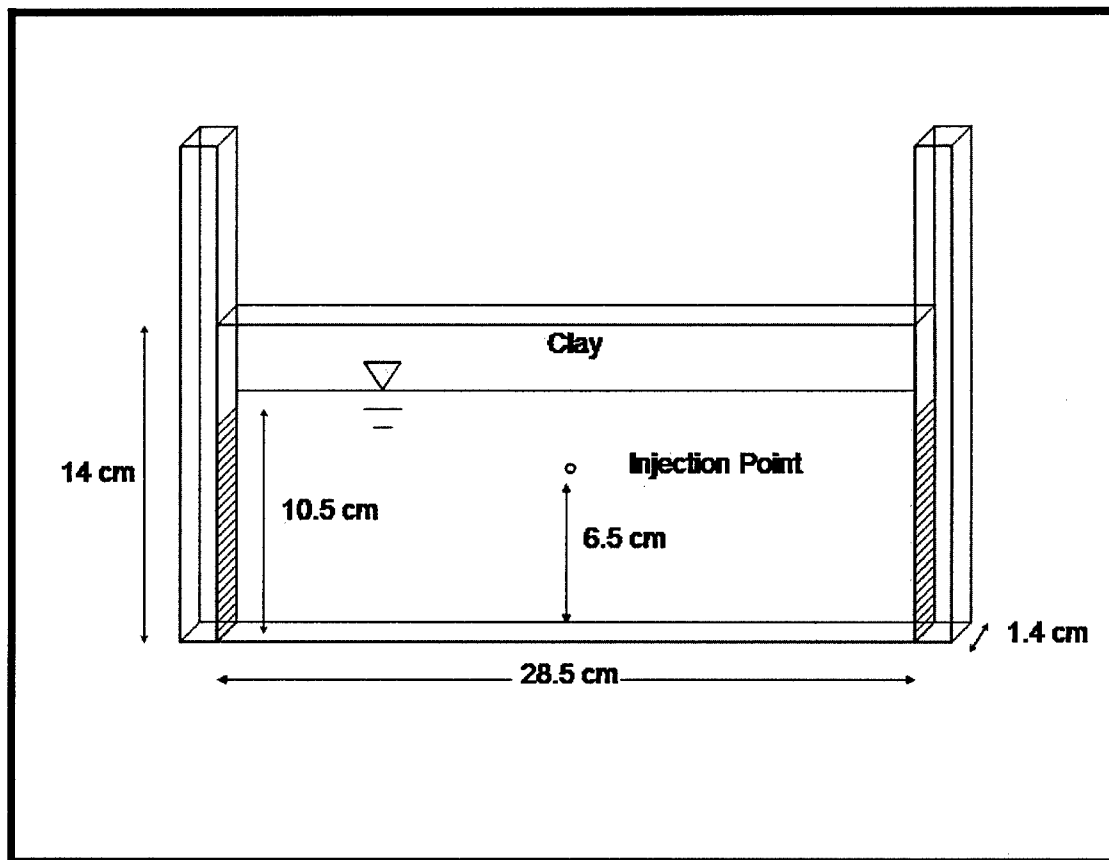
Figure 1.7. Two-dimensional flow chamber design

The two dimensional flow chamber was packed uniformly with the appropriate

medium for the specific objective. The top of the medium was covered with Bentonite

clay to maintain media pressure saturation and minimize volatile losses. NAPL was

injected into the side of the column at a specified rate using the syringe pump. The PCE

volume was injected in a stepwise fashion at a particular volume per injection up to a

predetermined total volume. All measurements were conducted under steady-state,

saturated flow conditions. Effluent samples were collected after the system achieved

steady state mass flux. The number of pore volumes required to achieve mass flux steady

state was experimentally derived. An Oil-Red-O dye tracer was added to the PCE to aid

in visual observation of the PCE in the 2-D column (Jeong et al., 2002). Flow rates were controlled to maintain a constant mass transfer rate from one experiment to another and to aid in comparisons of the various experimental results.

Samples collected throughout the experiment were analyzed using a Perkin Elmer AutoSystem XL Gas Chromatograph (GC) with a Flame Ionization Detector (FID). The FID was appropriate because it met the sensitivity requirements of the expected sample concentrations and its low selectivity was not impaired by the relatively clean samples (PCE being the only contaminant). Each sample was analyzed for PCE concentration which was used to calculate PCE percent mass flux.

Dissertation Organization

Each of the following chapters, 2-5, is written as a stand alone paper. Each chapter contains an Introduction, Methods and Materials, Results and Discussion, and Conclusion. Chapter 2 includes results of the wettability properties study. Chapter 3 discusses results of the media properties study. Chapter 4 presents the results of the fluid properties study. Chapter 5 presents the TCE mass loading and dissolution study. Chapter 6 is a summary of this research and presents major conclusions of the overall effort and identifies recommendations for future research.

CHAPTER 2
WETTABILITY STUDIES

Introduction

Wettability is the relative affinity of the solid media for fluids such as air, water or organic immiscible liquid (OIL) (Wilson, 1988). The degree of wettability is a function of the solid surface, OIL properties and composition of the water. Hydrophilic sands have an affinity for water because of their polarity and are considered water wet. Hydrophobic sands have more affinity for oil, or perhaps air, than water because they have a non polar surface and are considered oil wet. Moore and Slobod (1956) divided soil into three categories which include (1) water wet and (2) oil wet soils, and added (3) intermediate wettability soil. The intermediate wettability category has characteristics of both hydrophilic and hydrophobic media.

Understanding wettability is of great interest to both the environmental restoration and oil industries because oil and contaminant recovery is greatly influenced by this porous media property. Donaldson (1969) reported that oil recovery, as a function of water injected, is greater from water wet cores than oil wet cores. He went on to state that some findings indicate that oil recovery is better in intermediate wettability soil environments rather than either extreme.

According to Wilson (1988), it is typically assumed in reservoir engineering studies that rock is water wet. However, he reported that Treiber et al. (1972) studied reservoir rocks from 55 oil reservoirs, 15 being water wet, 3 of intermediate wettability and 37 as oil wet. Although these findings are related to oil reservoirs, it is an indication of the

variability in wettability conditions that are possible. Powers et al. (1996) found that a wide range of wetting conditions can be expected following spills of complex NAPL mixtures to the subsurface.

Silica surfaces are hydrophilic or naturally polar and can have their wetting characteristics changed in a variety of ways. Silica surfaces such as quartz sand can be altered by organic material becoming deposited on their surface and/or by the adsorption of polar oxygen-, nitrogen-, or sulfur-containing compounds. These deposition and adsorption processes can occur through physical (heat), chemical (adsorption), or biological means (Wilson, 1988). Wilson (1988) reported that fires convert heavy wax-like substances in the vegetative cover to an organic coating. This organic coating can alter the wettability of characteristics of the affected soil. Although this is an example of a physical mechanism, it appears that ultimately the coating had adsorbed to the surface of the media, altering wettability.

Powers and Tamblin (1993) found that polar molecules of high molecular weight or surfactants added to commercial gasoline as deicers, corrosion inhibitors, or carburetor cleaners increased hydrophobicity as they adsorbed to quartz slides. This indicates a potential for a wide range of wettability characteristics at sites where OIL products have been released.

The biological mechanisms that affect subsurface wettability are poorly understood (Wilson, 1988). However, it is apparent micro-organisms play an important role in affecting subsurface wettability. Wilson (1988) reported golf course putting greens at various courses around the country face management problems due to soil hydrophobicity. Under these conditions, a layer occur creating high water content and

anaerobic conditions. This favors growth of microorganisms that deposit hydrophobic coatings of organic metal sulfides on soil particles.

It is clear that the assumption of water wet subsurface media may not always be appropriate. This is an important assumption impacting a wide range of areas from golf course management, oil recovery, and contaminant remediation. For example, wettability conditions may impact the effectiveness of DNAPL remediation methods if there is an affinity between DNAPL and media surface. It is important to be able to quantify wettability conditions for better management practices.

Theoretical Background

Measurement of wettability can be made qualitatively and quantitatively. Donaldson et al. (1969) listed several methods for qualitatively assessing wettability. They determined that these methods could only classify a system as water wet or oil wet, but lacked the ability to satisfactorily classify intermediate wettability systems. Powers et al. (1996) demonstrated a qualitative bottle test that was able to visually distinguish between intermediate wetting systems. This method is qualitative because it determines system wettability based on observation of NAPL distribution between solid and aqueous phase and does not provide a quantitative value. This method is useful for relative system comparisons. This appears to be a quick method for determining relative wettability characteristics for a variety of systems and does not suffer from the same limitations of the methods listed by Donaldson et al. (1969). However, when developing oil recovery and remediation strategies, a more quantitative approach may be required.

Contact angle is often considered the best measure for quantifying wettability and is widely used (Bahrani et al., 1973; Bradford and Leij, 1995; Fink, 1970; Moore and Slobod, 1956; Letey et al., 1962; Powers et al., 1996; Watson and Letey, 1970). Powers

et al. (1996) and Bradford and Leij (1995) reported that the contact angle (θ) between

two fluids and a solid surface is the result of mechanical equilibrium or horizontal force

balance among the interfacial energies as described in Young's equation

$$\gamma^{so} - \gamma^{sw} = \gamma^{ow}\cos(\theta) \qquad (2\text{-}1)$$

where γ is interfacial energy and solid, organic, and aqueous phases are represented by

superscripts, s, o, and w respectively.

Direct measurement of the contact angle is one method for quantifying contact

angles. Contact angles can be measured by static or dynamic methods. For static

methods, advanced or receded contact angles are measured, while for dynamic methods,

the angles are referred to as advancing or receding. The contact angles are usually

measured through the aqueous phase with $0°$ to $90°$ being water wet and $90°$ to $180°$ being

oil wet, and neutral wetting around $90°$ (Figure 2.1).
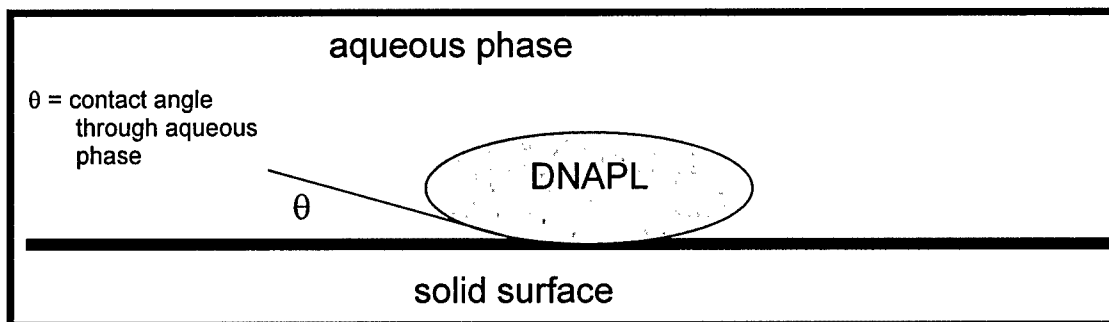
Figure 2.1. Contact angle through aqueous phase of a DNAPL

Powers et al. (1996) reported that various researchers used different ranges of

contact angles to categorize neutral wettability. For example, Powers et al. (1996)

reported that Treiber et al. (1972) used $72°$-$105°$ and Morrow (1976) used $62°$-$133°$.

Slobod and Moore (1956) used advancing contact angles of near $30°$ to describe water-

wet systems and angle greater that 90° to be oil wet with intermediate systems in between.

An example of a static method was used by Powers et al. (1996). They exposed a quartz slide surface to a variety of organic phases to achieve a variety of wetting conditions. These slides were then submerged in groundwater and exposed separately to a variety NAPLs including gasoline, diesel fuel, fuel oil, crude oil, creosote, coal tar, toluene, and TCE. The NAPLs formed drops on the treated slides. DNAPLs were placed on the top of the slides while LNAPL drops formed under the slides. After equilibration was achieved, a goniometer was used to directly measure the contact angle. Advanced angles were measured on each side of the slide. This method is similar to the sessile drop method used by Fink (1970). In this method, water is added to a flat level surface being tested until further additions increase the drop diameter, but not the height. The contact angle is a function of this height and therefore can be calculated. Since the water is being added, the advanced contact angle is calculated. These methods work well for quantifying homogeneously coated media. However, some media may be a combination of a variety of surfaces, some organic and some not.

The contact angle of a porous media can be calculated by measuring infiltration rates (Bahrani et al., 1973; Jamison, 1946; and Letey et al., 1962). Letey et al. (1962) used the following equation to calculate contact angles:

$$Q'' = \frac{nr(\rho rgh + 2\gamma \cos\theta)}{8L\eta} \tag{2-2}$$

where Q" is the water entry rate at the soil surface, n is porosity, r is the capillary radius, ρ is the density of solution, h is the capillary length plus depth of solution above capillary, γ is surface tension of solution, L is capillary length and η is viscosity of the

solution. In this equation, r and θ are unknown so a reference fluid such as ethanol with a

known θ is used to experimentally measure r to be used for other treatments. Water entry

rates were then experimentally measured for various media treatments altering contact

angle. With all other data known, contact angle θ was calculated using the above

equation. Similarly, Bahrani et al. (1973) used infiltration rates to experimentally derive

penetrability coefficients used to calculate contact angle. They derived these

penetrability coefficients after each of six wetting and drying cycles. They determined

that wetting, leaching and drying cycles change contact angles significantly from one

cycle to the next. However, they also determined that changing surface tension of the

water and changes in soil porosity showed no significant impact on wetting.

Letey et al. (1962) determined that infiltration rates did not hold true for sand

columns and resorted to capillary rise at equilibrium, $p_c = p_g$. They experimentally

measured h using sand columns and calculated contact angle using the following

equation:

$$h = \frac{2\gamma \cos(\alpha)}{\rho g r} \qquad (2\text{--}3)$$

Contact angle can be represented by capillary pressure by the following equation:

$$p_c = p^{nw} - p^w = \frac{2\gamma^{ow} \cos(\alpha)}{r} \qquad (2\text{-}4)$$

where p_c = capillary pressure, p^{nw} = non-wetting fluid pressure, p^w = wetting fluid

pressure, γ^{ow} = interfacial tension between oil and wetting phase, α = contact angle and r

is capillary tube radius. This relationship between capillary pressure and contact angle

can be used to quantify the wetting characteristics of a two phase system. The United

States Bureau of Mines (USBM) (Donaldson et al., 1969; Powers et al., 1996) and the

Amott-Harvey (Powers et al., 1996) methods are commonly used. Each method uses data

obtained from comparing imbibition and drainage capillary pressure/saturation curves

(Figure 2.2).
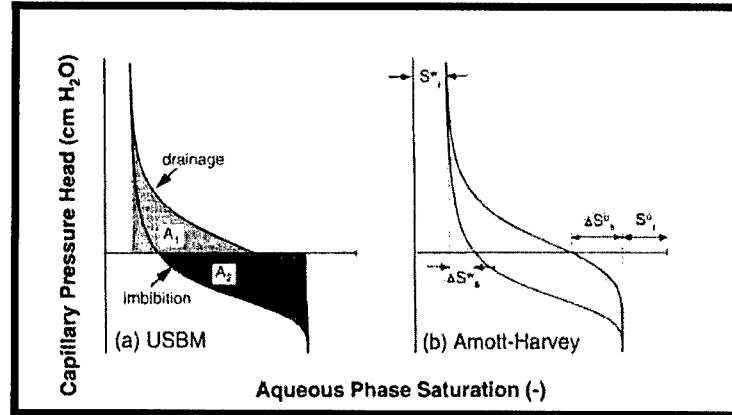
Figure 2.2. Example capillary pressure curves illustrating paramenters used for : (a)
USBM; (b) Amott-Harvey wettability indices (Powers et al. 1996)

The USBM method compares imbibition and drainage areas to assign a wettability index
using the following equation (Powers et al. 1996):

$$I_{usbm} = \log(A_1/A_2) \tag{2-5}$$

where A_1 is the area under the drainage curve to the horizontal axis and A_2 is the area

above the imbibition curve to the horizontal axis (Figure 2.2). The Amott-Harvey

method uses different data from capillary pressure curves to calculate a wettability index

using the following equation (Powers et al. 1996):

$$I_{ah} = \frac{(\Delta S_s^{\,w} - \Delta S_s^{\,o})}{(1 - S_r^{\,o} - S_r^{\,w})} \tag{2-6}$$

where $\Delta S_s^{\,w}$ = difference between saturation at $P_c = 0$ and the residual saturation of the

water phase, $\Delta S_s^{\,o}$ = difference between saturation at $P_c = 0$ and the residual saturation of

the oil phase, and $S_r^{\,o}$ = residual saturation of the oil phase and $S_r^{\,w}$ = residual saturation of

the water phase. None of these methods directly calculate the contact angle, however

they do give a numerical value for system wettability that is directly related to contact angle.

Fink (1970) experimentally measured breakthrough pressure for water repellent soils to quantify system wetting. This is essentially equivalent to the entry pressure or h_d that can be readily identified and quantified on a typical Brooks-Corey capillary pressure curve. Fluid entry pressures can be determined for air in the presence of water or oil, water in the presence of oil or air, and oil in the presence of water or air. An example would be oil penetrating water saturated hydrophilic porous media. Depending on conditions of the system such as type of oil, water composition, and surface type, the oil will require a certain amount of head or entry pressure to displace the water in the porous media. These entry pressure values are directly related to system wettability. Fink (1970) used the experimentally determined h (entry pressure) value in equation 2-3 to calculate θ. He compared the calculated θ values from the sessile drop method to the θ values calculated using the breakthrough pressure method. He assumed theoretically they would be equal but determined that they were not. However, he noted that they each showed similar trends, and therefore each could be used to make relative comparisons between wetting systems.

There are many methods for quantifying system wettability. It appears that most methods cannot be compared to each other directly. However trends can be compared from one method to the next as well as wetting systems can be quantified and compared to each other if a consistent method of measurement is used.

Study Objective

The objective of this study was to conduct water entry pressure, air and oil entry pressure tests for silica sand with various fractions of organic (silane) coated media. This was to quantify system wettability for a water wet, oil wet and intermediate wet systems.

Methods and Materials

Water/Air Entry Pressure Measurements

A series of water entry pressure (WEP) and air entry pressure (AEP) tests were completed for sands with octadecyl trichlorosilane (OTS) treatment percentages of 0, 25, 40, 50, 60, 75, and 100%. Organosilanes such as OTS are effective for changing the surface polarity of the media resulting in an oil-wet environment. Hydrophobic sand was created using an OTS treatment method used by Bradford and Leij (1995) and Le Grange (1993) as follows: 475 ml of denatured or reagent alcohol mixed with 25 ml of OTS to create a 5% OTS mixture; 575 ml of 30/40 Accusand was added to the 5% OTS solution and mixed for 5 hours. At the completion of mixing, the excess solution was drained off and the sand was rinsed again with denatured or reagent alcohol. The sand was then heat dried for several hours. To create each of the hydrophobic/hydrophilic percent volume combinations listed earlier, the appropriate amount of OTS treated sand was mixed with untreated sand to create the desired OTS/untreated sand percent ratio. Denatured alcohol was used for all experiments. Additionally, reagent alcohol treated sand was used for a second 100% OTS experiment.

The WEP and AEP for OTS/untreated sand mixtures listed above were determined using the apparatus shown in Figure 2.3. For the WEP measurements, each mixture listed in above was packed to a depth of 6 cm in the bottom of a long glass column. The column was plugged at the bottom with a rubber stopper with a hole in the center. The

stopper had a stainless steel mesh filter placed on top to support the sand in the glass tube. The stopper was attached to a burette using a section of ¼" tubing. The burette was placed so that the top was level with the bottom of the sand in the column. Water was placed in the burette to contact the bottom of the soil column.
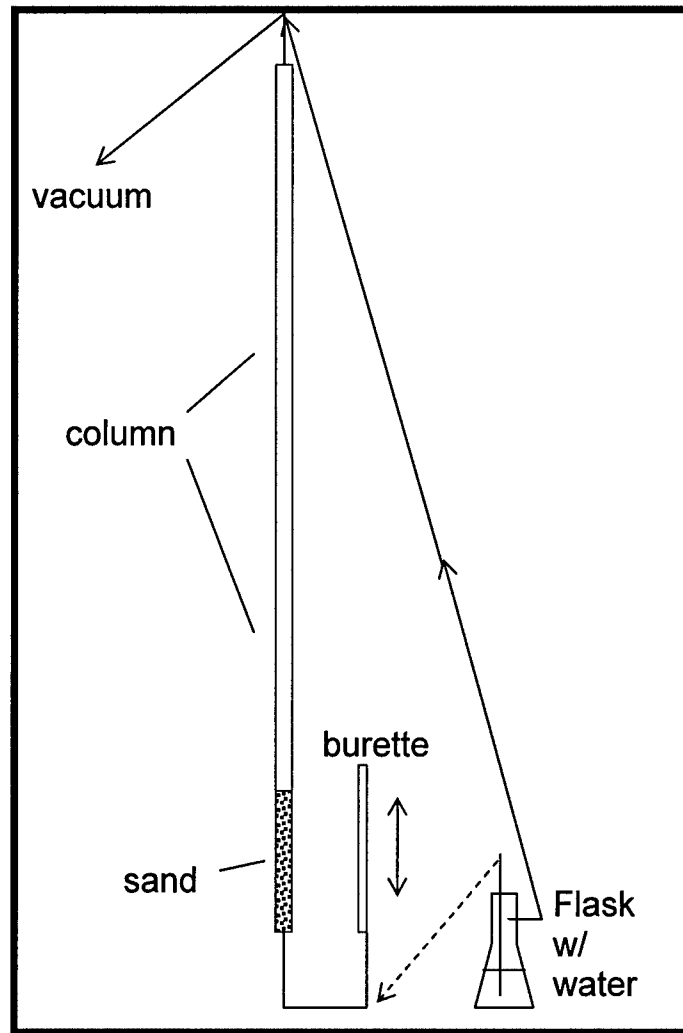
Figure 2.3. Water entry pressure/Air entry pressure column design

The burette was then raised in approximately 0.5 to 2 cm increments increasing the head of water at the bottom of the sand and allowed to stabilize for several minutes. The volume in the burette was recorded for each increment. The height at which the volume

of water began to enter the sand column was used as the head required for water entry or

WEP (See Figure 2.4).
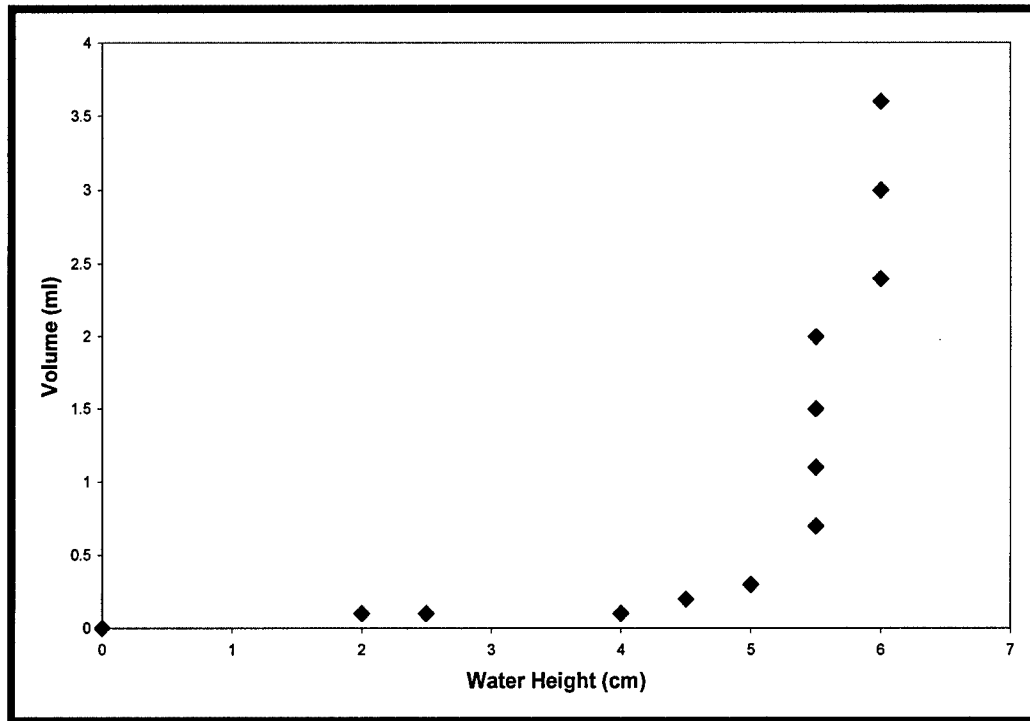
Figure 2.4. Volume change as a function of water entry head for 50% OTS treated sand

For the AEP tests, approximately 6 cm of sand for 0, 25, 40, 50, 60, 75, and 100%

mixtures was placed in the bottom of a long glass column (Figure 2.3). The top of the

column was plugged with a stopper attached to a T valve. The T valve was connected to

a vacuum source and the side port of an Erlenmeyer flask. The flask was filled with

water and sealed at the top with a rubber stopper. The stopper had a glass straw with one

end submerged in the water. The top of the flask was attached via rubber hose to the

stopper at the bottom of the column. This system was closed looped, preventing the

water from leaving the flask. The vacuum was turned on for 15 to 20 minutes to de-gas

the water in the flask. The tube attached to the side port of the flask was then crimped,

allowing the vacuum to draw the water through the top of the flask and into the bottom of

the column. A vacuum was used to facilitate water saturating the OIL and intermediate wet sand mixtures. Water was allowed to enter the column, saturating the sand as the water was drawn up by the vacuum. When the sand was completely saturated with water, the vacuum was shut off and the top of the flask was detached from the hose. This hose was then placed on the bottom of a burette. Water was allowed to exit the bottom of the column filling the burette until the top of the water table in the column was equal to the top of the sand. The height of the burette and volume of water in the burette was adjusted such that with the water table at the top of the sand, the level of the water was at the bottom of the burette. The burette was then lowered in increments of 0.5 to 1.5 cm. For each height, the volume in the burette was measured and recorded. The height at which the volume of water began to enter the burette was assumed to be the head required for air entry or AEP (See Figure 2.5).
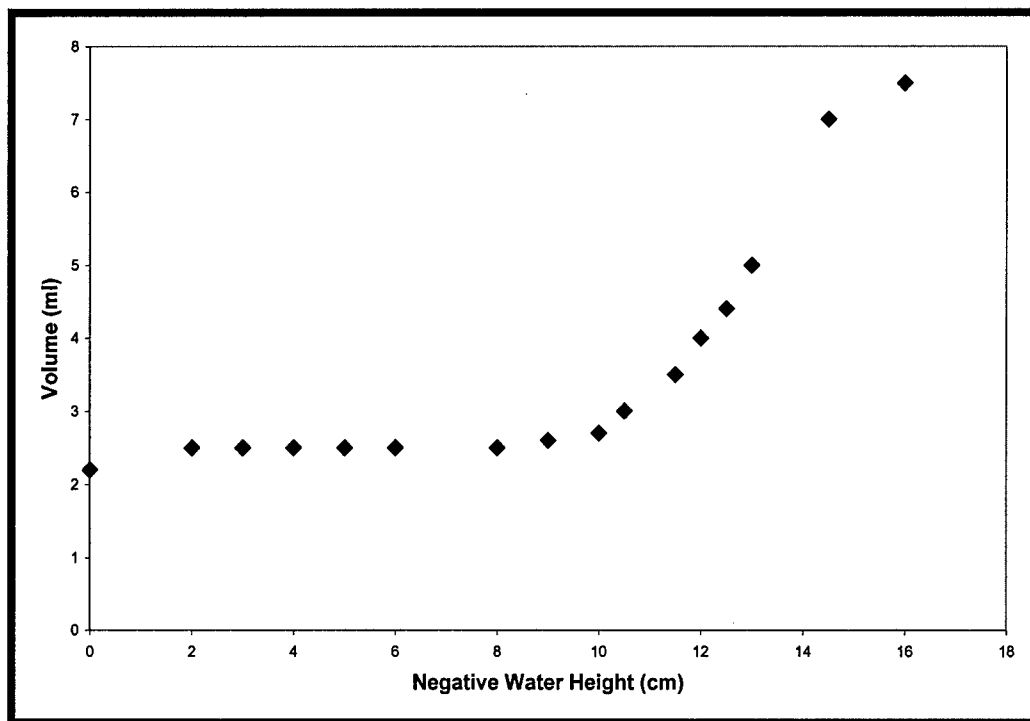
Figure 2.5. Volume change as a function of air entry head for 50% OTS treated sand

Oil Entry Pressure Measurements

A series of oil entry pressure (OEP) tests using PCE in the presence of water were completed for sands with OTS treatment percentages of 0, 25, 50, 75 and 90%. The OEP for these OTS/untreated sand mixtures were determined using the apparatus shown in Figure 2.6. Each mixture listed was wet packed to an approximate depth of 5 cm in the bottom of a short glass column. The column was plugged at the bottom with a rubber stopper with a hole in the center. The stopper had a stainless steel mesh filter placed on top to support the sand in the glass tube. A rubber tube was attached to the stopper at one end and a burette at the other end. There was a three way valve in the closed position between the burette and column. The water used for wet packing was degassed with helium for approximately 15 minutes prior to packing. This is necessary because silane coated sand has an affinity for air in the presence of water.
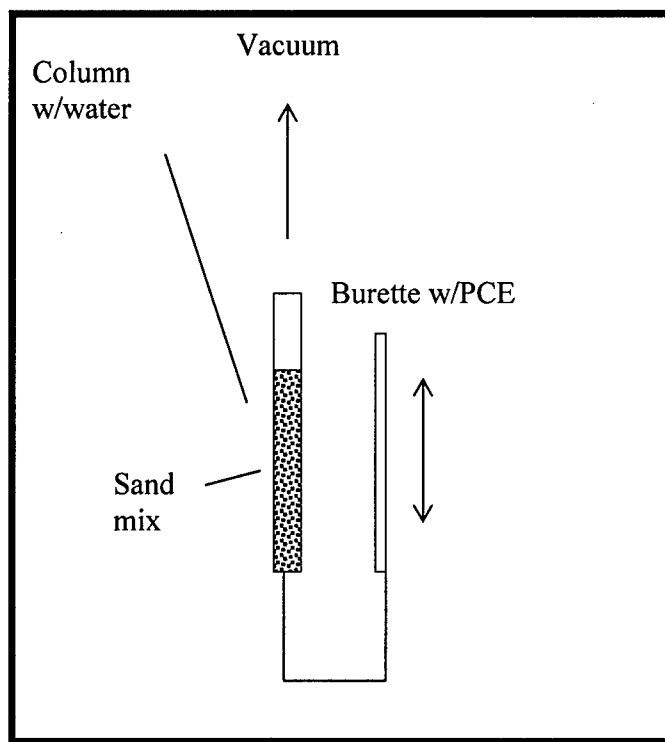
Figure 2.6. Oil entry pressure in the presence of water column set-up

Regardless of degassing, air bubbles were still present during the packing process. The column was sealed and a vacuum applied to further remove the air from the system. The column was then reopened and the sand was tamped down into the column to achieve a tight sand packing. A vacuum was applied again followed by compacting of the sand. This process was repeated until all visible air was removed. The burette was placed so that its top was level with the bottom of the sand in the column. Perchloroethylene was placed in the burette and drained through the three way valve to remove any air from the line while maintaining the water level in the column. After the air had been drained, the valve was placed as such to allow the PCE and water to contact. The burette was raised such that the PCE contacted the bottom of the soil column. The burette was then raised in approximately 0.5 to 2 cm increments increasing the head of PCE at the bottom of the sand and allowed to stabilize for several minutes. The volume in the burette was recorded for each increment and the height at which the volume of PCE began to enter the sand column was assumed to be the head required for Oil entry or OEP similar to the process for water entry pressure in the presence of air.

Results and Discussion

The pressure breakthrough curves for each sand mixture are displayed in Appendix A. Calculated contact angle values are shown in Table 2.1. The contact angles were calculated using equation 2-3 (Fink, 1970) and the WEP_a AEP_w, and OEP_a values as height (cm). Water contact angles decreased as OTS percentage decreased. All contact angles were >90, indicating oil wet system. Contact angles for 25% and 0% mixtures were estimated from the projected capillary rise shown in Figure 2.7. Air contact angles did not vary indicating air is always the non-wetting fluid. Oil contact angles decreased as OTS percentage decreased, indicating the media becoming more water wet. The

WEP$_a$, AEP$_w$ and OEP values as a function of hydrophobic media percentage are displayed in Figure 2.7. The WEP$_a$ for the hydrophobic sand decreased from a maximum of 9 cm to 5 cm as the hydrophobic percentage decreased. The mixtures exhibited hydrophobic behavior down to 40% OTS (hydrophobic) sand content. Water entry pressure for the 25% OTS sand content could not be measured because the water rose by capillary action, indicating the switch from hydrophobic to hydrophilic behavior. The air entry pressure with respect to OTS percentage showed a slight decline from 15 cm to 12 cm in AEP$_w$ from 0% to 75% OTS percentage respectively. The 100% OTS sand showed a slight increase back to 13 cm. This is a slight indication that the untreated sand retains the water or requires more pressure to begin draining water when compared to the OTS treated sand mixtures. Oil entry pressure was affected by the changing hydrophobicity, requiring less entry pressure as hydrophobicity increased. The point at which entry pressure is no longer required and PCE is drawn into the sand by capillary action appears to be between 75% and 90% OTS treated sand content.

Table 2.1. Calculated contact angles

% OTS	Water θ (in air) degrees	Air θ (in water) degrees	OIL θ (in water) degrees
100	128.5	25.8	
90			90.0
75	121.2	33.8	86.1
60	114.5	33.8	
50	114.5	25.8	80.3
40	110.2	28.8	
25	90.0	25.8	78.3
0	0.0	0.0	66.1

Conclusions

The change in percent OTS treated sand influences water entry and oil entry pressure values. The displayed trend shows that as OTS percentage decreases, water

entry pressure values decreased from 15 cm of capillary rise to -9 cm of entry head. As

the OTS percentage increased, the oil entry pressure values decreased from 6 cm of entry

head until reaching 90% at which the sand displayed hydrophobic characteristics and

drew the PCE into the media by capillary action. The trend related to air entry pressure

showed that AEP values were not sensitive to OTS percentage changes. Bradford and

Leij (1995) noted that air is always considered the non-wetting fluid, therefore, water

would be the wetting fluid regardless of soil treatment. This might explain the

insensitivity of the AEP values.
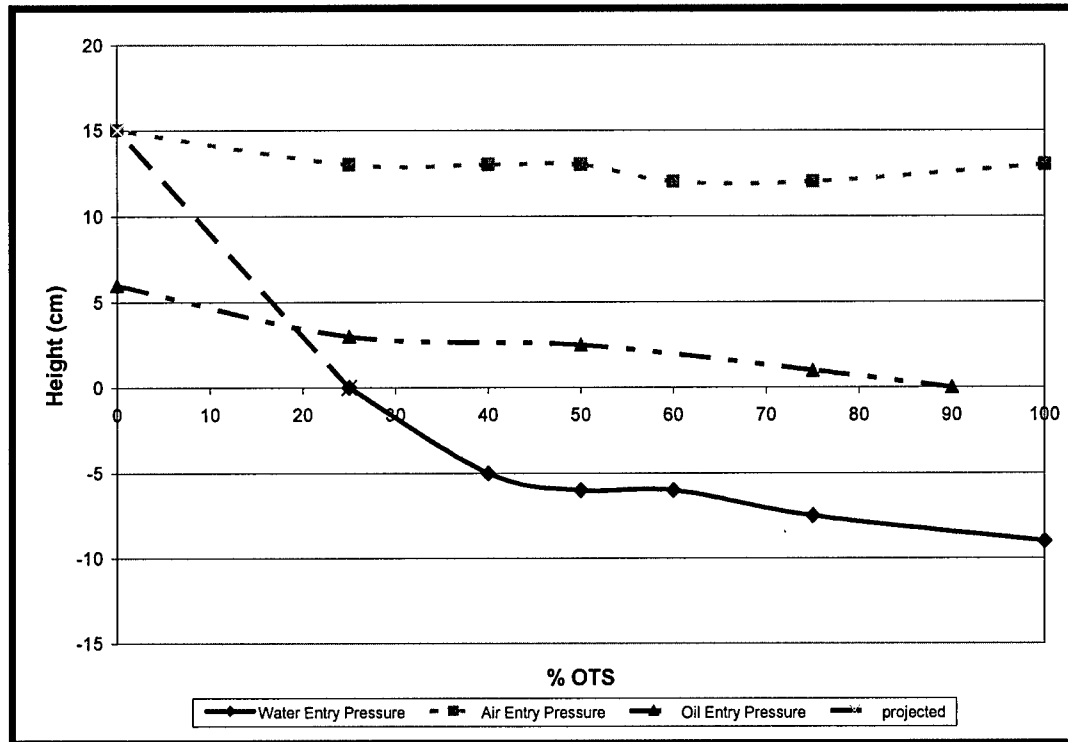
Figure 2.7. Water (air), air (water), and oil (water) Entry Pressure Values for each
mixture percentage Note – data points +/- 1cm

CHAPTER 3
INVESTIGATION OF THE RELATIONSHIP BETWEEN MEDIA PROPERTIES (GRAIN SIZE AND WETTABILITY) AND MASS FLUX

Introduction

As Dense Non-Aqueous Phase Liquids (DNAPL) migrate in the subsurface, media and fluid properties influence how and where they will travel and distribute. DNAPLs, serve as long term contaminant sources slowly dissolving into the aquifer. Typically, the solubilities of NAPLs in water are quite low; however, they are usually orders of magnitude higher than applicable drinking water/clean up standards. An understanding of how porous media and fluid properties affect travel and distribution behavior is needed to develop effective remediation strategies to manage these long term contaminant sources. Media properties such as soil type, media heterogeneity or homogeneity, grain size, grain shape, and wettability characteristics are needed to characterize DNAPL source zones. These properties influence contaminant behavior in sub-surface systems. What remains after migration is contaminant residual that is suspended or trapped in the porous media as residual and/or pooled on an impermeable layer at a low point in the aquifer. The residual and pooled NAPL surfaces provide a contact area based on geometry and orientation for NAPL to transfer to the aqueous phase.

Theoretical Background

Porous media grain size and contact angle (wettability) are the common components governing NAPL migration and entrapment processes.

Grain Size

Grain size is an important parameter that affects the flow, gravitational and capillary pressures acting on a DNAPL globule in the subsurface. Pennell et al. (1996) proposed a pore entrapment model describing the forces acting on a NAPL globule that affect its mobilization after entrapment. A similar model can be used to observe the forces acting on a NAPL globule during migration processes. Figure 3.1 displays the forces acting on a NAPL globule in a pore.

Figure 3.1. Schematic diagram of pressures/forces action on a NAPL globule

Capillary forces are represented by P_c, injection forces P_i and gravitational forces are P_g. The forces identified are similar to those identified by Pennell et al. (1996) shown in equation 3-1 with the exception of the injection force.

water flow + gravity　　= capillary

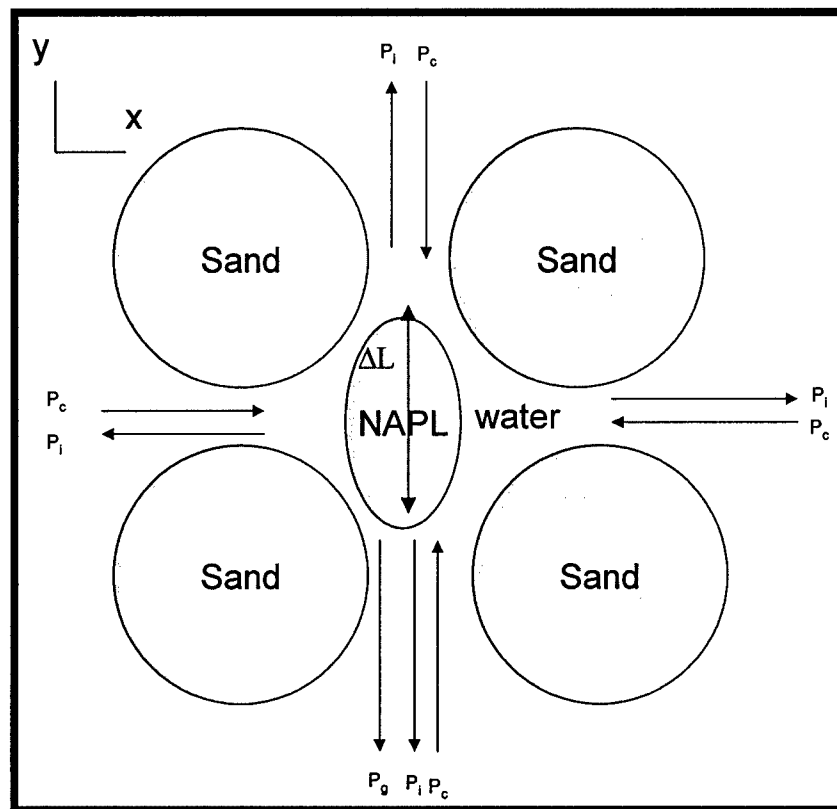$$\frac{\mu_w \Delta\rho}{k_w} q_w + \Delta\rho g \Delta l \sin\alpha = \frac{2\beta_{ow} Cos\theta}{r_n} \qquad where \beta = 1 - \frac{r_n}{r_b} \qquad (3\text{-}1)$$

where μ_w is the fluid viscosity, $\Delta\rho$ is the density differential, q_w is the darcy flux, k_w is intrinsic permeability, Δl is average length of DNAPL globule, α is the angle with respect to flow, θ is the contact angle, r_n is neck or throat radius, and r_b is blob radius. As grain size changes, intrinsic permeability changes affecting the flow conditions, the potential length of the globule changes affecting globule size and weight, and the throat radius changes affect capillary pressure. In a system where groundwater flow is perpendicular to gravitational forces, the flow force will be less significant compared to gravitational forces when determining migration behavior in the direction of gravity and transverse to the flow field. Additionally, the flow force is a magnitude smaller through a range of sand sizes when compared to the gravity forces (Table 3.1).

Table 3.1. Calculated bond, capillary and total trapping numbers using equations 1-4 and 1-5

Seive	K (cm/sec)	$K_i(cm^2)$	N_{bond}	$N_{capillary}$	N_T
20/30	0.149	1.35E-06	6.55E-06	1.50E-07	6.55E-06
30/40	0.143	1.29E-06	6.25E-06	1.50E-07	6.25E-06
40/50	0.091	8.31E-07	4.00E-06	1.50E-07	4.01E-06
40/60	0.088	7.97E-07	3.84E-06	1.50E-07	3.84E-06
50/70	0.063	5.72E-07	2.75E-06	1.50E-07	2.76E-06

The injection force or pressure is the pressure imposed on the NAPL by the injection of the NAPL into the system. This pressure is a function of injection rate and fluid viscosity. This is unique to the lab environment since NAPL injection through a syringe is a common method of NAPL introduction into two-dimensional columns. As grain size decreases, the P_c increases against the NAPL globule, requiring higher entry

pressure to move the globule from one pore to the next. As the P_c increases, the effect P_g has decreases and P_i becomes more significant near the point of injection. This may cause the globule to migrate in all directions rather than be dominated in the direction of gravity. This effect becomes less significant the further away the NAPL migrates from the injection port. This effect may possibly cause more spreading of the NAPL as the grain size decreases.

Entrapment processes are also affected by grain size. Maintaining all other components of the N_T constant, changing the grain size diameter will change the Bond Number and the N_T. NAPL residual saturation appears to be sensitive to changing N_T (Dawson and Roberts, 1997; Saripalli et al., 1997) and as N_T increased, saturation decreased. This is consistent with the findings of Pennell et al. (1996).

Wettability

Wettability is a property of interest because of its effect on oil (NAPL) recovery. Wettability in porous media is the relative affinity of the solid component of the media for fluids such as air, water or oil (Wilson, 1988). Hydrophilic soils have an affinity for water while hydrophobic soils have an affinity for oil. Soils can become oil wet through physical, chemical, or biological mechanisms (Bradford and Leij, 1995; Wilson, 1988). According to Wilson (1988), physical mechanisms such as heat can aid in depositing organic material on the soil. The chemical mechanism involves adsorption of compounds that change the surface polarity of the media. It has been reported that cationic surfactants and additives in gasoline can cause water-wet material to become oil-wet (Bradford and Leij, 1995; Powers and Tambin, 1995; Powers et al., 1996). Additionally, Powers et al. (1996) found that complex NAPL mixtures can create a wide range of wetting conditions.

Biological mechanisms are the least understood and beyond the scope of this study (Wilson, 1988).

Wettability is typically measured by the advancing contact angle for water displacing oil (Bahrani et al., 1973; Moore and Slobod, 1956; Powers et al., 1996). The contact angle formed between two fluid phases and a solid surface is a result of equilibrium among interfacial energies between interfaces and is defined by Young's equation as follows (Powers et al., 1996):

$$\gamma^{so} - \gamma^{sw} = \gamma^{ow} \tag{3-2}$$

where γ is the interfacial energy with s, o, and w representing solid, oil, and water, respectively. Strongly water wet systems have contact angles θ near 30° while oil wet systems are assigned contact angles of greater than 90°. Contact angle is an important physical parameter when considering vertical movement of DNAPLs. It is represented as a required parameter in equation 1-1 in chapter 1. Additionally, it affects the capillary pressure acting on a DNAPL in a pore. Figure 3.2 displays the pressure forces acting on residual DNAPL in a pore. It is similar to Figure 3.1, however, the capillary pressure can act against the DNAPL trapping it in the pore or it can act by pulling the DNAPL out of the pore similar to capillary "wicking". The direction in which capillary forces act is dependent on the contact angle between the aqueous phase and DNAPL with respect to the media surface. As the contact angle increases and the media becomes oil wet, capillary forces may act in favor of drawing the DNAPL into the media by capillary "wicking". Equation 3-1 shows that contact angle has a great effect on the capillary pressure of the system. Considering only gravitational and capillary pressures, as the capillary pressure grows, gravitation forces become less influential. As the capillary

forces decrease, gravitational forces become more influential until potentially the contact

angle exceeds 90° and becomes an oil wet system.

Contact angle is also represented in both the Bond and Capillary Numbers in the

denominator as $Cos\theta$. As θ approaches 90° or an oil-wet system, $Cos\theta$ approaches zero

increasing both the Bond and Capillary numbers and thus the N_T. This may reduce
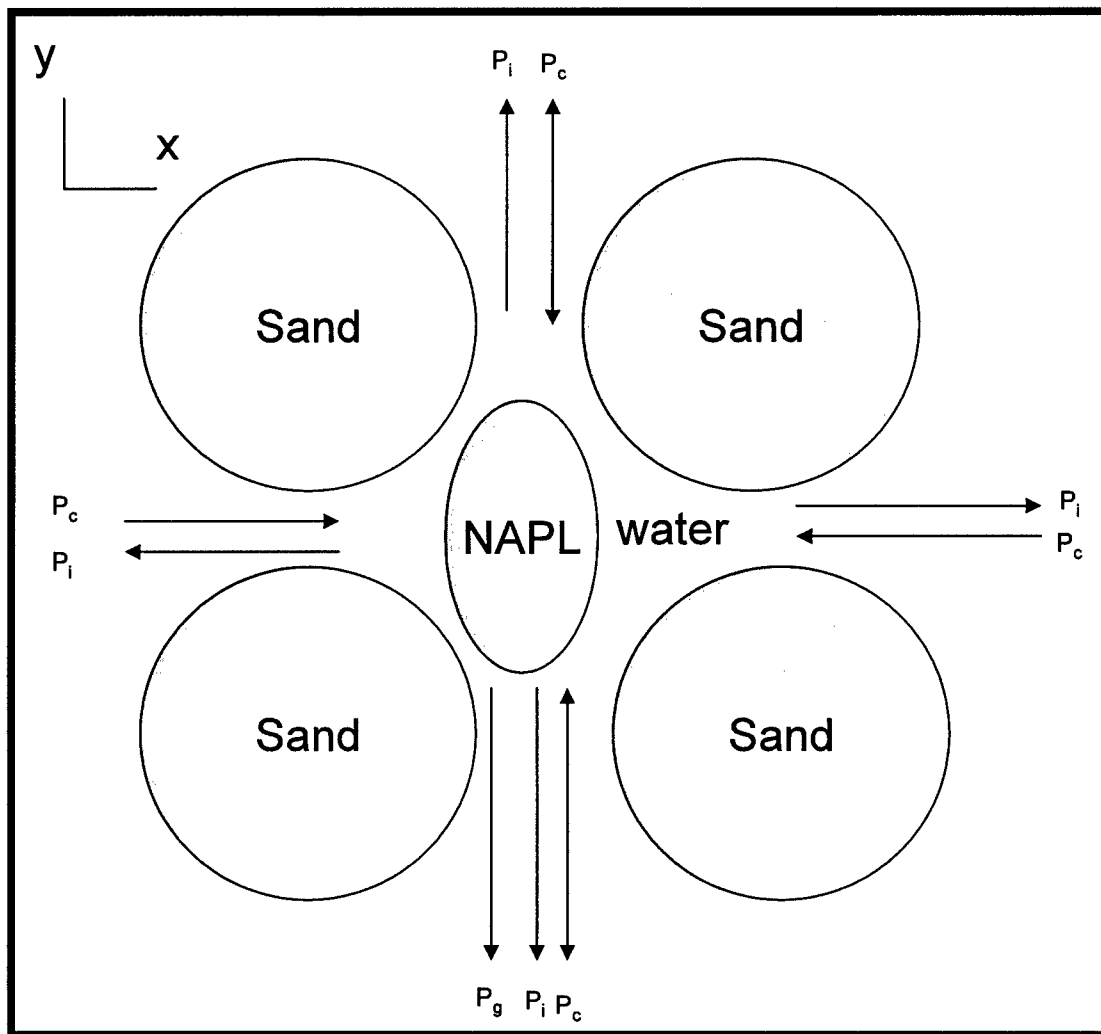
entrapment potential.

Figure 3.2. Schematic diagram of pressures/forces action on a NAPL globule with
variable capillary pressure

Study Objective

The objective of this study was to conduct two types of two dimensional chamber studies designed to investigate soil media modifications and their effect on contaminant geometry and orientation, and ultimately, contaminant mass flux and system efficiency. A set of experiments was completed varying grain size and generate mass loading versus mass flux curves. Another set was to completed changing the media polarity creating an oil-wet environment and generate mass loading versus mass flux curves. Finally, a two dimensional chamber experiment was conducted to quantify a contaminant pool's percent contribution to mass flux compared to the residual mass contribution. Maximum contaminant mass flux values and system efficiency (β) values were investigated.

Materials and Methods

General Experimental Procedure

A two-dimensional (2-D) chamber as described in Chapter 1 (Figure 3.3) was used for each media study. An experiment was conducted for each sand size listed in Table 3.2 and for each hydrophobic media percentage as follows: 25%, 50%, 75%, 90%, and 100% hydrophobic sand.

A total of 11 combinations were investigated. Each experiment lasted approximately two weeks in length. The experimental endpoint was determined when a physical parameter of the chamber was exceeded, e.g. when PCE infiltrated one or both wells.

Hydrophilic Sand Packing Procedure

Sand was added through the top of the chamber in approximately 5 cm thick intervals. After each interval, the sand was mixed with a stir bar and then the box was vibrated to settle and compact the sand. All packing was done under water wet

conditions to minimize air entrapment. This procedure was continued until the chamber

was filled with enough sand to cover the well screens (approximately 10 cm). A layer of

bentonite clay was added on top of the sand to simulate a confined aquifer and eliminate

the complexities of a capillary fringe. Enough clay was added to create a wet clay

thickness of approximately 2-3 cm. This packing procedure was followed for each sand

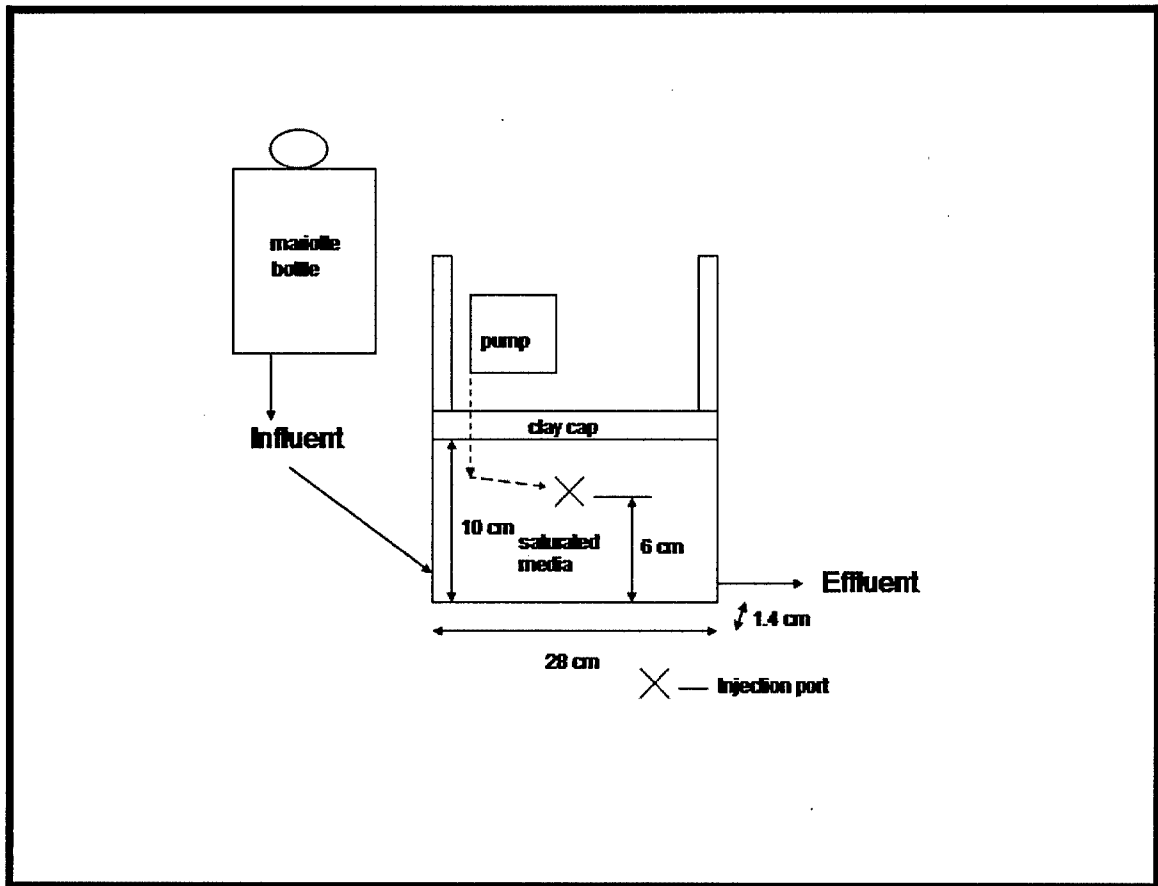size to provide hydraulic and media consistency from experiment to experiment.

Figure 3.3. Two dimensional chamber set-up

Table 3.2. Media properties

	Grain Size Diameter in mm		
Seive Size	min	max	avg
20/30	0.50	0.85	0.68
30/40	0.33	0.60	0.48
40/50	0.25	0.42	0.35
40/60	0.21	0.42	0.32
50/70	0.15	0.30	0.23

Hydrophobic Sand Packing Procedure

Due to the nature of hydrophobic media, a different packing method was required to ensure that a saturated environment was created. The chamber was dry packed with hydrophobic sand in a similar fashion described using 5cm thick layers and stirring. Dry Bentonite clay was added to the top of the sand layer and hydrated with a water bottle to create a clay seal over the dry hydrophobic sand. Carbon dioxide was introduced into the influent port of the chamber to purge the chamber of air. Carbon dioxide was selected because of its high solubility in water. Initially the wells and the effluent port were left open to prevent any air from being trapped in the casing portion of the wells. The wells were then sealed and effluent gas was collected in a 0.5 L Tevlar bag attached to the effluent port. The bag was filled and evacuated to track the number of pore volumes displaced in the chamber by CO_2. Approximately 50 pore volumes were displaced. Water was then introduced into the influent and effluent ports of the chamber to facilitate saturating the sand from the sides of the chamber to the center. The trapped CO_2 was dissolved into the water. As most of the chamber became saturated, an area of trapped CO_2 was created in the center of the box as the water front from each side of the chamber moved towards the center. At this point, the effluent port was released from the water source and water was allowed to flow through the chamber. As the water flowed through

the chamber, the remaining trapped CO_2 in the center of the box was dissolved into the water creating a water saturated media.

PCE Introduction and Sampling

HPLC grade PCE (CAS 127-18-4), colored red with Oil-red-O dye ($\leq 1X10^{-4}$ M, CAS 1320-06-05) was used for each experiment. The PCE was injected into the center of the rear of the chamber 6.5 cm from the bottom and approximately 4.0-4.5 cm from the top of the sand layer, except for the pooling experiment. In the pooling experiment, the injection port was 1 cm from the bottom of the chamber. The PCE was injected through a 20 gauge stainless steel needle glued into the rear of the box. The needle entered the box at a 90° angle to the glass side and protruded 0.7 cm into the box so PCE entered in the center of the width (1.4 cm) of the box. The needle was attached to a 10 ml gastight syringe attached to a syringe pump.

A baseline effluent sample was collected prior to PCE injection. PCE was then injected at a rate of 0.1 ml/min for 5 minutes for a total of 0.5 ml injected. A sufficient number of pore volumes (>8) were passed through the chamber to allow the injected PCE to reach a quasi steady state dissolution. Samples were collected after injection to determine the breakthrough characteristics. The number of pore volumes at which concentration did not vary was the point at which steady state was assumed to be achieved. An effluent sample was collected in a two ml vial to measure PCE concentration. This was used with the measured flow rate to quantify the mass flux generated from the injection. Another 0.5 ml of PCE was then injected and allowed to reach quasi steady state with a subsequent effluent sample collected. Additionally, an outline of the PCE distribution (light red coloration in the sand) was traced on transparency paper attached to the side of the chamber to maintain a qualitative record of

the PCE geometry and orientation after each injection. Reflected light was used to help identify the PCE when producing the outline. The outlines only represent one side of the column and distributions across the thickness of the box were not observed. This procedure was repeated until a physical parameter of the chamber was exceeded. This was usually after a total of five to five and a half ml of PCE was introduced into the box over period of approximately two weeks. Samples collected in the two ml vials were analyzed using a Perkin-Elmer Gas Chromatograph Auto XL with a Flame Ionization Detector. Turbochrome Navigator 4.1 software was used. The method for detection used was as follows: Carrier Pressure – 7.0 psig, 35 °C oven hold for six minutes, Temperature ramp from 35 °C to 110 °C at 5 °C/min, Injection Temp 180 °C, Detector Temperature 250 °C.

Hydraulic Controls

A constant head was maintained at the influent well using a Marriott Bottle controlling the effluent discharge height. The head was maintained at approximately two to three cm above the surface of the sand media to accommodate the clay layer. The effluent rate was maintained by adjusting the effluent discharge height. The rate was approximately 0.7 ml/min. This produced a specific discharge of 68 cm/day. Based on a porosity of 0.377, this gives a pore velocity of 180 cm/day.

Octadecyl Trichlorosilane Treatment and Retardation Factor

Hydrophobic sand was created using an octadecyl trichlorosilane (OTS) treatment method (Bradford and Leij, 1995; Le Grange, 1993). Organosilanes are effective for changing the surface polarity of the media resulting in an oil-wet media. Hydrophobic sand was created as needed by the following method: 475 ml of denatured/reagent alcohol mixed with 25 ml of OTS to create a 5% OTS mixture. Accusand (575 ml of

30/40 mesh size) was added to the 5% OTS solution and tumbled for 5 hours. At the completion of mixing, the excess solution was drained off and the sand was rinsed again with denatured/reagent alcohol. The sand was then dried for 24 hours. To create each of the hydrophobic/hydrophilic percent combinations listed in Table 3.2, the appropriate amount of OTS treated sand was mixed homogeneously with the untreated sand to create the desired percent ratio. As annotated in Table 3.2, denatured alcohol was used for all experiments. Duplicate experiments were run for the 50%, 75%, and 100% mixtures using the reagent alcohol during the mixing procedure. This sand mixture was then tumbled for an hour to create a homogeneous distribution.

Bradford et al. (2000) determined the Freundlich distribution coefficient (K_f^{sw}) f and n for PCE in an OTS treated 20/30 (0.68) sieve sand to be 2.01 and 1.06, respectively. This is nearly a linear relationship. Using the following equation:

$$R = 1 + \frac{\rho_b K}{\theta} \tag{3-3}$$

where ρ_b is the bulk density (1.55 g/ml), K_f^{sw} is substituted for K and θ is the volumetric water content (0.3). The retardation factor was approximately 11. A minimum of 11 pore volumes were used to achieve temporary steady state.

Results and Discussion

To gain an appreciation for how some of the distributions and their associated flux values differed, the hydrophobic and hydrophilic system results are shown in Figures 3.4-through 3.7. The hydrophobic or 100% OTS treated sand distribution is shown in Figure 3.4 with its associated flux curve shown in Figure 3.5. The untreated or hydrophilic system is shown in figures 3.6 and 3.7. It is obvious how much the geometries differ between these systems and how those differences are reflected in their respective flux

curves. The remainder of this section will discuss the grain size experiments and
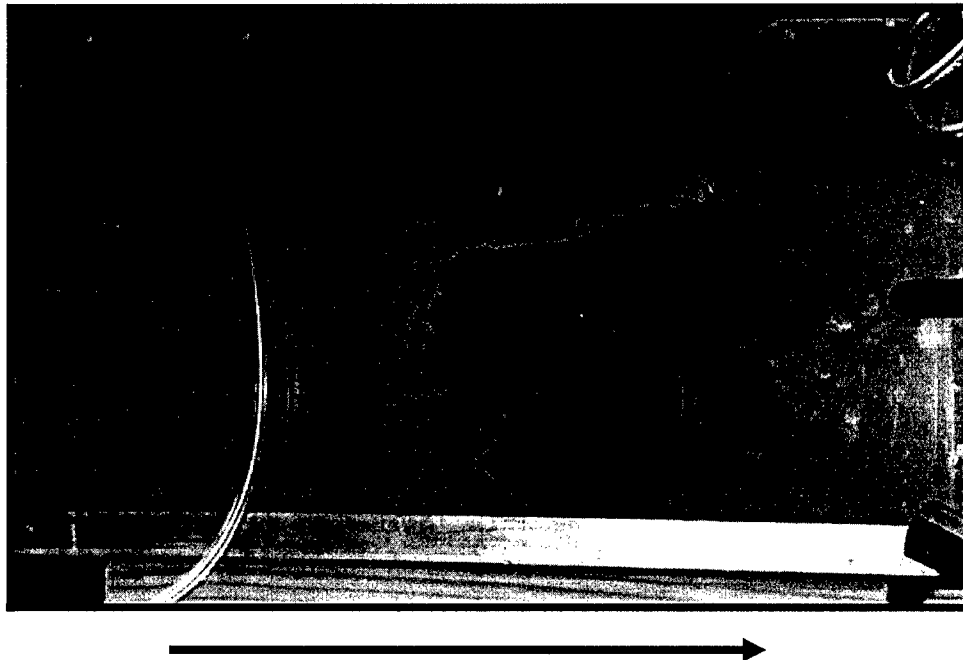
wettability experiments separately.

Figure 3.4. 100% OTS treated 30/40 (0.48) sieve sand at 2.5 ml of PCE
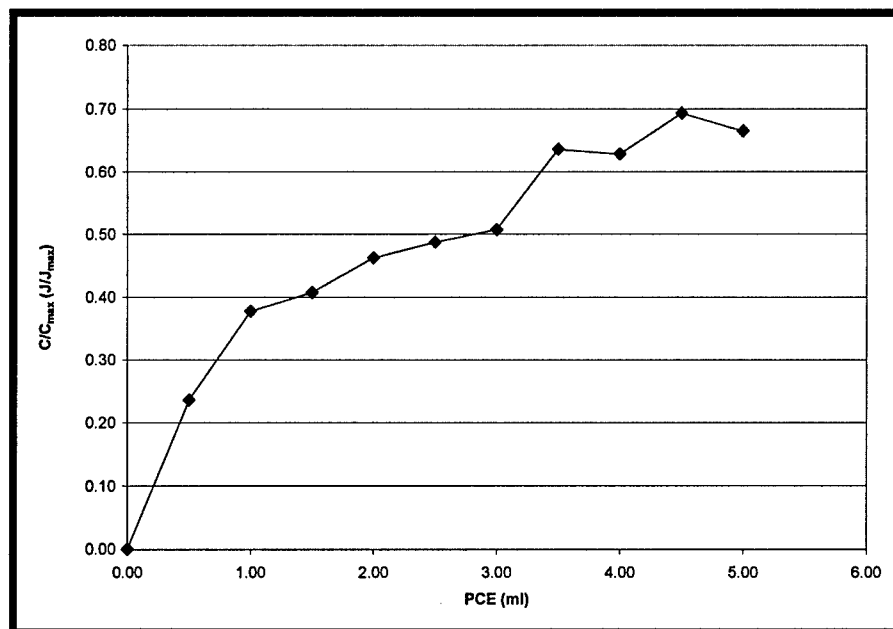

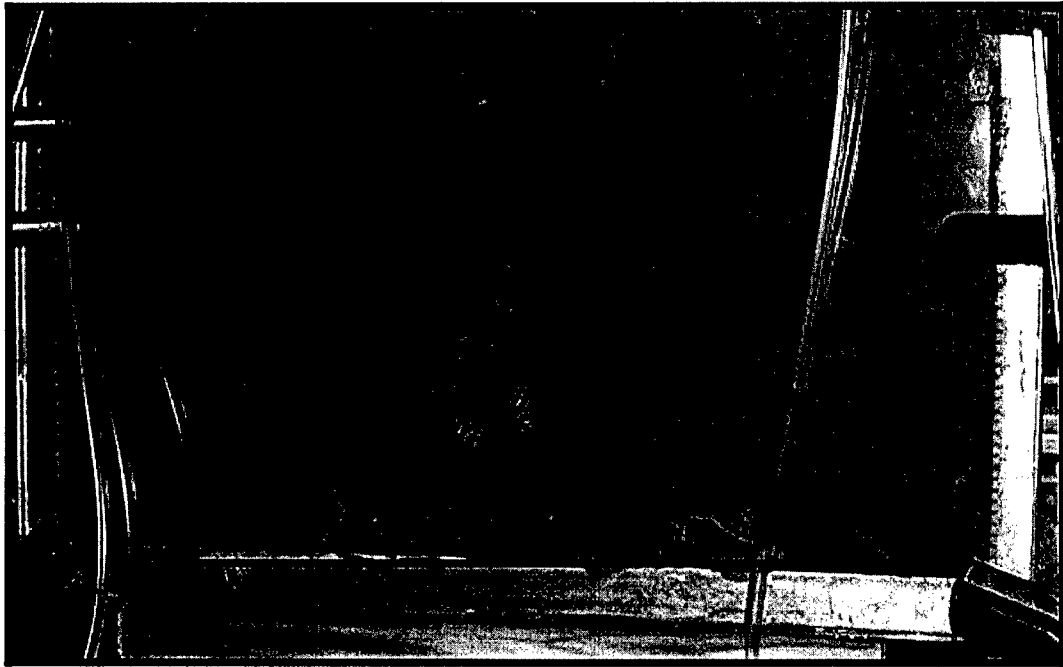Figure 3.5. 100% OTS treated 30/40 (0.48) sand contaminant volume versus flux

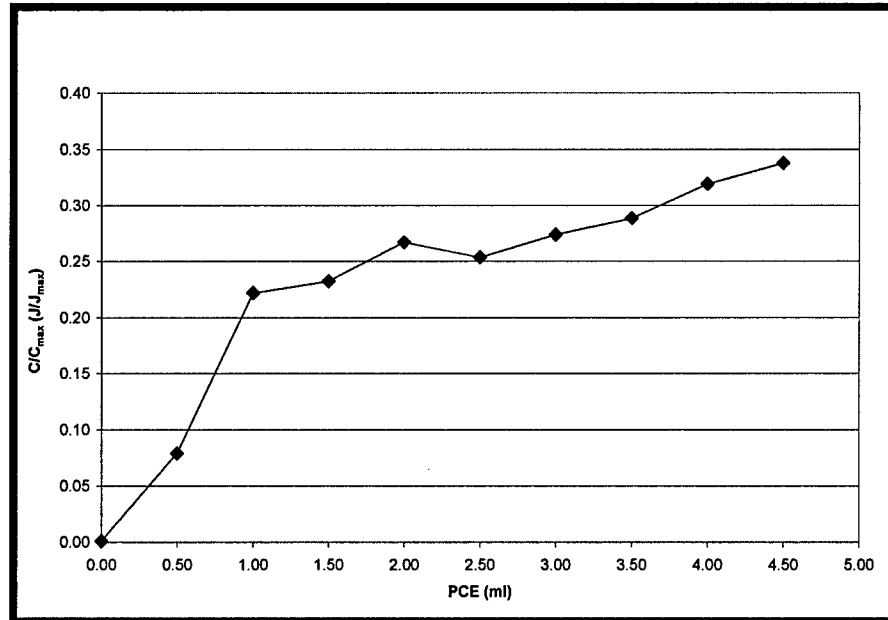Figure 3.6. Untreated 30/40 (0.48) sieve sand at 4.5 ml PCE content

Figure 3.7. Untreated 30/40 (0.48) sand contaminant volume versus flux

Grain Size Comparison Results and Discussion

For each experiment conducted with different size porous media, a trace sketch of the PCE distribution was generated. A trace of the distribution was drawn after each injection reached steady state on a single transparency, resulting in a cumulative distribution drawing (Appendix B). Figures 3.8 and 3.9 are examples of these drawings for the 30/40 (0.48) sand and pooling experiment respectively. A qualitative comparison of the final geometry for each sand size was made using the drawings in Appendix B. In general, predictability of geometry and PCE behavior based on sieve size was not obvious. Pooling began in each experiment by the second injection or one ml with the exception of the 40/50 (0.35) sieve experiment, which appeared to have begun after the fourth injection or two ml. Figure 3.10 shows the quantitative comparison of each volume versus percent mass flux curve for each sieve size and the pooling experiment. In this figure, the C/Cmax values were generated by dividing calculated flux values generated from measured PCE concentrations and flow rates by a calculated maximum flux value based on equilibrium solubility limit and applied flow. The values can be thought of as scaled concentration of mass flux. These values were then graphed against their associated injection volumes. Each of the curves appears to be non-linear in shape with the exception of the pooling curve. The logarithmic shape indicates an initial rapid establishment and increase in flux per unit volume of PCE, followed by a plateau. These results show the first several injections are the largest contributors to flux with the later injections having minimal impact. This is possibly because the first several injections contribute to the residual geometry with the later injections contributing more to the pool.
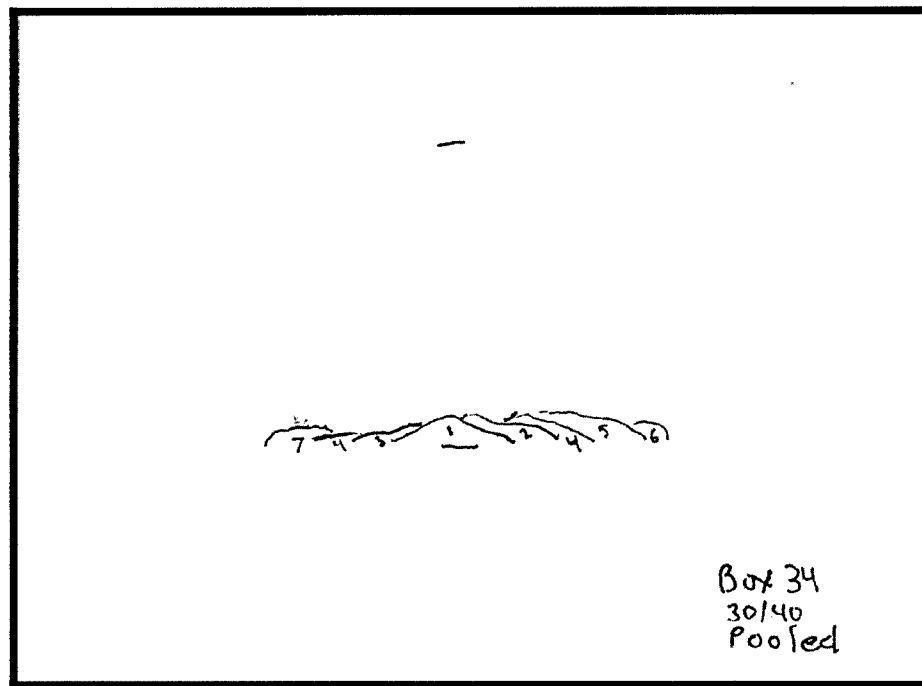
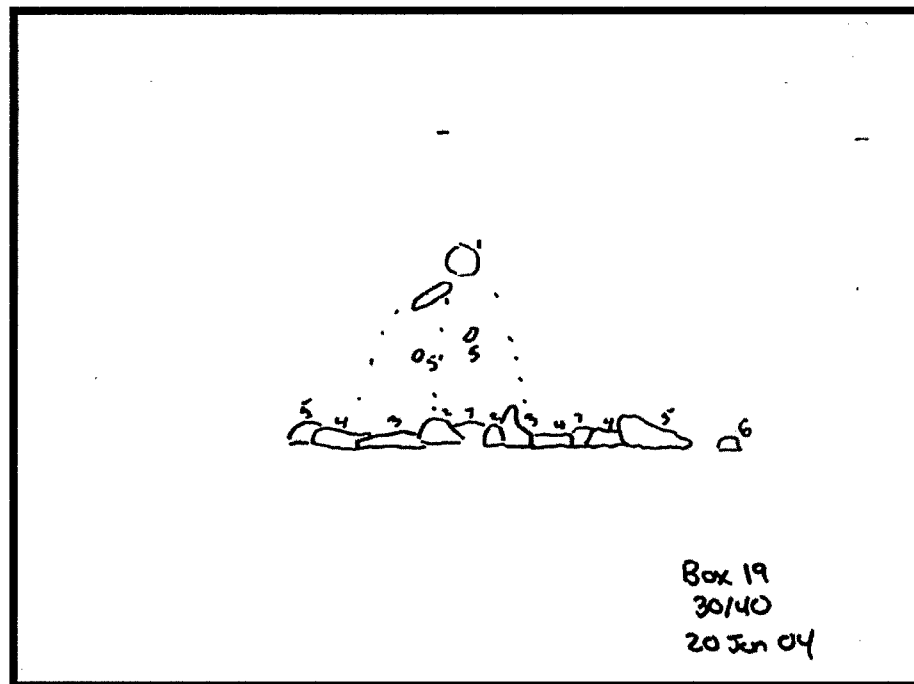Figure 3.8. 30/40 (0.48) sand pooling experiment

Figure 3.9. 30/40 (0.48) sand experiment PCE distribution
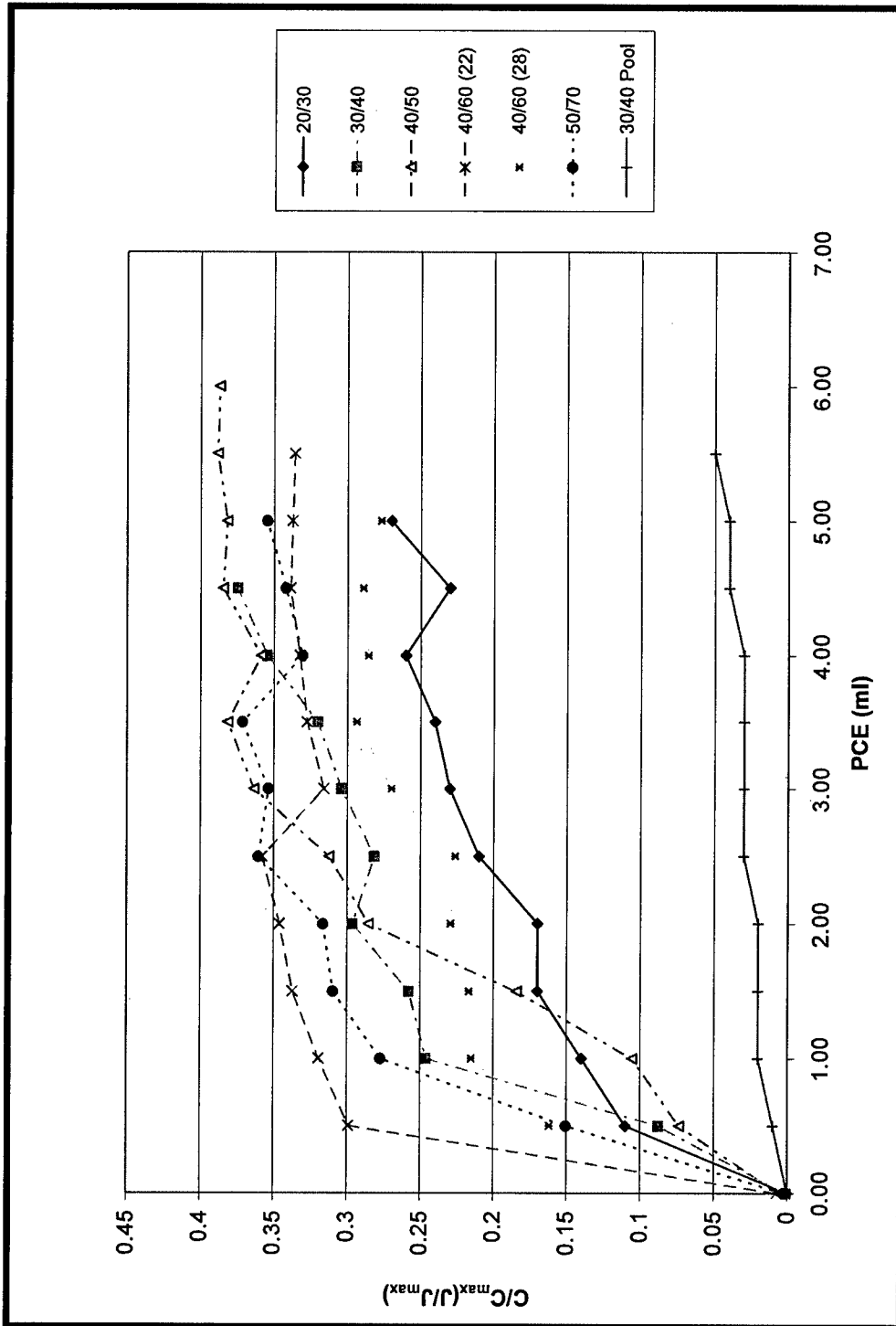
Figure 3.10. Volume versus percent mass flux grain size comparisons

This is supported by the results of the pooling experiment, which show the pooling contributes significantly less mass flux per unit volume when compared to the combined residual and pooled values. The 20/30 (0.68) sieve sand has the lowest C/C_{max} value of 0.27 and the 40/50 sieve sand has the highest C/C_{max} value of 0.38. Using the binary model, the maximum C/Cmax value is estimated to be 0.60. This is based on the injection point position of 6cm from the bottom of the 10 cm chamber and assumes residual distributed homogeneously (vertical and depth) from injection point to chamber bottom. The values observed during each experiment are lower because migration did not produce homogeneously distributed PCE in the vertical plane.

There was no clear pattern between sand size and flux values, but there was indication that as grain size decreased, flux values increase. To confirm this, additional experiments using 20/30 (0.68) and 50/70 (0.23) sand was performed. The results are shown in Figure 3.11 and confirm that finer sands produce higher flux values relative to the course sands. This is possibly due to more lateral spreading caused by the finer grain size resulting in a larger cross sectional area.

Curves were fitted to data using the $Y=X^{\beta}$ model. Figure 3.12 provides an example of collected data and the associated fit curve for the 30/40 sieve sand. Figure 3.13 displays the fitted curves for each grain size. These curves were generated from dimensionless/normalized data to facilitate comparison. The data was normalized by using the maximum mass and flux values for each respective experiment. These curves display the contaminant mass flux versus loading characteristics for the sands investigated. Sand sieves 20/30 (0.68), 30/40 (0.48) and 40/50 (0.35) each have virtually

the same β values and therefore curve shape. This indicates that the vertical migration
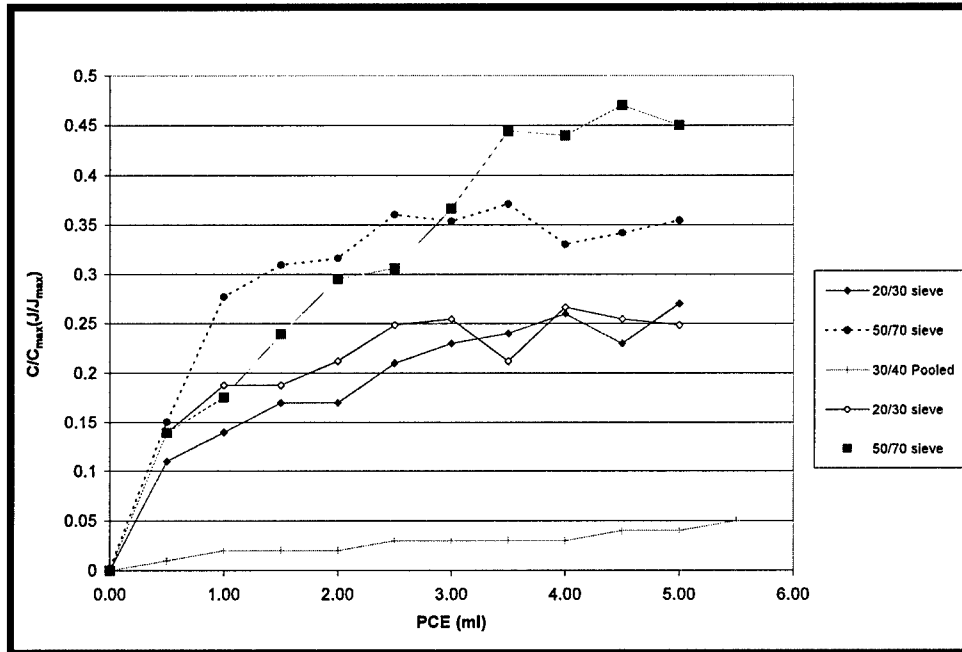from injection to injection of the PCE in each of these sands were similar.

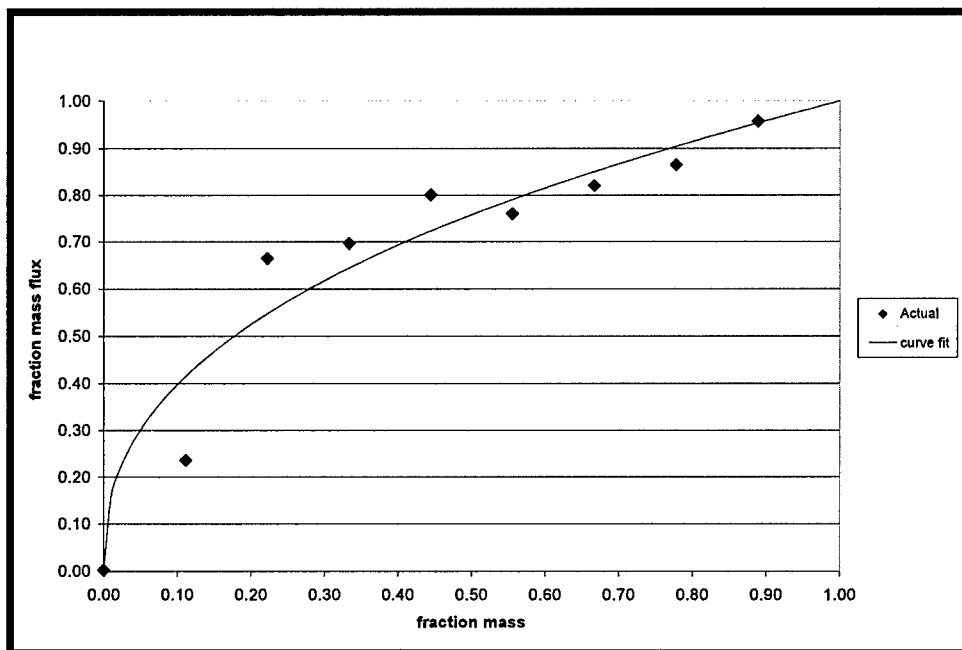Figure 3.11. 20/30 (0.68) and 50/70 (0.23) duplicate experiment

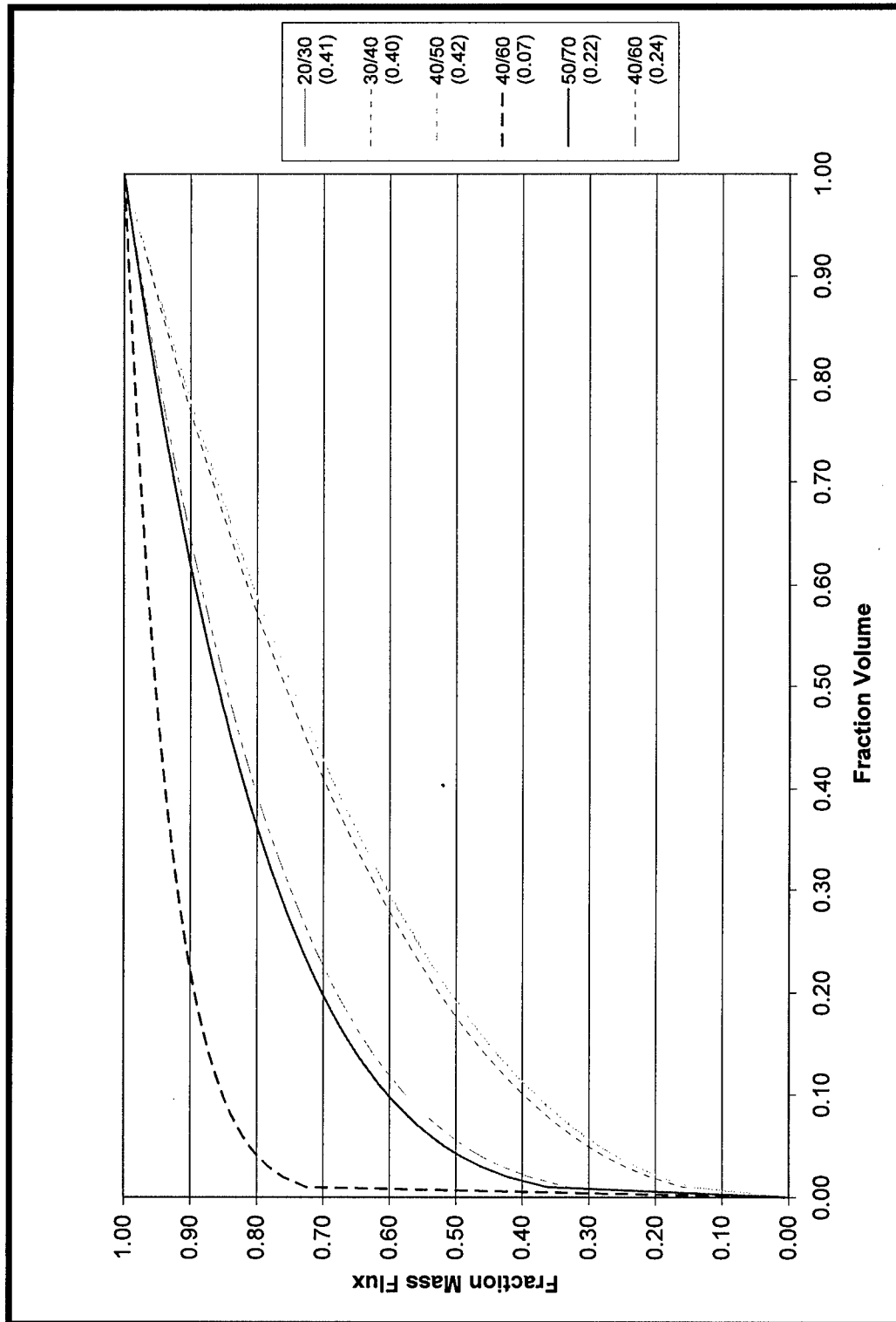Figure 3.12. 30/40 (0.48) sieve sand curve fit example

Figure 3.13. Curve fit comparisons (grain size)

The duplicate experiments for the 40/60 (0.32) sieve sands were performed and identified as boxes 22 and 28. A comparison of these two experiments displays the variability of migration characteristics. This could be due to the wider sieve range relative to the other sands. Figure 3.14 graphically displays the β and grain size relationship with one line representing box 22 data and the other using box 28 data.

The 50/70 sieve sand demonstrated the most efficient loading by developing the largest percentage of its flux value at a lower mass percentage. Tables 3.3 and 3.4 display the correlation analysis between each of the sand's physical characteristics and its estimated β value.
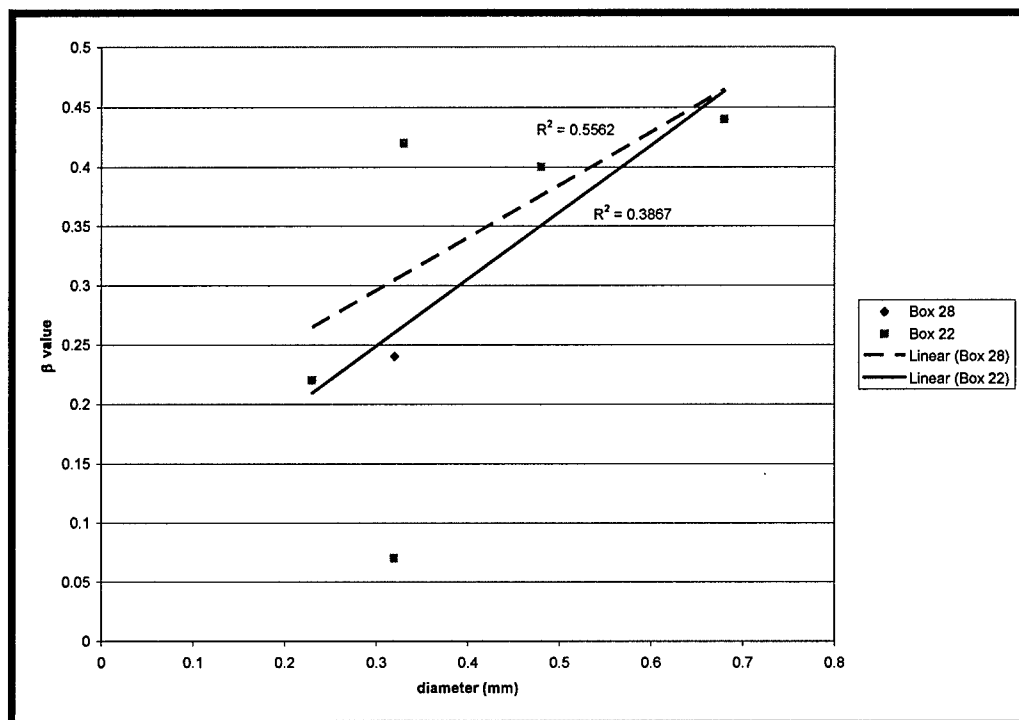

Figure 3.14. β versus grain size diameter

Table 3.3. Correlation analysis using box 28 40/60 (0.32) sand sieve β value

bx28

	diameter	variance	surface area	hydraulic conductivity	beta
20/30	0.68	0.27	146	8.98	0.44
30/40	0.48	0.12	275	8.57	0.40
40/50	0.33	0.08	301	5.49	0.42
40/60	0.32	0.13	307	5.27	0.24
50/70	0.23	0.05	423	3.78	0.22
				r	r^2
			diameter	0.75	0.55
			variance	0.53	
			surface area	-0.77	
			Hydraulic conductivity	0.78	

Table 3.4. Correlation analysis using box 22 40/60 (0.32) sand sieve β value

bx22

	diameter	variance	surface area	hydraulic conductivity	beta
20/30	0.68	0.27	146	8.98	0.44
30/40	0.48	0.12	275	8.57	0.40
40/50	0.33	0.08	301	5.49	0.42
40/60	0.32	0.13	307	5.27	0.07
50/70	0.23	0.05	423	3.78	0.22
				r	r^2
			diameter	0.62	0.38
			variance	0.35	
			surface area	-0.55	
			hydraulic conductivity	0.65	

Wettability Results and Discussion

As performed for the grain size comparisons, in each experiment (percent wettability) a trace sketch of the PCE distribution was generated. A trace of the distribution was drawn after each injection reached steady state on a single transparency, resulting in a cumulative distribution drawing (Appendix B). Figures 3.15 and 3.16 are examples of these drawings. A qualitative comparison between the geometries for 0%,

25%, 50%, 75%, 90% and 100% media mixtures was made using the drawings in
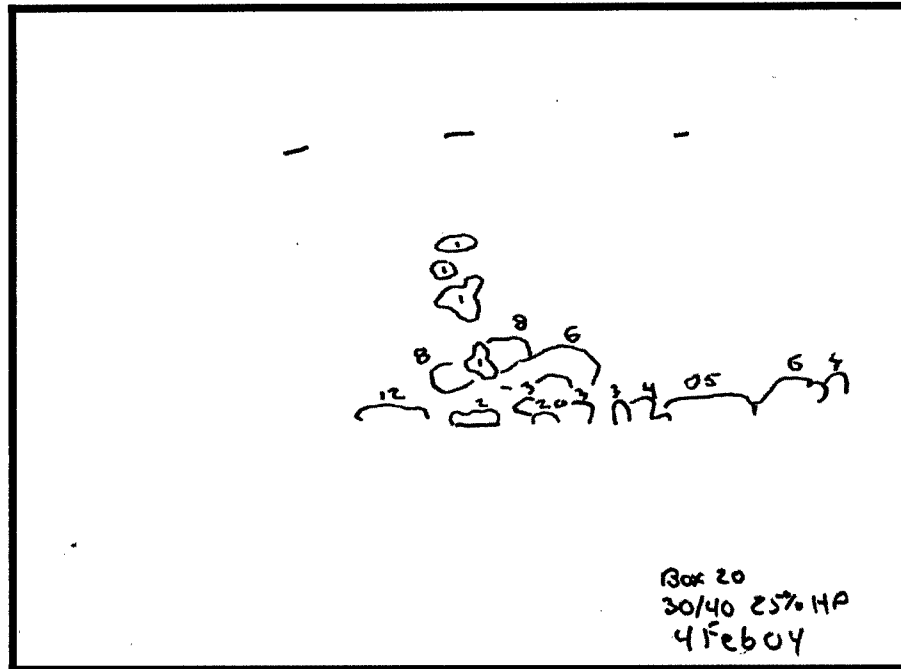
Appendix B.

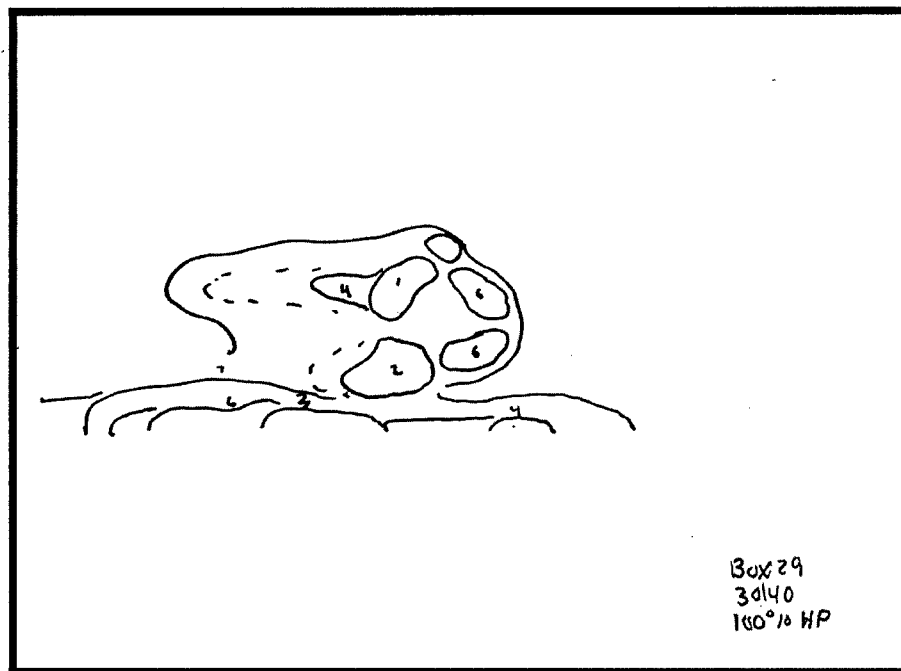Figure 3.15. 30/40 (0.48) Sand 25% OTS mix trace

Figure 3.16. 30/40 (0.48) Sand 100% hydrophobic mix trace

In general, as the hydrophobicity increased, the PCE distributed more uniformly and with increasing connectivity. Because of the water wet media used in the 0% experiment, the PCE was not subject to the "globbing" observed in the 25%, 50% and 75% mixtures and appears to have been more evenly distributed than the intermediate hydrophobic media. The "globbing" observed is when the PCE would collect in discrete concentrated sections in the media and did not have a more uniform distribution. The 0%, 25%, 50% and 75% mixtures displayed a fingered distribution with the 90% mixture beginning to transition to the more uniform spreading shown in the 100% mixture. Additionally, capillary "wicking" was primarily observed in 100% mixtures with some minimal "wicking" occurring in the 90% mixture. Apparently, a significant amount of the media ($\geq$90%) must be OTS treated to allow capillary forces to overcome gravitational forces and cause uniform lateral and vertical spreading.

A quantitative comparison was made and shown in Figure 3.17. The flux is presented as C/Cmax or J/Jmax since flow rate (Q) and area is constant is each experiment. In general, the 100% and 90% mixtures appear produce the higher maximum percent mass flux values when compared to the intermediate and 0% mixtures. Comparing these curves to their associated sketch, it appears the vertical movement of the PCE above the injection point was the differing factor in flux production. More PCE exposure to the horizontal aqueous flow appears to have resulted in higher flux values. There appears to be little difference in flux values between the 0%, 25%, 50% and 75% mixtures. This might be due to the intermediate mixtures providing similar overall surface area contact between the PCE and aqueous phase as the 0% sand
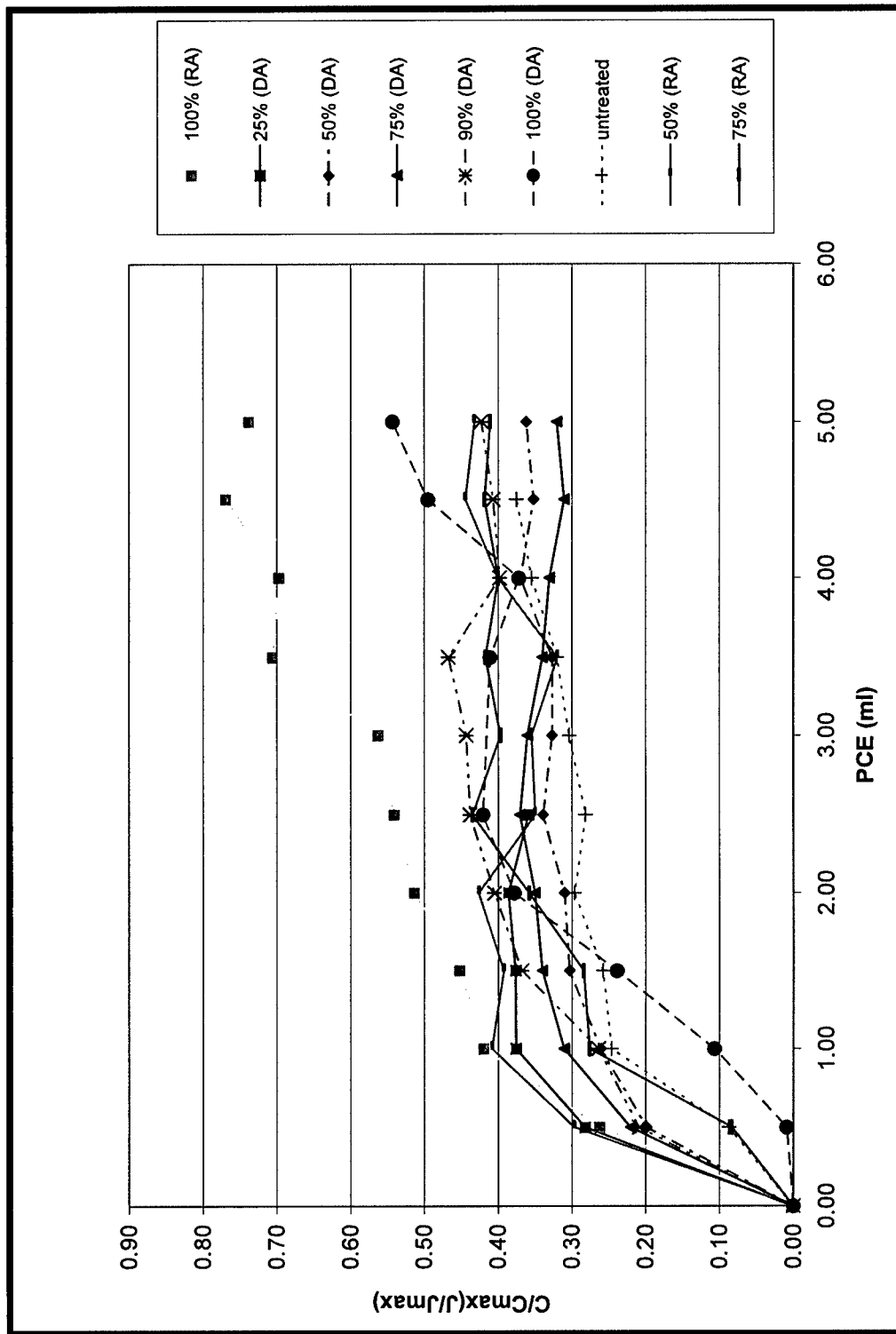
Figure 3.17. Volume versus percent mass flux hydrophobic comparisons

The intermediate soils tended to collect the PCE residual in disconnected globs while the 0% appeared to a more evenly distributed fingered residual. Additionally, Moore and Slobad (1956) found that porous media of the intermediate wettability had lower water imbibing tendency than in the strongly water wet system. They state that imbibition, though still present, is not the dominating displacement process. As a result, the capillary and viscous forces are of equal importance and the water will flow down both sizes of pores at nearly the same velocity. The result is lowered oil saturation at breakthrough compare to either wettability extremes.

As examples of the wettability curve fit data, Figure 3.18 displays the 75% and 100% OTS treated sands data and associated fit curves. Figure 3.19 displays the fitted curves for each wettability percentage. There is little difference between the shapes of the curves for 0%-90% hydrophobicity. The 100% RA treated sand and 100% DA treated sand are more linear relative to the other sands and demonstrated by their higher β values. This may be due to capillary forces countering gravitational forces, causing a slower vertical downward migration and thus, a less efficient system. This may be explained by the force balance performed using equation 3-1 and the system data listed in Table 3.5. Flow forces were ignored due to orientation of flow with respect to gravity. Table 3.6 displays the results of theoretical capillary rise, h, and both gravity and capillary pressures acting on the NAPL globule. The force balance indicates that gravity pressures remain constant with changing contact angle. However, as the contact angle increases and the system becomes oil wet, gravity may become more significant. Additionally, in order to achieve capillary rise, the system must become oil wet as indicated by the 90° contact angle. According to the entry pressure findings in Chapter

two, the system becomes oil wet at approximately 90% OTS treated sand content. This supports why the system must be >90% treated sand in order to achieve capillary rise and overcome gravitation forces.
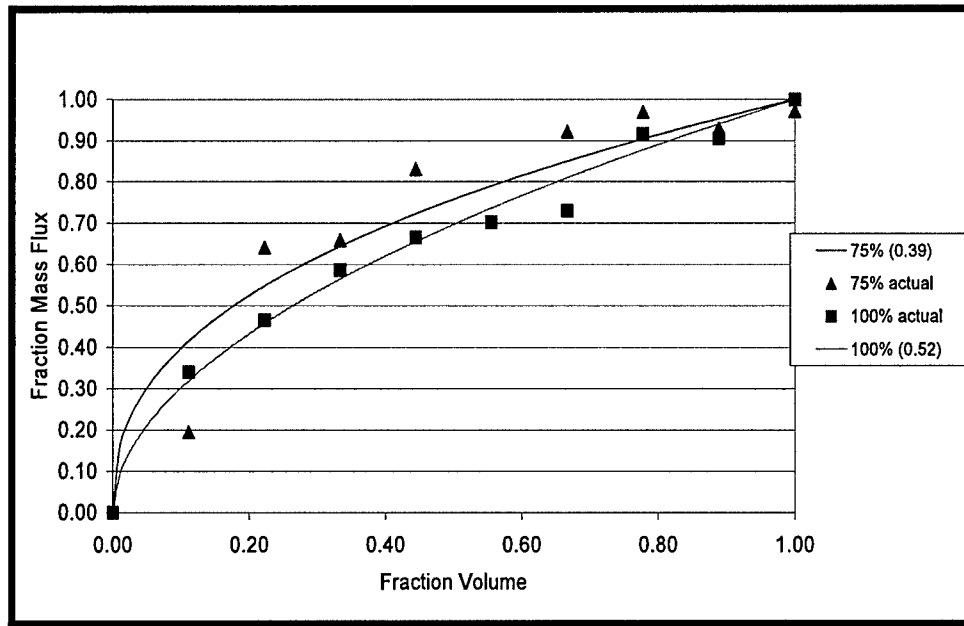

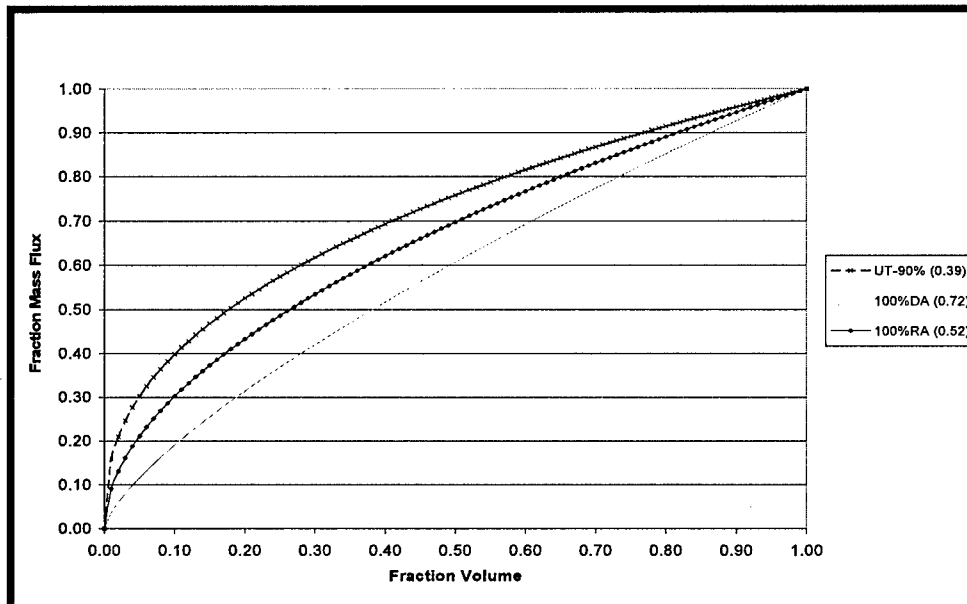Figure 3.18. 75% and 100% OTS treated data curve fit examples

Figure 3.19. Curve fit comparisons (wettability)

Table 3.5. Force balance data

α=	90	degrees	$r_p=$	0.0106	cm	Δl=	0.0212	cm
d=	0.05	cm	$r_t=$	0.00385	cm	β=	0.636792	
Δρ=	0.65	g/ml	g=	980	cm/sec^2	$ρ_{oil}=$	1.65	g/ml
σ=	47	dynes/cm						

Table 3.6. Theoretical force balance results

θ	Cos(θ)	h (cm)	capillary pressure
0	1.00	-38.3	155E2
10	0.98	37.7	153E2
20	0.94	36.0	146E2
30	0.87	33.2	134E2
40	0.77	29.3	119E2
50	0.64	24.6	9993
60	0.50	19.1	7773
70	0.34	13.1	5317
80	0.17	6.66	2699
82	0.14	5.33	2163
84	0.10	4.01	1625
86	0.07	2.67	1084
88	0.03	1.34	542
90	0.00	0.00	0.00
92	-0.03	-1.34	-542
94	-0.07	-2.67	-1084
96	-0.10	-4.01	-1625
98	-0.14	-5.33	-2163
100	-0.17	-6.66	-2699
110	-0.34	-13.1	-5317
120	-0.50	-19.1	-7773
130	-0.64	-24.6	-9993
140	-0.77	-29.3	-119E2
150	-0.87	-33.1	-134E2
160	-0.94	-36.0	-146E2
170	-0.98	-37.7	-153E2
180	-1.00	-38.3	-155E2

Flow By-passing and Rate Limited Mass Transfer

Concentrations of NAPL compounds in groundwater are usually less than their

aqueous solubility due to irregular distributions, non-uniform flow patterns, dilution and

sorption effects, and rate limited mass transfer (Hunt, et al., 1988; Soerens et al, 1998).

Powers et al. (1992) performed one-dimensional column experiments to determine the physical characteristics which affect mass transfer rates. These experiments were performed using homogeneously distributed NAPL source zones and determined that grain size, source zone length and Darcy velocity impact mass transfer coefficients under one dimensional column conditions. This method may overestimate mass transfer coefficients when applied to heterogeneously distributed NAPL source zones such as those created in this research.

Soerens et al. (1998) concluded that non-equilibrium or non-ideal dissolution of NAPL can be represented by mass transfer rate limitations, flow by-passing due to media or distribution heterogeneities, or a combination of these mechanisms. Experimental curves generated from this research were compared to ideal equilibrium curves and curves developed using mass transfer rate estimations to determine if potential flow by passing, rate limitation or both is occurring. The equilibrium and mass transfer curves were developed for the 20/30 (0.68) sand and 100% hydrophobic sand experiments. Figure 20 shows an example of a sketch superimposed over a 0.5 cm grid. The equilibrium curves were determined by assuming equilibrium dissolution has been reached after each loading event. The equilibrium curve was constructed by estimating the percentage of the flow field exposed to PCE after each loading event. This was done by adding the number of vertical grids containing PCE and dividing it by the total grid height. The mass transfer rate curves were developed by calculating the modified Sherwood number used by Powers et al. (1992). The Modified Sherwood number was then used to estimate the mass transfer rate and finally the C/C_s as a function of length of the PCE per each grid height.
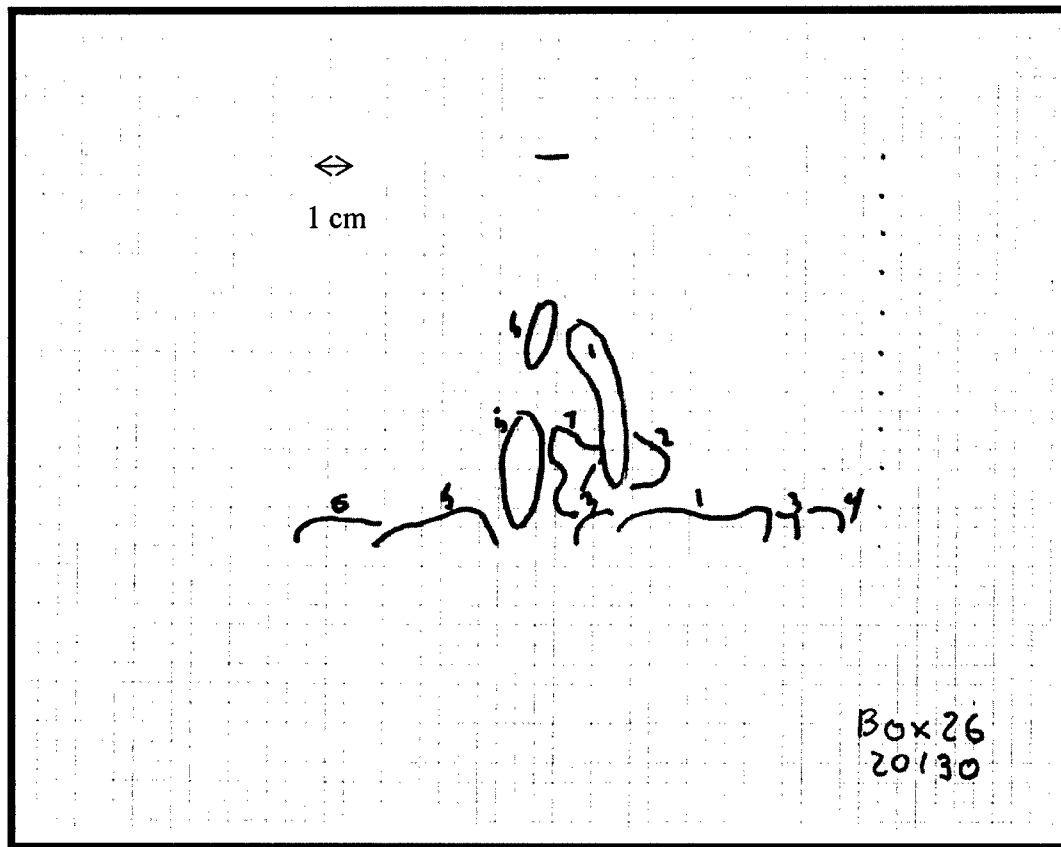
Figure 3.20. Example sketch superimposed over 0.5 cm grid

Figures 3.21 and 3.22 display the resultant equilibrium and mass transfer rate estimated curves in relation to the experimental data generated curves. Figure 3.21 displays the results for the 20/30 (0.68) sand and indicates that based on the length of the source zone after each loading event, that equilibrium may not have been achieved. Additionally, the experimental data curve is lower than the mass transfer rate generated curve. This indicates that both flow by-passing and mass transfer rate limitation may be occurring. Figure 3.22 shows the results for the 100% hydrophobic sand (30/40) and it indicates that the source zone is sufficient in length throughout the loading event that equilibrium is achieved. Additionally, the experimental data compares relatively well to the equilibrium and mass transfer rate curves, however still indicating some potential by-passing. The hydrophobic data compares more favorably than the 20/30 sand because it

achieves equilibrium and possibly has less by-passing because of the uniform distribution

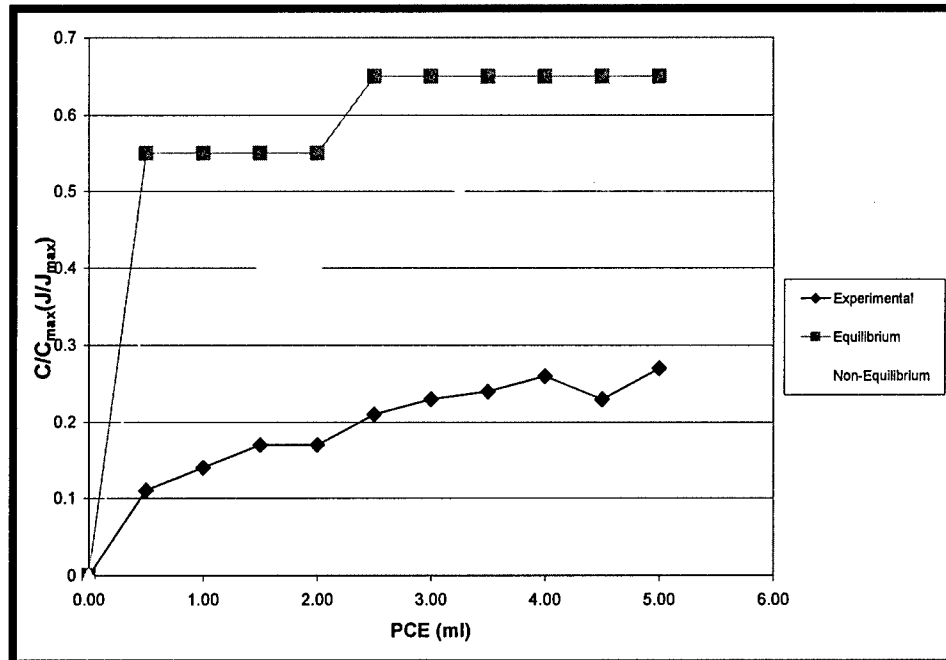of the PCE resulting from capillary wicking in the hydrophobic media.
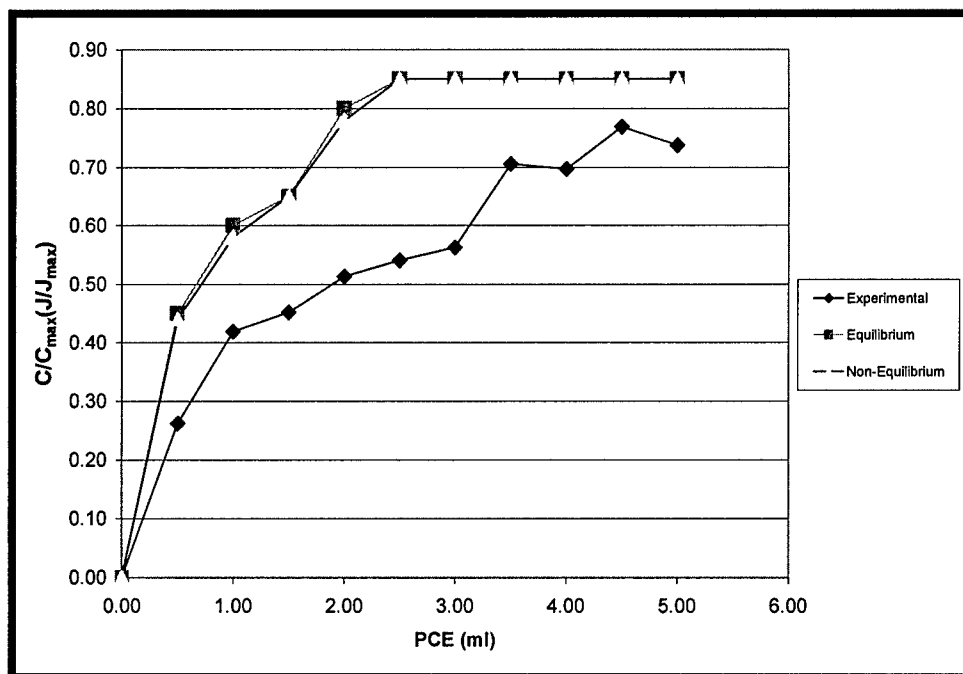

Figure 3.21. 20/30 curve comparison

Figure 3.22. Hydrophobic sand curve comparisons.

Conclusions

Grain size did not appear to affect the geometry of the residual and pooled PCE in such a way that was predictable. The grain size appears to affect the percent flux, with the flux increasing as the grain size decreases. It appears the determining factor for mass flux values was the cross sectional exposure of the PCE to perpendicular aqueous flow. The residual PCE portion was found to contribute the largest portion of mass flux relative to the pooled section, although the pooled section appears to be where the majority of the PCE collected. Assuming local equilibrium assumption, pores with PCE present may likely reach the solubility limit of the PCE, regardless of saturation percentage. Based on this assumption, each experiment should produce similar flux values because the vertical exposure of the PCE to the aqueous flow for each experiment was the same, however, the lateral distribution is not the same due to spreading. As the grain size decreases, more lateral spreading of PCE occurs, increasing flux. The pooled experiment supports the hypothesis that the residual mass produces the largest percentage of flux relative to the pooled source flux. The pooled source flux produce 0.05% of C/C_{max} with the combined residual and pooled sources producing a range from 0.27 to 0.38 C/C_{max}. In general, remediating the residual may remove relatively small amounts of PCE compared to the possible total mass, but could provide the greatest reduction in flux values. However, pooled flux values are still greater than clean-up requirements and will be a persistent flux source.

The mass loading/mass flux efficiency or β values are somewhat correlated to grain size. The wettability experiments showed that nearly all ($\geq$90 %) of the media must be OTS treated top affect residual geometry and percent mass flux values. As the media

approached 100% hydrophobicity, the capillary forces were able to overcome gravitational forces and spread the PCE above the point of injection. Although lower hydrophobic mixture percentages may not produce increased mass flux values, because of capillary forces retaining the PCE, removal of PCE from the pore may be difficult because of its affinity for the media surface.

The mass loading/mass flux efficiency (β) only became affected after a significant portion of the sand was treated (>90%). Otherwise, there is consistency in β values for the remaining sands.

Flow by-passing and mass transfer rate limitation may be occurring resulting in lower than expected experimental values. Qualitatively, most of the source zones produced are of sufficient length to achieve equilibrium indicating that by-passing is the most likely cause of lower than expected values.

CHAPTER 4
INVESTIGATION OF THE RELATIONSHIP BETWEEN FLUID PROPERTIES (INTERFACIAL TENSION AND DENSITY DIFFERENTIAL) AND MASS FLUX

Introduction

Chlorinated solvents such as perchloroethylene (PCE) are commonly found at many contaminated sites. They have been popular as industrial degreasers and because of past poor management practices and the threat they pose to human health, they have become a major concern at many contaminated sites throughout the country. It is likely that many chlorinated solvents have been used with a variety of different chemicals during various industrial processes and activities. The chemicals comprising these mixtures could interact creating a single "new" mixture, causing them to behave in the sub surface in very different ways than as single separate components. Depending on the mole fractions of each component, miscibility, and a variety of other conditions, surface and bulk properties for the "new" mixture can be vastly different from its individual separate predecessors (Brusseau, 1993; Seo and McCray, 2002). Surface activity such as interfacial tension and bulk properties such as density differential between aqueous and non-aqueous phases can be affected (Brusseau, 1993; Seo and McCray, 2002).

Theoretical Background

Entrapment and Migration

The common fluid to fluid properties represented in both the entrapment and migration processes are density differential and interfacial tension between aqueous and non-aqueous phases. As previously discussed in Chapter 1, contaminant flux is a

function of surface contact area between aqueous and non-aqueous phases and contact

area is a function of geometry and orientation to flow of the contaminant source zone.

Entrapment and migration were the two processes discussed that influence source zone

geometric and orientation development. DNAPL vertical and horizontal migration

processes are governed by the following equations:

$$Ho = \frac{2\sigma Cos\theta(1/r_t - 1/r_p)}{g(\rho_w - \rho_o)} \tag{4-1}$$

$$\frac{dP}{dx} = \frac{2\sigma}{L_o(1/r_t - 1/r_p)} \tag{4-2}$$

where H_o is the critical height or head required to displace water in a pore, γ is the

interfacial tension between liquids, θ is wetting angle, r_t pore is throat radius, r_p is pore

radius, g is acceleration due to gravity, L_o is the length of the continuous DNAPL phase

in the direction of flow, r_w is water density and r_o is DNAPL density. Additionally, using

the force balance equation from Chapter 3, it can be seen that changes in density

differential affect the gravitational pressure, and changes in the interfacial tension can

affect the capillary pressure of the system. These parameters also affect the entrapment

process which is described using the Capillary and Bond numbers discussed in Chapter

one.

Interfacial Tension

Interfacial tension (IFT) results from the co-existence of immiscible liquids at

different pressures and is measured by the force that exists in the interface separating the

two fluids (Pankow and Cherry, 1996). The interfacial tension between water and

another chemical only exist when the fluids are immiscible. In particular, the surface

tension of chlorinated solvent DNAPLs with respect to water has a significant impact on

how chlorinated solvents penetrate the capillary fringe and migrate through the saturated

zone. As the chlorinated solvent migrates through the capillary fringe, it is held up by the capillary retention of water until enough head is built up to overcome retention. The capillary retention is directly proportional to the interfacial tension and inversely proportional to radius of curvature (Lowe et al., 1999). As interfacial tension increases and pore size and density decreases, more head is required to produce downward migration. This may result in a lateral movement of liquid along layers of finer grain sands. Interfacial tension properties of DNAPLs are important when considering remediation techniques.

Surfactants alter interfacial tension between immiscible fluids by altering fluid interfaces. They accomplish this through the nature of their amphiphilic structure. Surfactants are typically molecules with a hydrophilic group or head at one end attached to a long hydrophobic hydrocarbon chain or tail. The hydrophilic head will have an affinity for water while the hydrophobic tail will have an affinity for non-aqueous contaminants or oils. Surfactants are classified by the nature of their hydrophilic groups, which are anionic, cationic, and non-ionic. Anionic surfactants give rise to a negatively charged surfactant ion and a positively charged counter-ion upon dissolution in water. They are sensitive to the presence of salts in solution. Cationic surfactants yield a positively charged surfactant ion and a negatively charged counter-ion upon dissolution in water. Cationic surfactants are not widely used because of their potential toxicity (Lowe et al., 1999). Nonionic surfactants do not ionize in water and are insensitive to the presence of salts in solution.

The amphiphilic structure allows the surfactant to accumulate at the NAPL-water interface. The hydrophilic group resides in the aqueous phase with the hydrophobic tail

residing in the NAPL. Depending on the concentration of surfactant at the interface, NAPL solubility and/or interfacial tension will be modified.

The manner in which the surfactant distributes in a surfactant-water-NAPL system is categorized by three systems. Winsor Type I, II, and III. The Winsor Type I system has micelles of oil droplets in the aqueous phase. Winsor Type II creates "reverse micelles" with droplets of water in the oil phase. Winsor Type III is a middle phase micro-emulsion with ultra-low interfacial tensions.

Density

Density plays an important role in DNAPL migration. It is the property which defines a liquid as being dense or light relative to water. If a liquid is determined to be dense, it has a specific gravity greater than one and if it is light, its specific gravity is less than one. In many situations, NAPL density varies from water by 10-50%, with only a 1% difference being needed to influence fluid movement (Mercer and Cohen, 1990). Because of the density differential, DNAPLs may move down a physical gradient counter to the hydraulic gradient; however, this can be impeded by capillary and/or impermeability resistance. DNAPL spreading will occur along pathways of least capillary and permeability resistance (Mercer and Cohen, 1990). This must be considered when determining the location of DNAPLs in groundwater, because the liquid may not simply sink to the lowest point in an aquifer. Additionally, the unique spreading of DNAPLs must be considered when conducting co-solvent or surfactant assisted remediation.

<div align="center">

Study Objectives

</div>

The objectives of this study was to conduct two dimensional chamber studies designed to investigate fluid, fluid property effects on contaminant geometry and

orientation and ultimately contaminant mass flux and system efficiency as discussed in chapter 3. The first objective was to vary density differential and generate mass loading versus mass flux curves. The second objective was to change the interfacial tension between the fluids and generate mass loading versus mass flux curves. Maximum contaminant mass flux values and system efficiency (β) values were investigated.

Materials and Methods

General Experimental

A two dimensional chamber as described in chapter one was used for each experiment. The hydrophilic packing procedures and hydrological controls described in chapter three were followed. The PCE material and injection methods described in chapter 3 were used. A total of nine experiments using 30/40 and 40/50 sieve sand were completed.

Density Modification

An experiment for each density and sieve size combination listed in Table 4.1 was completed.

Table 4.1. Density sieve size experiments

PCE Density (g/ml)	1.0	1.1	1.4	1.6
30/40 Sieve	x	x	x	x
40/50 Sieve		x		x

To achieve the densities listed in Table 4.1, the appropriate mole fractions of PCE and decane were mixed together (Table 4.2). Decane was selected because of its density (0.73 g/ml), and its low solubility in water to ensure limited partitioning from the non-aqueous to the aqueous phase.

Table 4.2. Decane/PCE densities and respective mole and volume fractions

ρ	volume fraction		mole fraction	
	PCE	Decane	PCE	Decane
1	0.3	0.7	0.45	0.55
1.1	0.41	0.59	0.57	0.43
1.4	0.75	0.25	0.85	0.15
1.65	1	0	1	0

Additionally is has similar interfacial tension properties (52 dynes/cm) compared to PCE in relation to water. The IFT of 50/50 mole fraction of PCE and Decane mixture was measured using a tensiometer to determined if the resultant mixture had an IFT value in between the IFT values for pure PCE and Decane. The IFT for decane and water was measured to be 43 dynes/cm, PCE and water was 37 dynes/cm, and the mixture resulted in an IFT of 39 dynes/cm. This supports that Seo and McCray (2002) determined there is a linear relationship between multi-component mole fractions and IFT properties of the mixture.

Interfacial Tension Modification

Interfacial tension between PCE and water was modified by adding 0.0025%, 0.005%, 0.01%, 0.025%, 0.05% and 0.1% by volume Span 80 to PCE. Span 80 (sorbitan monooleate) was selected because of its low hydrophile/lipophile balance (HLB) value of 4.3. A low HLB surfactant was required to limit partitioning of the surfactant into the aqueous phase. The relationship between % surfactant added and interfacial tension between PCE and water is shown in Figures 4.1. The relation ship between C_{max} and percent surfactant is shown in Figure 4.2.
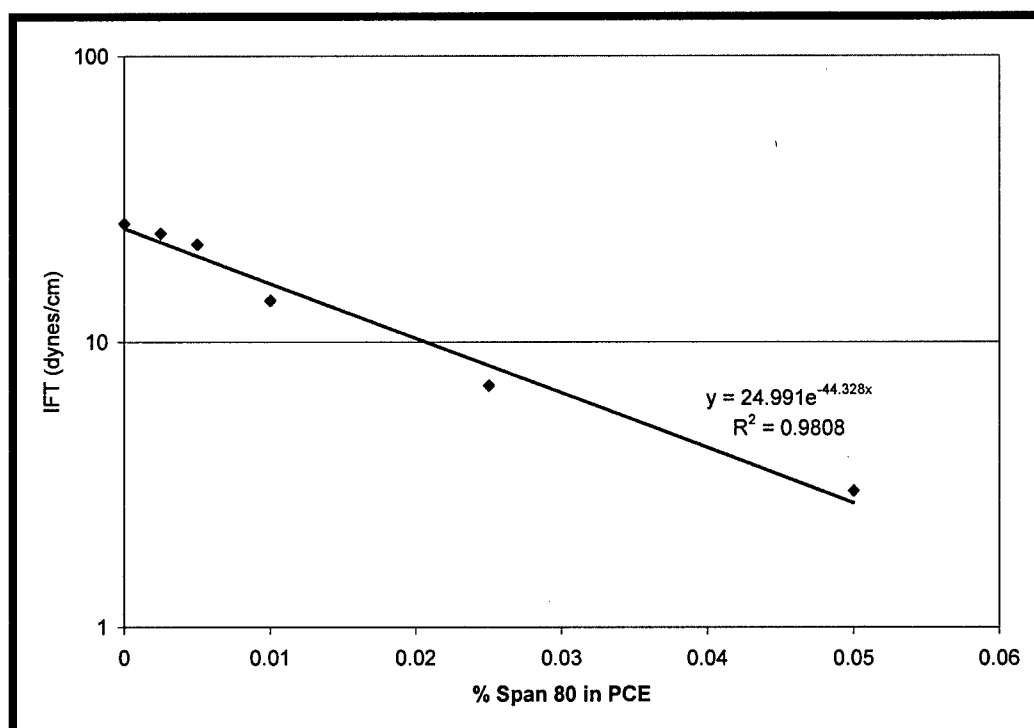
Figure 4.1. Span 80 percentage and resultant interfacial tension Semi-Log

The equation in Figure 4.1 reads:
$$y = 24.991e^{-44.328x}$$
$$R^2 = 0.9808$$
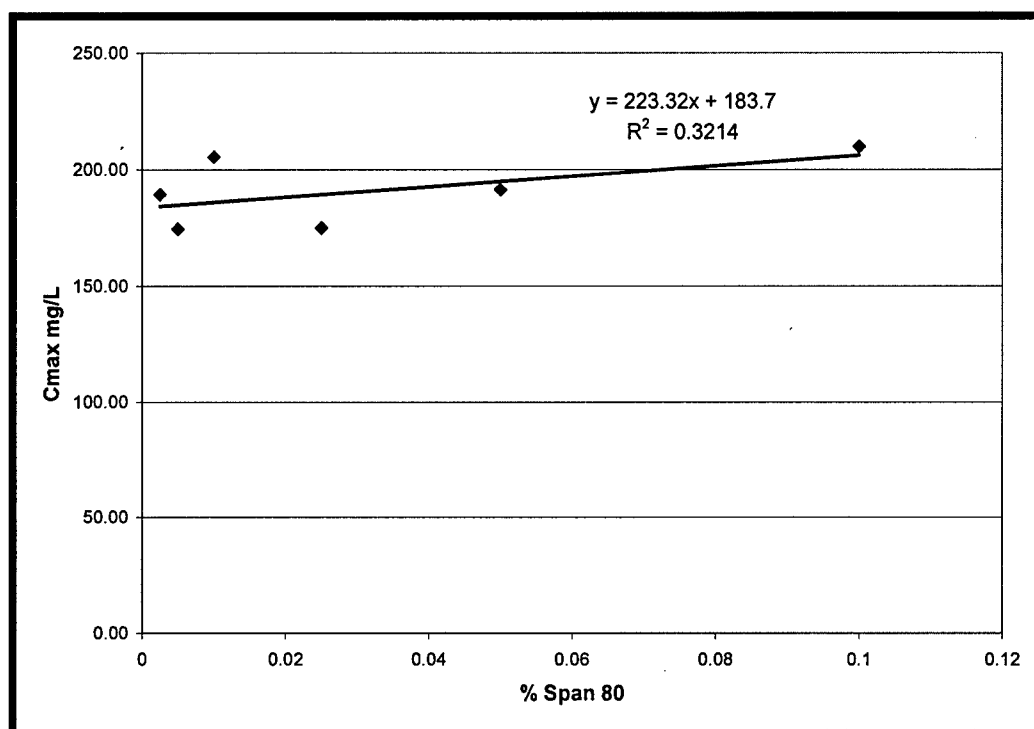
Figure 4.2. Maximum PCE concentration as function of percent surfactant (Span 80)

The equation in Figure 4.2 reads:
$$y = 223.32x + 183.7$$
$$R^2 = 0.3214$$

An experiment for each interfacial tension value listed in Table 4.3 was completed. The low IFT of 3 dynes/cm was selected because at greater Span 80 percentages cloudiness occurred.

Table 4.3. Interfacial values tested and respective Span 80 percentage

Interfacial Tension (dynes/cm)	3* 0.05% Span 80 *not shown on graph - estimated based on curve fit equation shown in Figs 4.1 and 4.2	13 0.025% Span 80	47 0% Span 80

Results and Discussion

IFT Modification Results and Discussion

For each experiment (interfacial tension) a trace sketch of the PCE distribution was generated. A trace of the distribution was drawn after each injection reached steady state on a single transparency, resulting in a cumulative distribution drawing (Appendix C).

A qualitative comparison using sketches in Appendix C was made between each interfacial tension experiment shows a difference in migration characteristics as IFT decreases. As the IFT decreased, the residual geometry became more spread out. Figures 4.3 and 4.4 are an example in how the distribution behavior of PCE changes as the IFT is lowered. This may be from the lower IFT influencing the migration of the PCE in a horizontal direction in addition to vertical movement. Pooling for each began by the second injection, so the vertical migration was not affected by lowering the IFT, indicating that density differential controlled vertical migration.
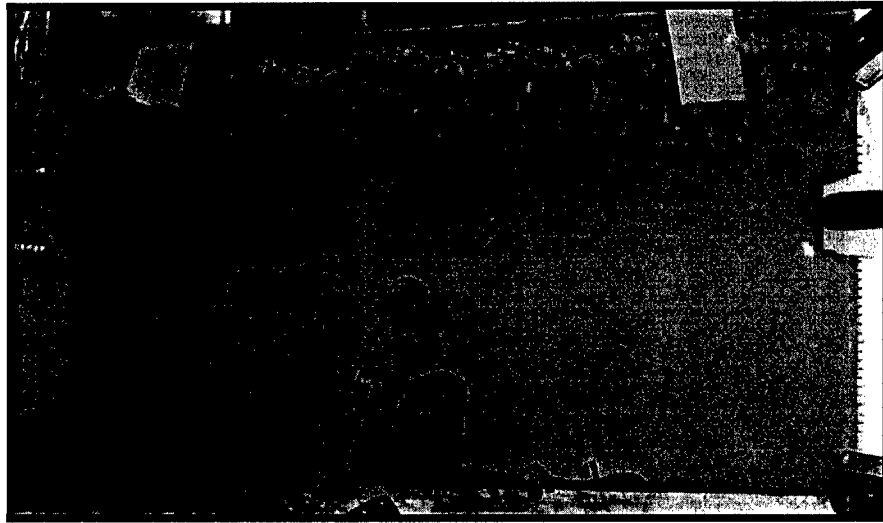
Figure 4.3. 3 dynes/cm interfacial tension distribution
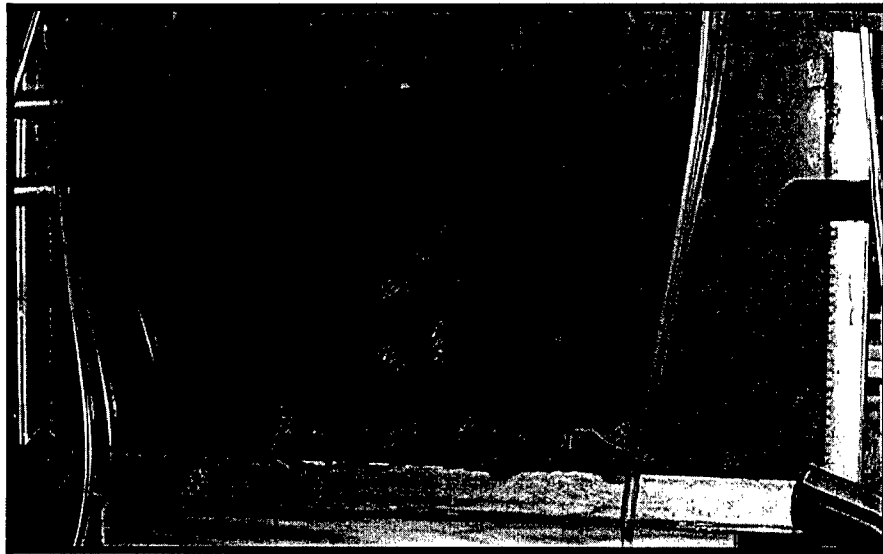
Figure 4.4. 47 dynes/cm interfacial tension distribution

Figure 4.5 displays similar results between each IFT experiment. As the IFT decreased, the relative C/C_{max} values appear to increase slightly. This may be due to more uniform migration occurring in the thickness of the chamber as the PCE migrates vertically. The maximum values appear to be bounded by injection point location.
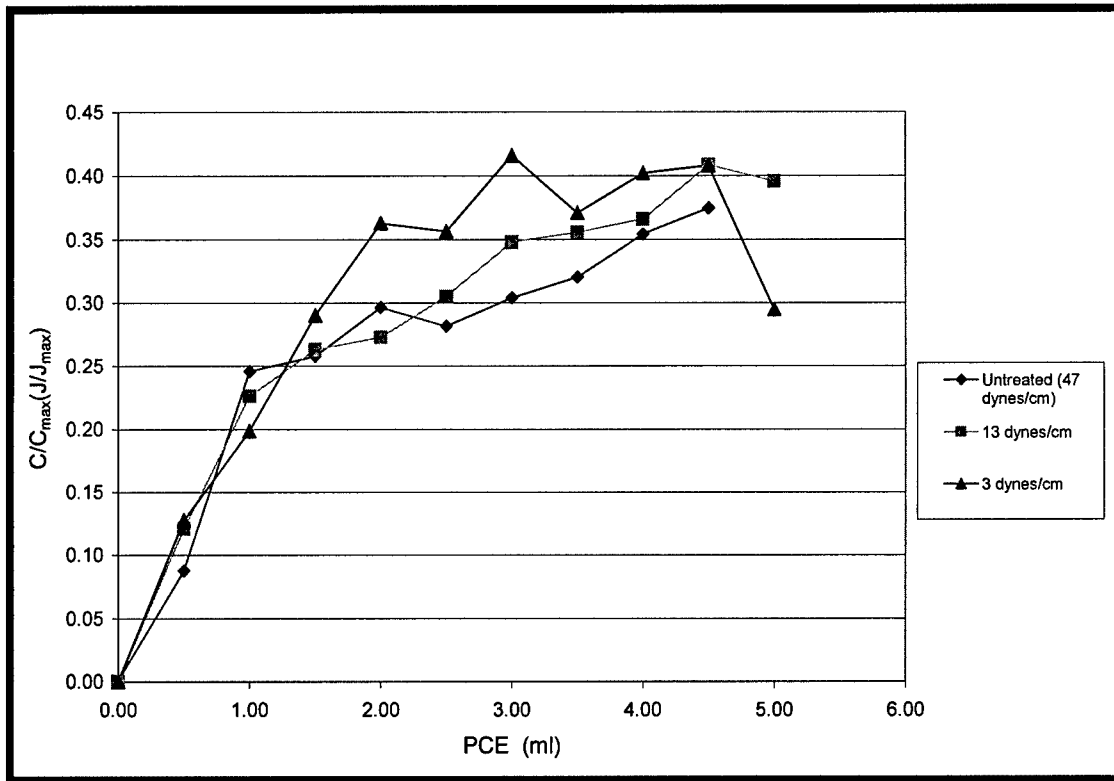
Figure 4.5. Interfacial tension comparisons

Figure 4.6 displays the relative curve fits for each IFT with the associated data.

They are essentially the same, indicating regardless of IFT, vertical migration

characteristics appear to be the same for each. Ultra low IFTs may be required to affect

migration or prevent entrapment. Table 4.4 tabulates the bond, capillary and total

trapping number for each IFT. These values indicate that entrapment will still occur,

because Pennell et al. (1996) reports mobilization when $N_T = $ 1E-3. However, to achieve

these ultra low IFTs, solubility would increase dramatically (Pennell et al., 1996).

Table 4.4. Calculated bond, capillary and total trapping number for each IFT

IFT (dynes/cm)	N_{Bo}	N_{Ca}	N_T
47	9.8E-5	2.3E-6	9.8E-5
13	2.3E-5	5.4E-6	2.3E-5
3	6.2E-5	4.9E-6	6.2E-5
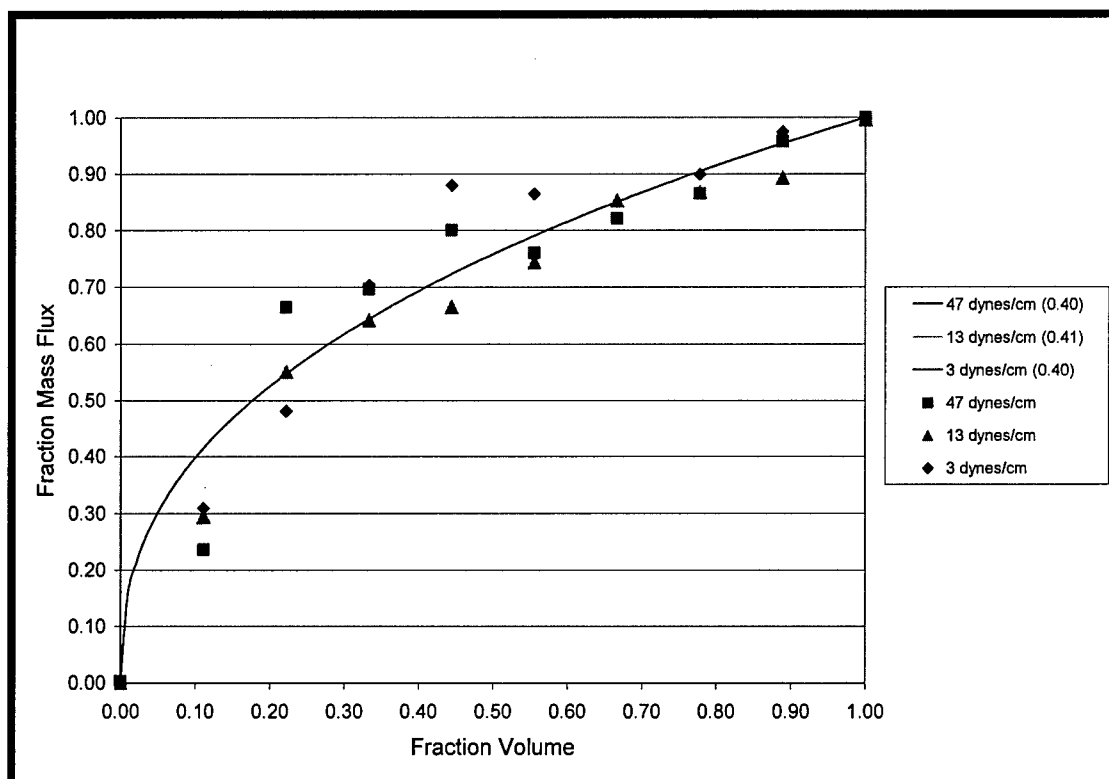
Figure 4.6. Interfacial tension curve fit

Density Modification Results and Discussion

For each density experiment a trace sketch of the PCE distribution was generated. A trace of the distribution was drawn after each injection reached steady state on a single transparency, resulting in a cumulative distribution drawing (Appendix C).

A qualitative comparison between density experiments reveals interesting results using the drawings in Appendix C. As the density decreased, vertical and lateral migration characteristics changed. Figures 4.7 and 4.8 provide a qualitative comparison between distributions of PCE and PCE treated to achieve 1.1 mg/l (ρ).
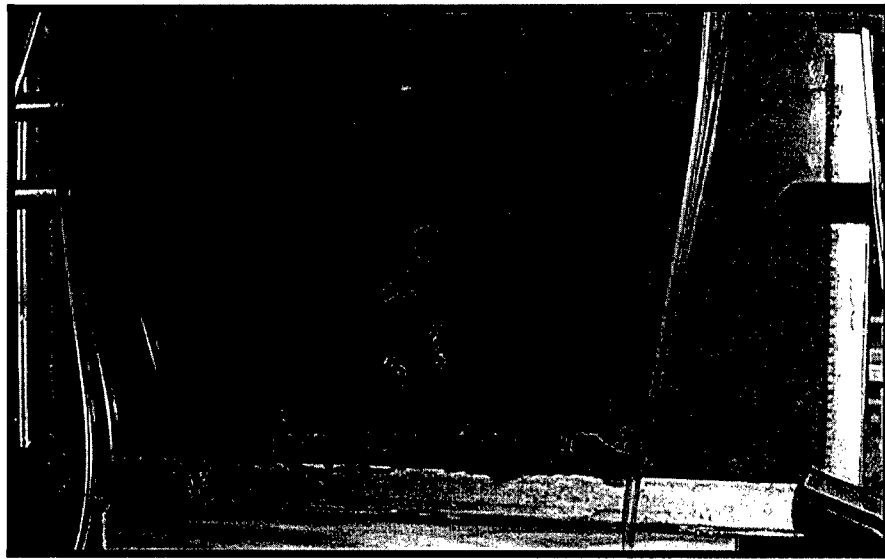
Figure 4.7 Untreated PCE distribution

Figure 4.8. 1.1 density distribution

The comparison shows how differently PCE migrates and distributes as ρ is decreased. Vertical migration was slower from injection to injection in the lower density experiments when compared to the untreated PCE experiments. In the untreated experiments pooling usually began by the second injection (1.0 ml), indicating complete vertical migration from injection port to chamber bottom. The lower density experiments required as many as nine injections (4.5 ml) to cause full migration from injection port to

bottom and in the case of the 1.0 density PCE, no pooling occurred indicating no full downward migration. The C/C_{max} values were similar with the 1.1 ρ in the 30/40 sieve sand showing the largest value followed by the 1.0 density PCE in the 30/40 sand (Figure 4.9). These results are probably due to the PCE being able to migrate above and below the injection port, providing a larger cross sectional area exposure to flow compared to the untreated PCE experiments.

Figure 4.10 compares the fitted curves for each density experiment. The lower density experiments displayed a linear mass loading/mass flux relationship compared to the untreated experiments which were more non linear. These curves coupled with the traces indicating reduced vertical migration per each injection indicate the curves are a function of density differential. A faster downward migration results in higher flux values at low masses when compared to slower downward migration results. The 1.4 ρ and β values were expected to be in between the 1.0, 1.1 and 1.65 density β values. However, the 1.4 β value was closer to the lower density β values. This may be explained by Figure 4.11. The downward migration appeared to be delayed by possible layering. This caused the vertical migration to behave similarly to the migrations seen at the lower densities. This resulted in a more linear β value.
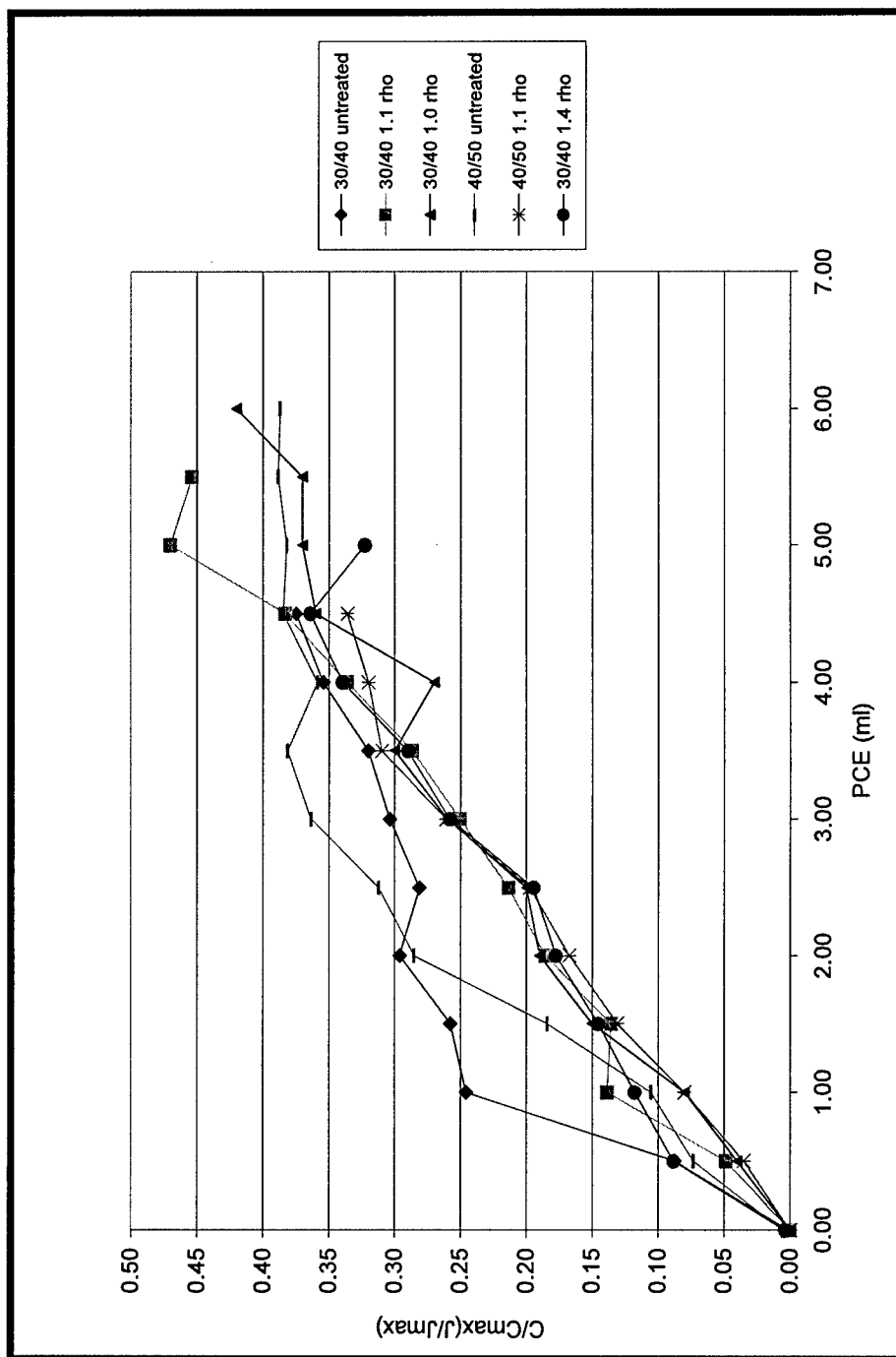
Figure 4.9 Density comparisons
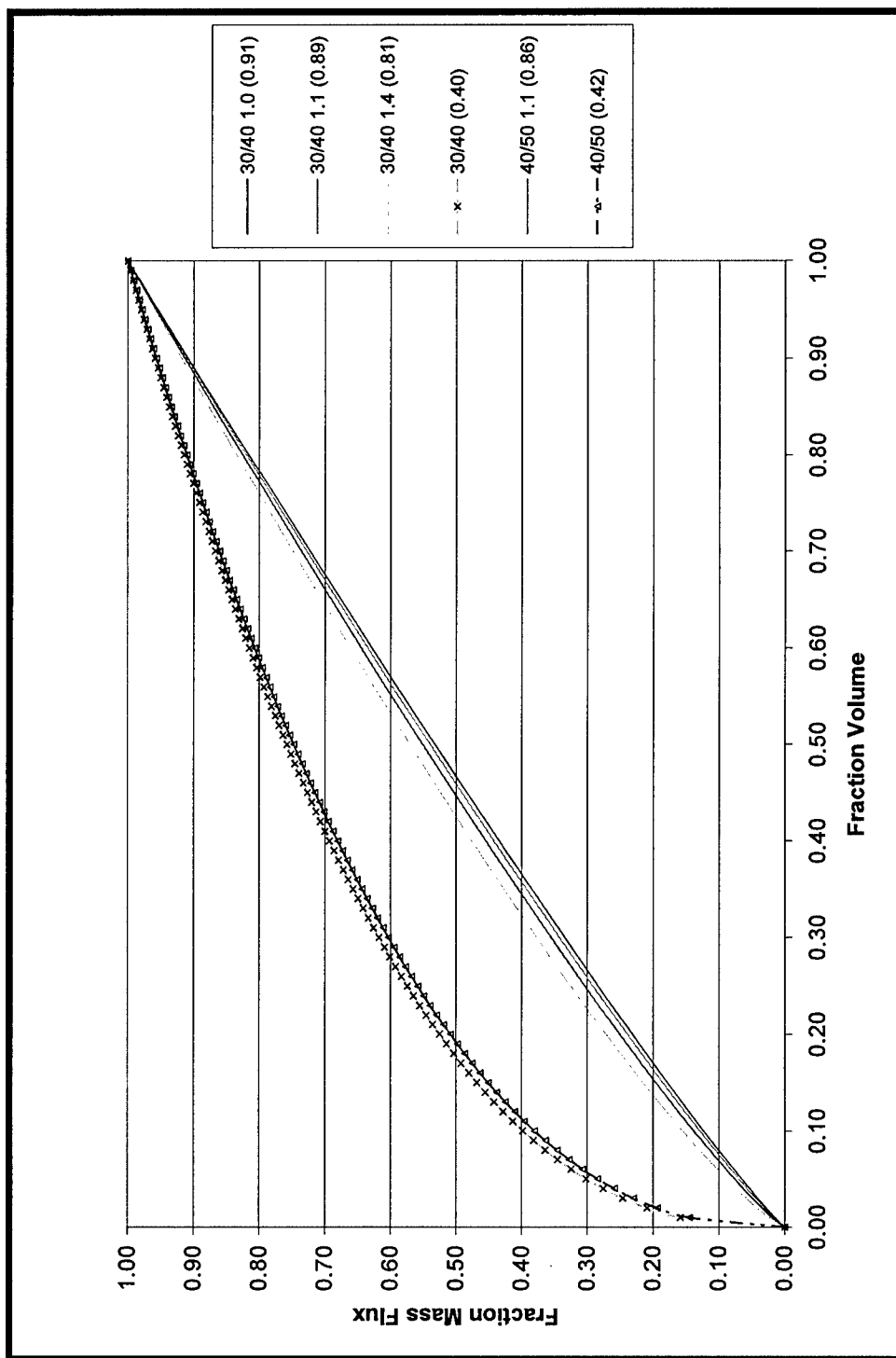
Figure 4.10. Density curve fit
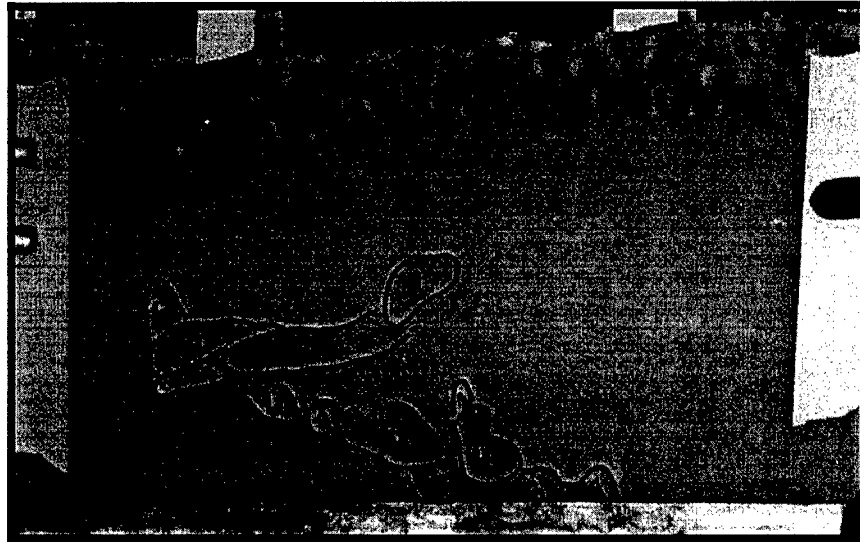
Figure 4.11. 1.4 density distribution
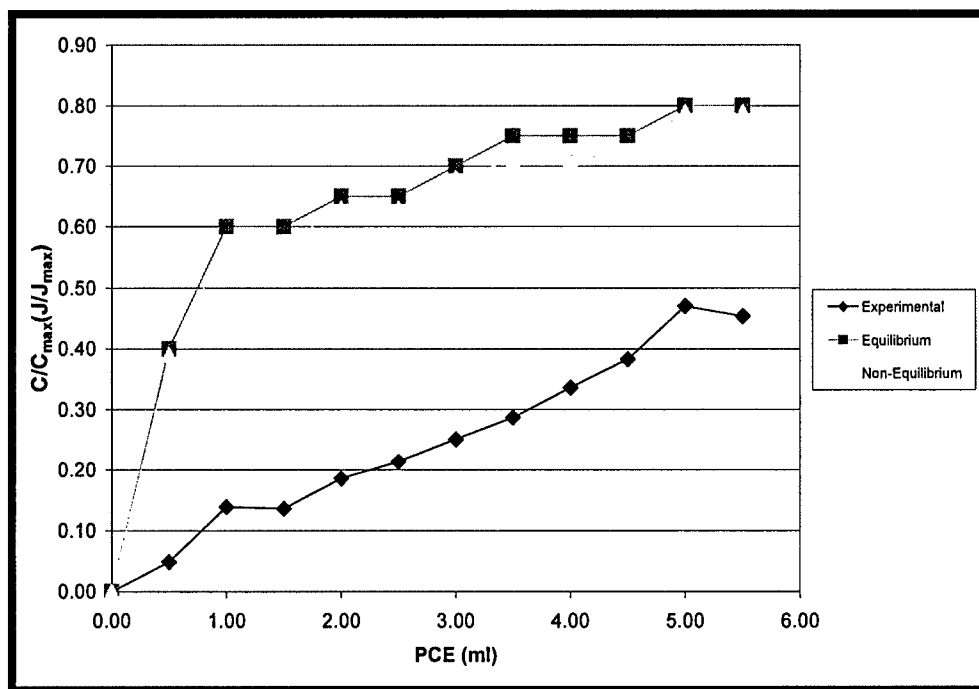
Figure 4.12. Curve comparisons for 1.1 density PCE in 30/40 sand
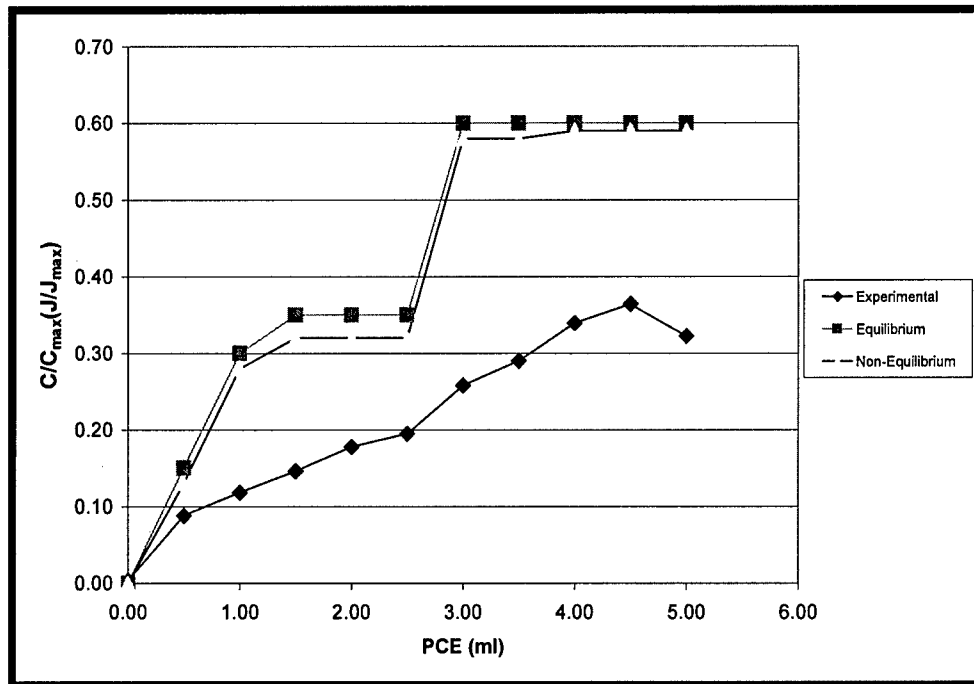
Figure 4.13. Curve comparisons for 1.4 density PCE in 30/40 sand

Flow By-Passing and Mass Transfer Rate Limitation

Figures 4.12 and 4.13 shows a comparison of mass flux versus mass loading curves based on equilibrium, mass transfer rate, and experimental data.

For both the 1.1 and 1.4 density source zones, sufficient contact length is produced during the loading process, indicating that equilibrium is achieved. The lower flux values shown from the experimental data indicate that flow by-passing is likely occurring and accounts for most of the reduction from expected equilibrium values. This is due to the PCE not being homogeneously distributed across the width of the domain.

For both the 1.1 and 1.4 density source zones, sufficient contact length is produced during the loading process, indicating that equilibrium is achieved. The lower flux values shown from the experimental data indicate that flow by-passing is likely occurring and accounts for most of the reduction from expected equilibrium values. This is due to the PCE not being homogeneously distributed across the width of the domain.

Conclusions

Changes in density appear to slightly affect both the C/C_{max} and β values. Decreasing density slows vertical migration and delayed pooling leading to less efficient, more linear mass loading /mass flux behavior and higher β values when compared to untreated PCE values. As the density differential decreased, the residual geometry became more uniformly spread out. As density differential decreased, residual geometry more uniformly spread.

The interfacial tension for the range considered did not affect flux values. It appears that interfacial tension must be ultra-low in order for the PCE not to become entrapped (Pennell et al., 1996). The IFTs tested were not low enough to cause instantaneous mobilization of the PCE, therefore a residual zone was left after migration resulting in similar flux values compared to the untreated system.

Finally, flow by-passing is occurring and producing lower than expected flux values when compared to equilibrium conditions.

CHAPTER 5
INVESTIGATION OF CONTAMINANT MASS FLUX HYSTERESIS

Introduction

Currently, there is little research investigating the life cycle of a contaminant spill and the manner in which contaminant flux values vary through mass increase and eventual mass reduction and dissolution. Most source zone contaminant research has focused on mass fraction or volume fraction removal of contaminant (Rao et al. 1997, Jawitz et al. 1998b, Martel et al. 1998, McCray and Brusseau 1998, Lowe et al. 1999, Fiorenza 2000, Jawitz et al. 2000, Meinardus et al. 2002). In particular, field investigations are typically limited to this focus because of their retrospective nature. Other research has gone further to investigate theoretical models by evaluating the relationship between mass reduction and contaminant flux reduction (Berglund, 1997; Rao and Jawitz, 2003; Sale and McWhorter 2001). The focus of this research topic is retrospective since it focuses on source zone and flux characteristics after the contaminant has been introduced into a particular setting. The mass loading process and its contaminant flux behavior in relation to the mass reduction and dissolution process has not been considered. Flux behavior as a function of loading is a more convenient method for associating flux values to known contaminant mass values. If a relationship between flux loading curves and flux reduction curves can be made, flux loading curves may be a more convenient predictor of flux reduction behavior which pertains to mass reduction.

Theoretical Background

Typically, hysteresis in the context of hydrology is associated with soil-water retention curves and the relationship between drying and wetting curves. When the drying curve and the wetting curve are not the same, there exists hysteresis (Fetter, 1999). This concept may be applied to contaminant mass-contaminant flux curves associated with Dense Non-Aqueous Phase Liquids (DNAPL).

When a spill occurs into the subsurface, it may happen as a chronic event as opposed to one catastrophic, acute event. The chronic spill may occur as a continuous event or a series of spills from the same source into the same location such as an aquifer. Considering the series of spills scenario, after each spill, mass would be added to the source zone. Each addition of contaminant mass contributes to the development and geometry of the source zone. The source zone is divided into the residual mass which is suspended in the porous media and the pooled mass which collects on top of a lower permeability layers. As contaminant mass is added, the residual geometry is developed and eventually a pooled portion begins to develop. During this loading process, there is an associated mass flux with each contaminant mass amount added. Local equilibrium is assumed as well as a contaminant that has a suitably low solubility to allow a steady state flux condition to be reached in between contaminant mass additions. After the loading process is complete, eventually the source zone mass would begin to decrease through dissolution. The residual mass would be removed first with the pool source persisting longer. During the dissolution removal process, there will be an associated mass flux with each remaining contaminant mass.

The mass loading/flux increase curve can relate to the mass reduction/flux reduction curve in two ways; the process is reversible or it is hysteretic. The reversible

process is the dissolution flux curve and it follows the same curve established during the loading process. Figure 5.1 shows some examples of reversible curves. In the hysteretic process, the dissolution flux curve does not follow the same curve back to the origin as shown in Figure 5.2.
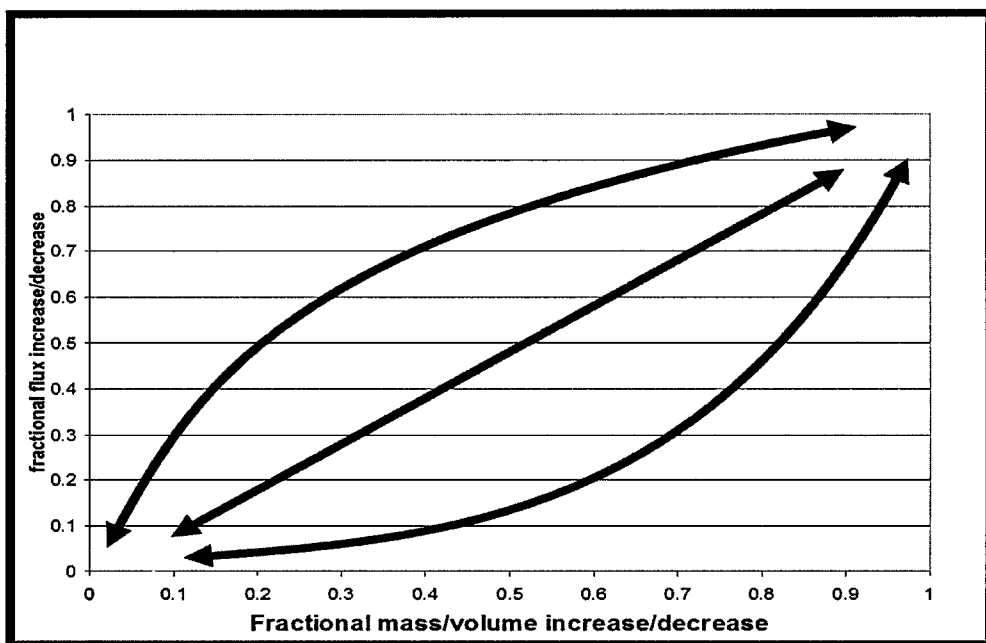
Figure 5.1. Reversible flux loading and dissolution processes
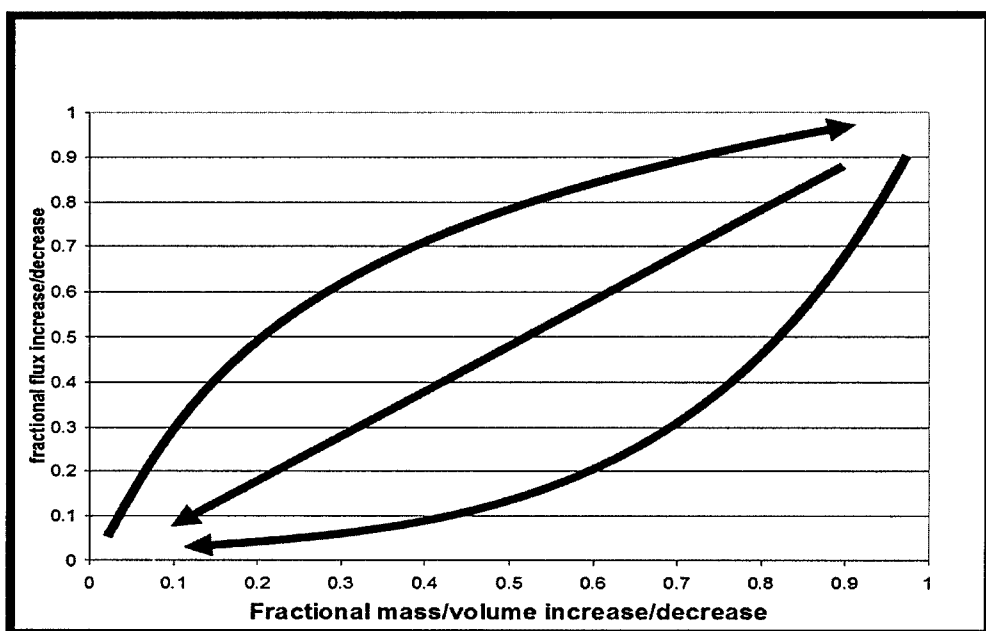
Figure 5.2. Hysteretic flux loading and dissolution processes

The physical events associated with the reversible process are those events which occurred last during the loading process and will occur first during the dissolution process. For example, as a spill occurs, the residual geometry is created and if a lower permeability layer exists below the spill source, pooling will occur on the layer. The associated flux behavior with this loading event would be a rapid establishment of flux followed by a plateau as pooling becomes more prevalent. An example of this is shown as the top curve in Figure 5.1. For the dissolution flux behavior to follow this curve in reverse, the pool would have to be removed first followed by the residual. If the residual were to be removed first, the process would than be hysteretic and the dissolution curve would be different than the loading curve (Figure 5.2). It is important to note that the physical conditions of the media such as heterogeneities and flow conditions will have an impact in mass loading/mass reduction relationship.

Study Objective

The objective of this study was to determine the relationship between DNAPL mass flux curves associated with contaminant mass loading and mass flux curves associated with contaminant mass removal. Flux loading curves were compared to flux removal curves to determine if the relationship was hysteretic.

Materials and Methods

A two dimensional chamber as described in chapter one was used for this experiment. The hydrophilic packing procedures using 30/40 sieve sand and hydrological controls described in chapter three were followed. Trichloroethylene (TCE) was the DNAPL used because of its moderate water solubility (1100 mg/L) and concern for its toxicity and ubiquity. This is low enough to allow steady state conditions to occur before significant mass has partitioned into the water, while still being high enough to

allow mass to dissolve in a timely fashion. The injection and sampling methods described in chapter three were used.

Results and Discussion

Two experiments were run to compare the mass loading flux curves to the mass dissolution flux curves. The results of the first experiment are shown in Figure 5.3. A total of 7000 mg of TCE was introduced in increments of 700 mg. Accounting for dissolution of the TCE during the loading process resulted in approximately 6000 mg of mass present at the point loading was discontinued and dissolution to construct the mass reduction curve began. There were approximately three pore volumes in between each injection and sampling event during mass loading and mass dissolution. This resulted in the curve shown in Figure 5.3. There appears to be a rapid decrease in flux within 10 pore volumes of PCE introduction discontinuation. As discussed in chapter 3, the residual source zone produces the largest percentage of dissolution flux when compared to the pooled source zone. The rapid decrease in flux observed indicates that the residual was removed rapidly with the pool remaining and being removed more slowly. This indicates that the mass that is loaded first is removed first or first in is first out. This produces a hysteretic process. A non-hysteretic process would have the pool removed first since it represents the mass last introduced.

The second experiment yielded similar results. During this experiment, 1400 mg of TCE was introduced during two injections of 700 mg each. Two separate injections were done to remain consistent with previously used loading procedures. Reduced mass introduction was done to facilitate timeliness of the experiment. Figure 5.4 displays the breakthrough curve and Figure 5.5 displays the mass reduction, flux reduction curve. Again, there appears to be a rapid decrease in flux within 10 pore volumes of PCE

introduction discontinuation, indicating the residual was removed first and while the pool

was removed more slowly, resulting in a hysteretic process.
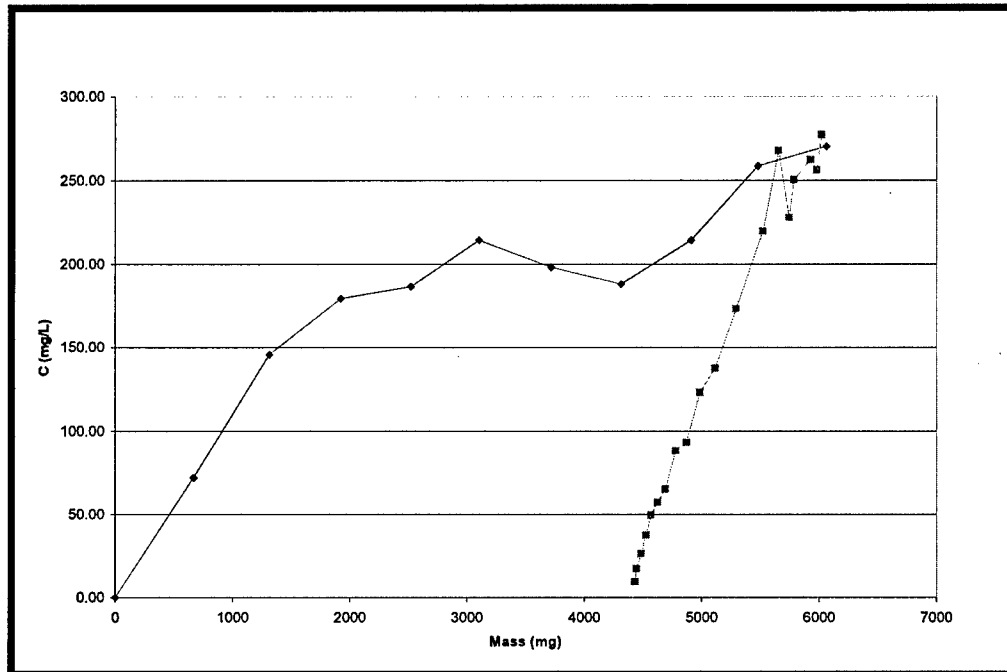
Figure 5.3. TCE mass increase/dissolution experiment one - Note the rapid flux
decrease following stoppage of mass introduction
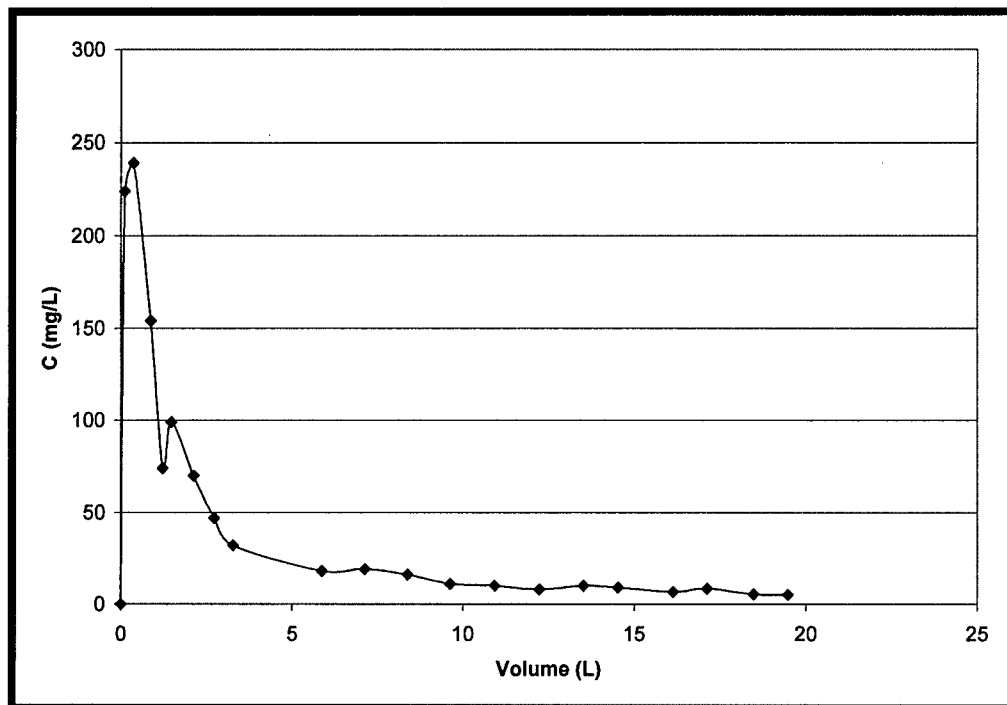
Figure 5.4. Breakthrough curve
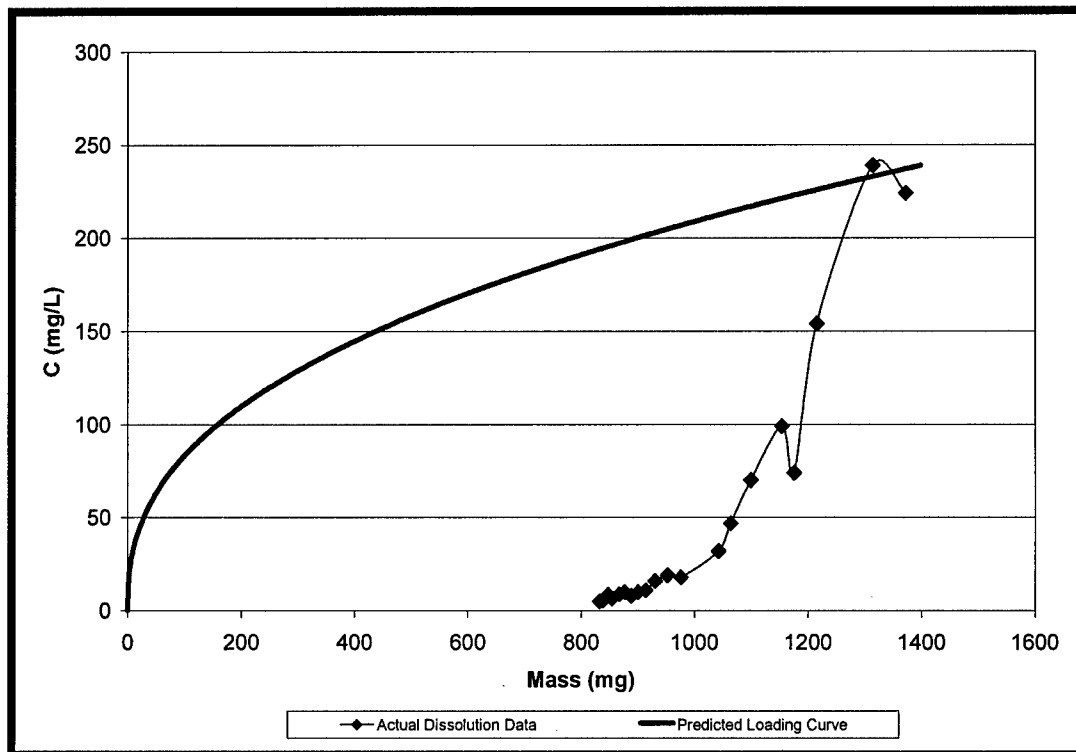
Figure 5.5. TCE mass increase/dissolution experiment two - note the rapid flux decrease following stoppage of mass introduction

Conclusions

When considering homogenous media systems where pooling of a DNAPL occurs, the relationship between the mass loading flux and the dissolution mass flux appears to be hysteretic. This indicates that during the loading process, the residual source zone is constructed followed by the pool source zone construction. However, during the dissolution process, the residual source zone appears to be removed more quickly than the pooled source zone resulting in a rapid reduction in flux. This results in a hysteretic process. This hysteretic relationship could potentially be used for predicting mass dissolution, mass removal behavior using mass loading, mass dissolution information. For a homogeneous media, it appears that the mass that is first introduced and is retained in the residual zone is the mass that is first removed from the system.

CHAPTER 6
SUMMARY, CONCLUSIONS AND RECOMMENDATIONS

Summary

The overall goal of this research was to study the effect of media and fluid

properties on DNAPL migration geometry and contaminant mass flux. The major

objectives were as follows: (1) Determine the relationship between hydrophobic media

content and water, air and oil entry pressure and related entry pressure values, (2)

Determine the relationship between contaminant mass flux and media properties, (3)

Determine the relationship between contaminant mass flux and fluid properties, (4)

Determine the mass loading and dissolution behavior of TCE. The findings from the

hydrophobic media study indicate that water and oil entry pressure measurements are

sensitive to media wettability and can be used as a relative indicator of system

wettability. Grain size and wettability properties of the media affected flux values and

mass loading, flux value relationships. In general, each media size produced a non-linear

relationship between mass loading and dissolution flux. As grain size decreased,

dissolution flux increased. Nearly oil wet media increased dissolution flux and produced

a more linear relationship between mass loading and dissolution flux relative to water wet

media. Density differential between the DNAPL and water had no apparent effect on

total flux values, however, a near linear relationship between mass loading and

dissolution flux was observed as density differential approached zero. Interfacial tension

had no apparent effect on flux values for the range of IFTs considered. The relationship

between flux produced during loading events is hysteretic when compared to the flux

94

reduction mass reduction relationship. Specific conclusions and recommendations are listed below.

Conclusions

The following conclusions are drawn as they relate to the research performed to meet this study's objectives:

- As oil wettability of the media decreases, water entry pressure decreases and oil entry pressure increases

- There is no apparent effect of oil wettability on air entry pressure due to air being the non-wetting fluid regardless of media type

- Grain size affects lateral PCE migration, thereby increasing contaminant flux as grain size decreases

- The residual source zone is the greatest contributor of contaminant flux compared to the pooled source zone

- Grain size has a 0.75 correlation to β values

- 90% + oil wet sand using octadecyltrichloro silane (OTS) coating was required to affect residual geometry and influence contaminant mass flux values

- 90% + oil wet sand allows capillary forces to overcome ρ differential and gravity effects

- A reduced $\Delta\rho$ linearized relationship between mass fraction loading and flux fraction increase, indicating delayed pooling

- Interfacial tension (IFT) had no effect on flux values and β values for the range of IFT values considered

- Flux values are lower than expected due to potential flow bypassing

- Sufficient contact length between source zone and aqueous phase is required to reach equilibrium

- In considering homogeneous systems where pooling of DNAPL occurs, the relationship between mass loading flux values and mass dissolution flux values is hysteretic

Recommendations

The following recommendations are made to further the extent of knowledge relating to this research:

- A larger range of grain sizes should be considered to further clarify grain size effects on mass flux and β values

- Silane coatings other than OTS should be studied to further investigate wettability effects on DNAPL migration geometry and contaminant mass flux values

- Ultra low IFT values should be considered to investigate DNAPL entrapment behavior and its effect on contaminant mass flux and β values

- Geometries such as pooled only, residual only, or various pooled and residual combinations in heterogeneous media should be investigated to determine if loading/dissolution behavior is reversible or hysteretic for other system configurations

- Combinations of variables should be considered i.e. low density differential and low interfacial tension, etc.

- Fluid viscosity modification should be considered

- Contaminant injection rate should be varied to observe impact on source zone geometry development

AIR, WATER, AND OIL ENTRY PRESSURE BREAKTHROUGH GRAPHS FOR
HYDROPHOBIC MIXTURES
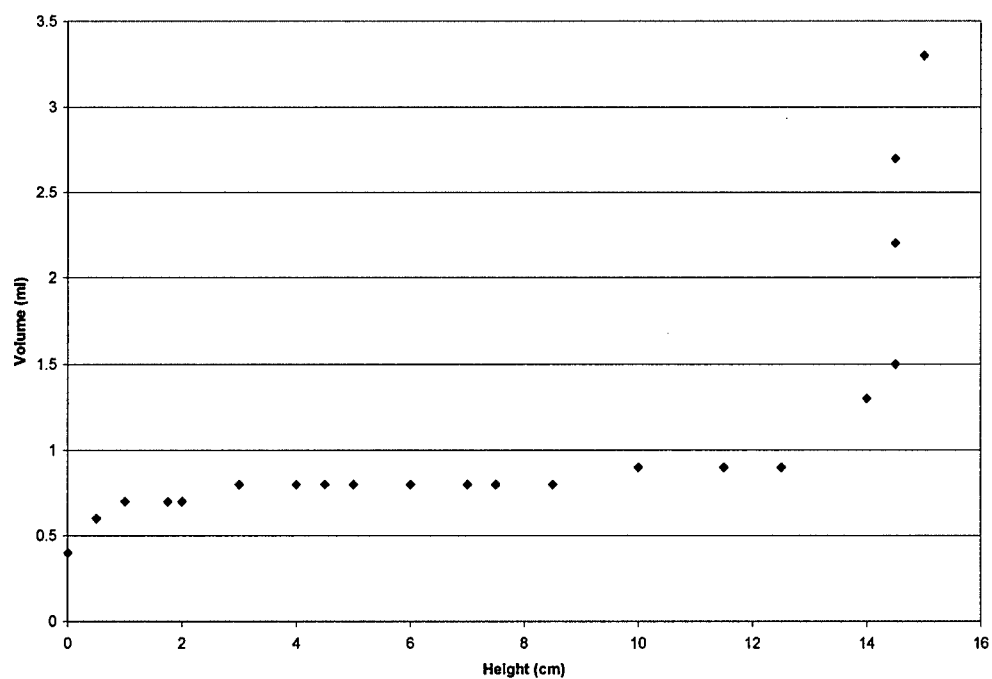
Figure A.1. Untreated sand air entry pressure (water saturated)
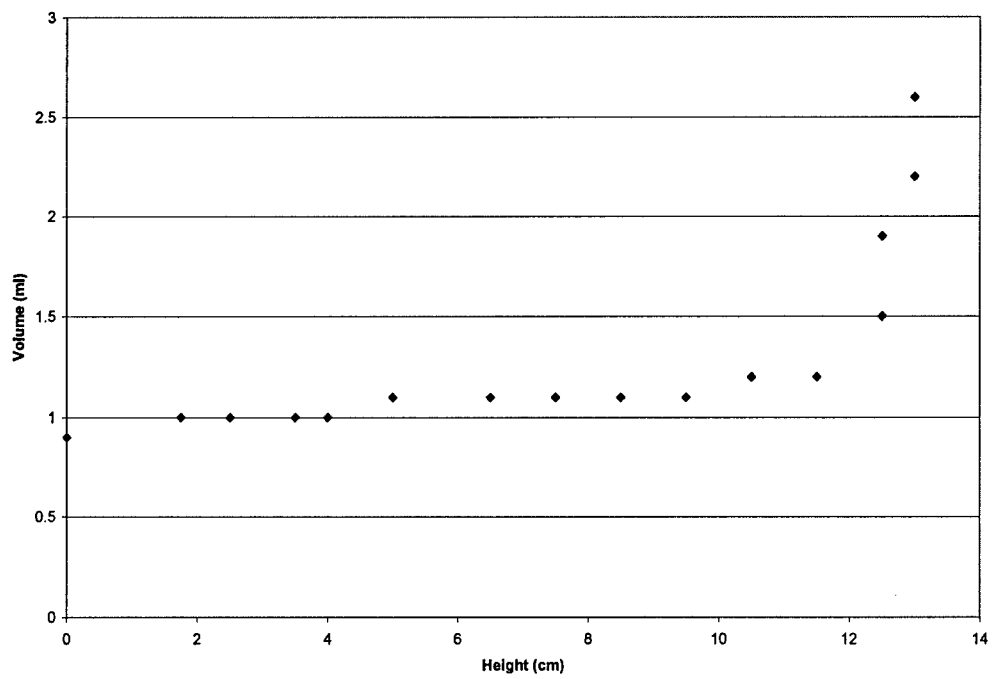
Figure A.2. 25% Octadecyltrichlorosilane (OTS) treated air entry pressure (water saturated)
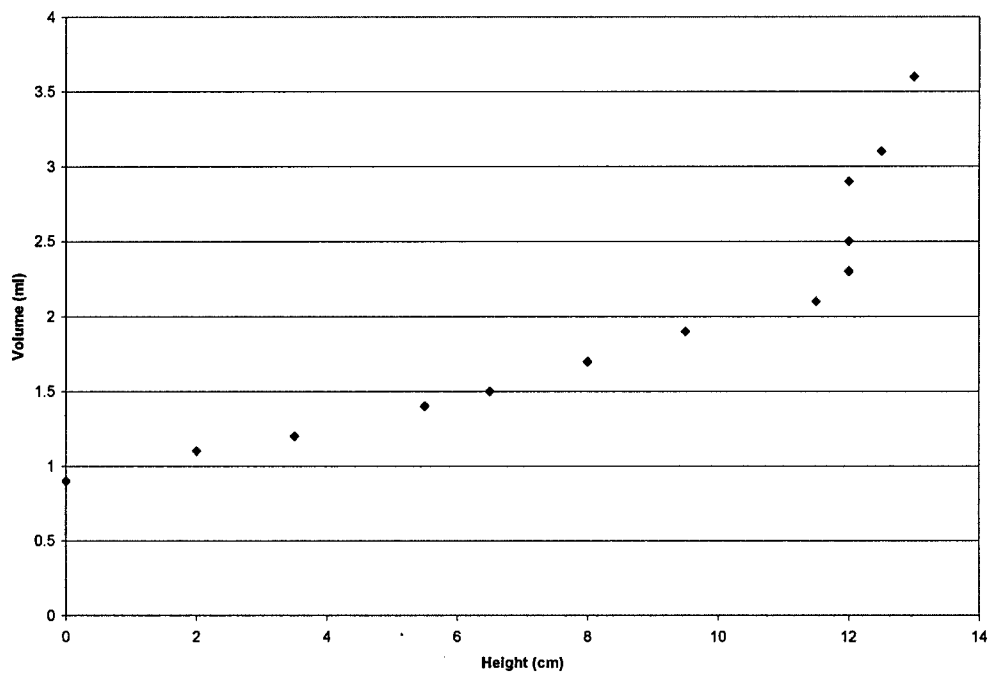
Figure A.3. 40% OTS treated air entry pressure (water saturated)
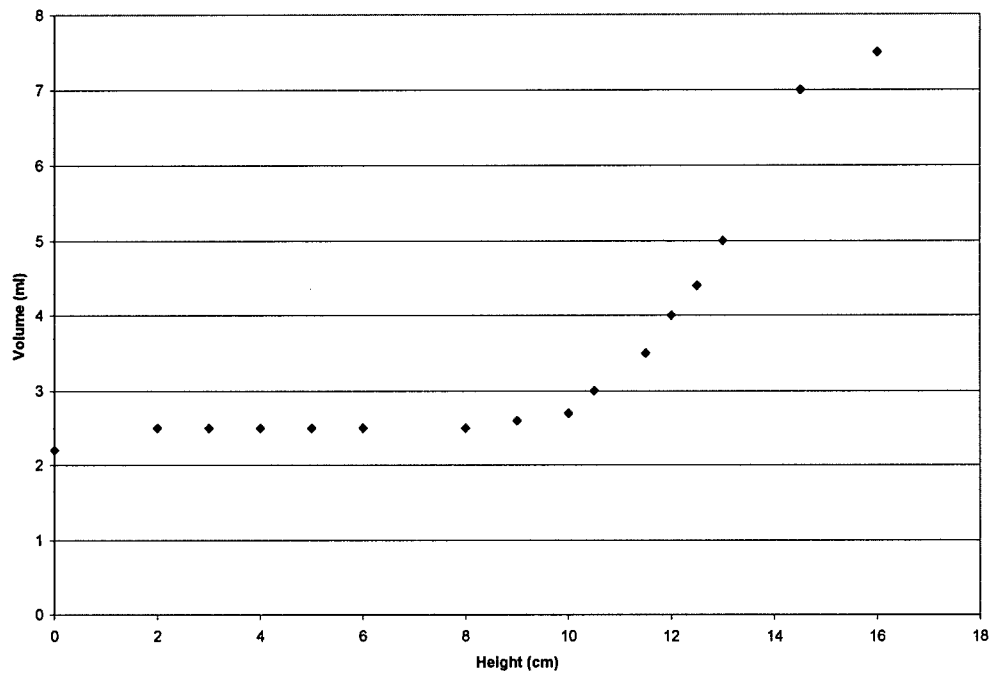
Figure A.4. 50% OTS treated air entry pressure (water saturated)
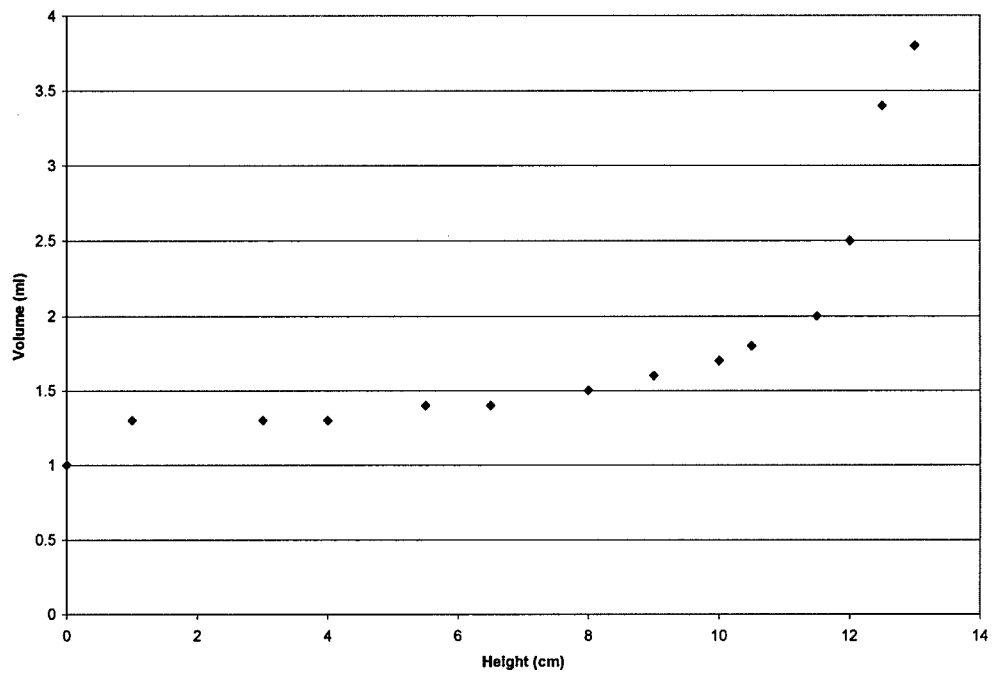
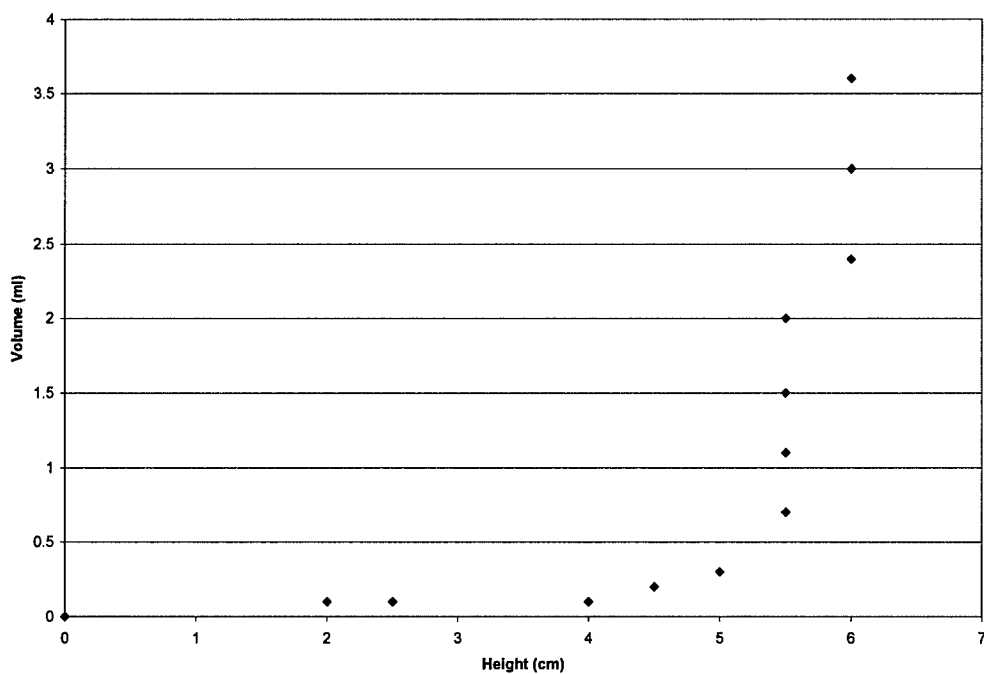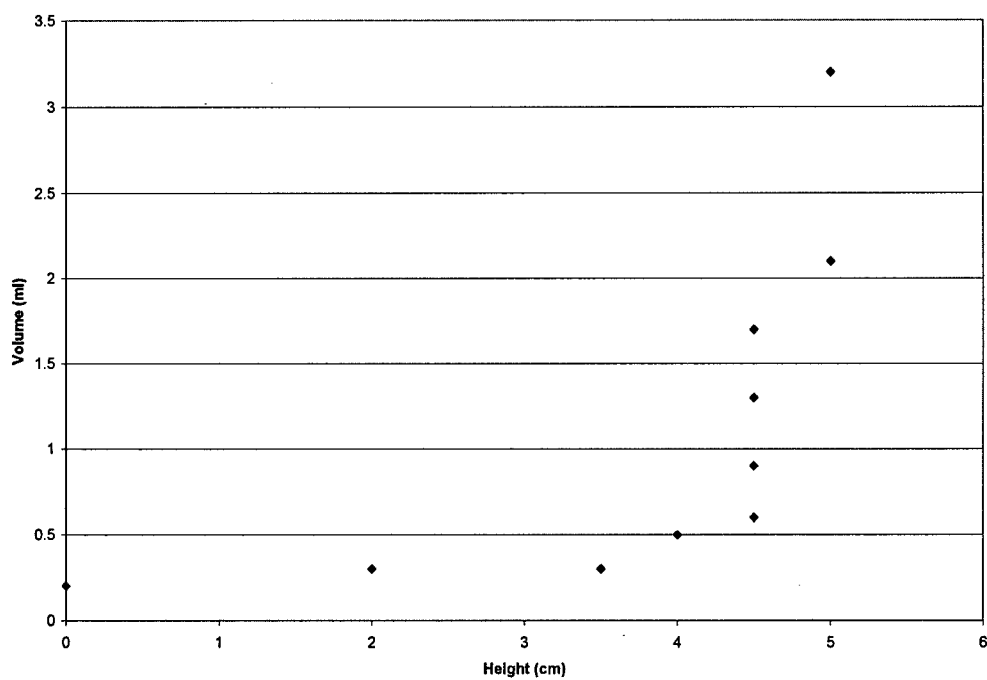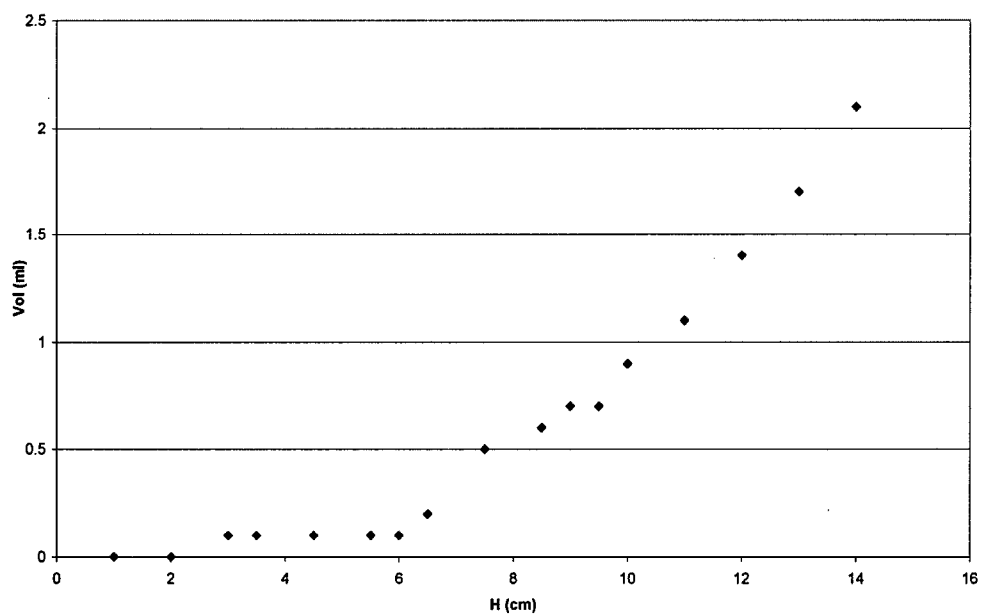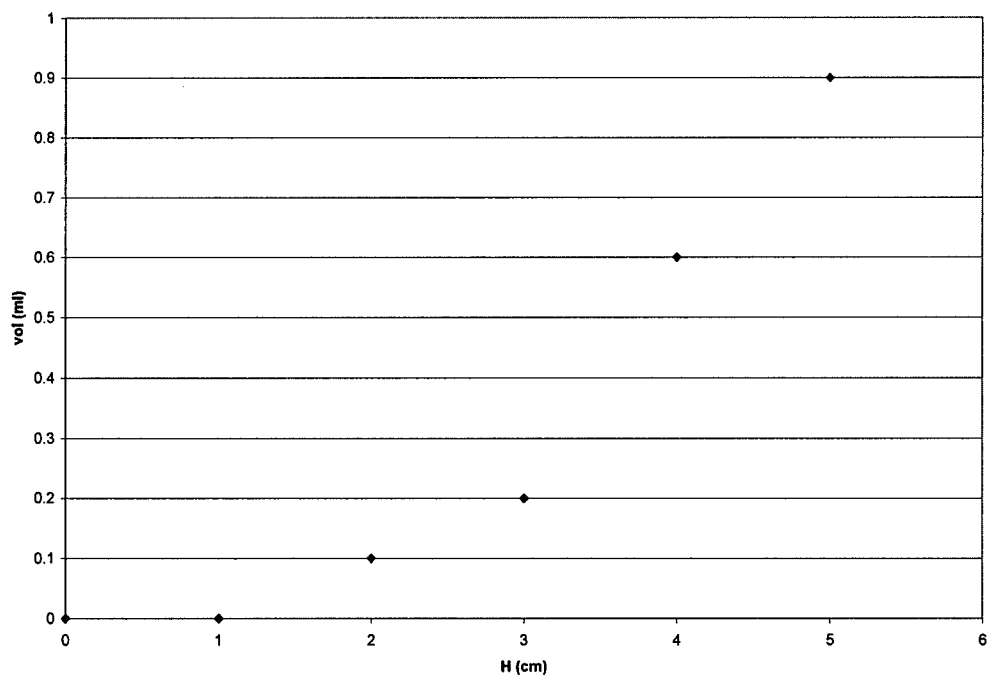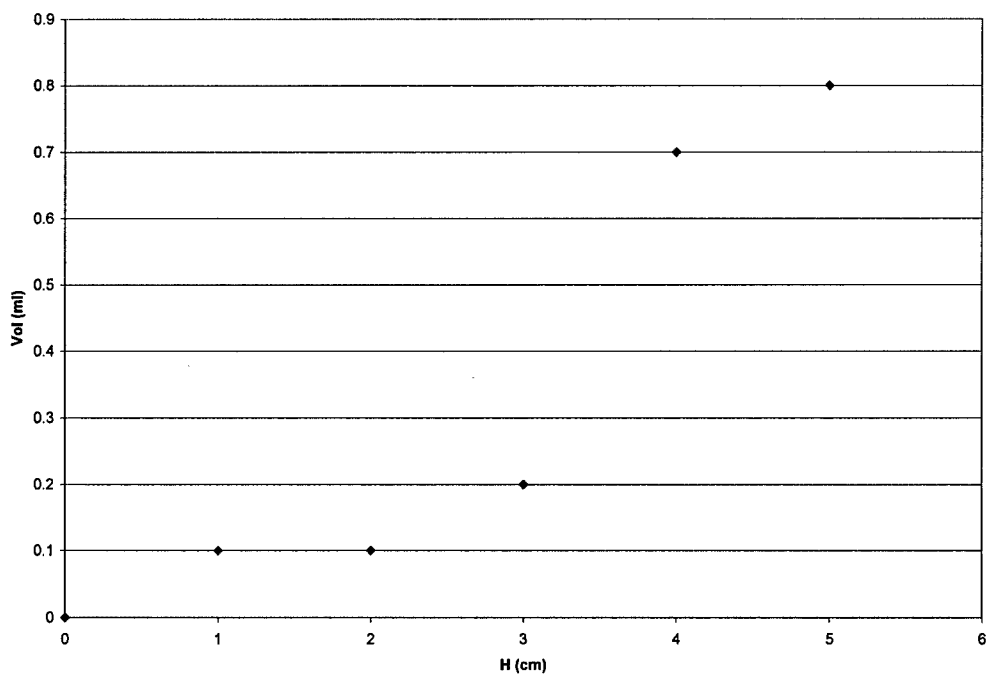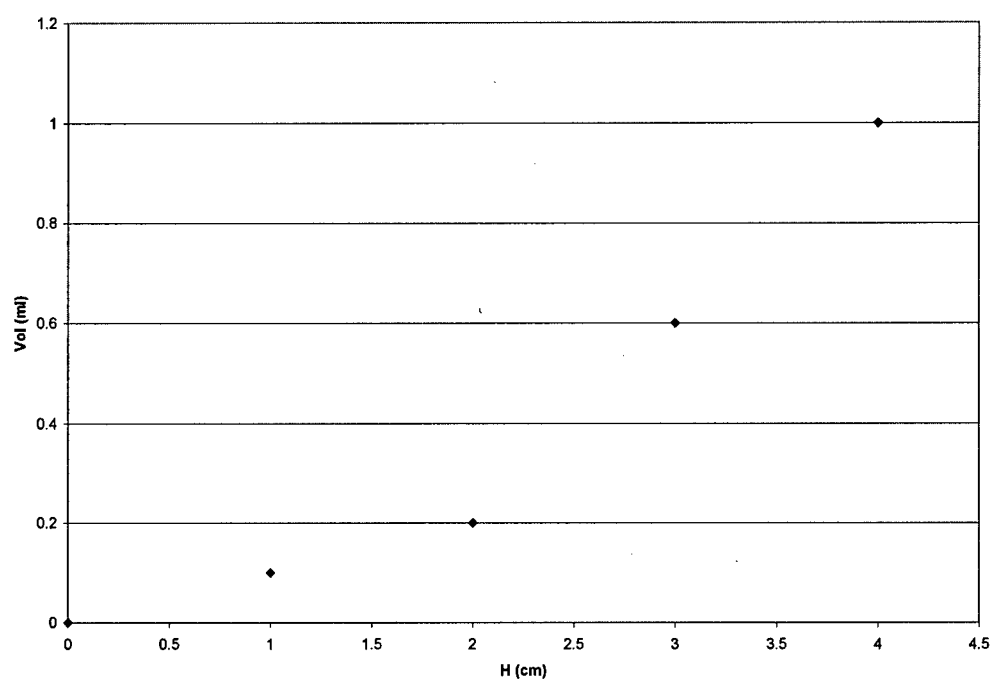Figure A.5. 60% OTS treated air entry pressure (water saturated)
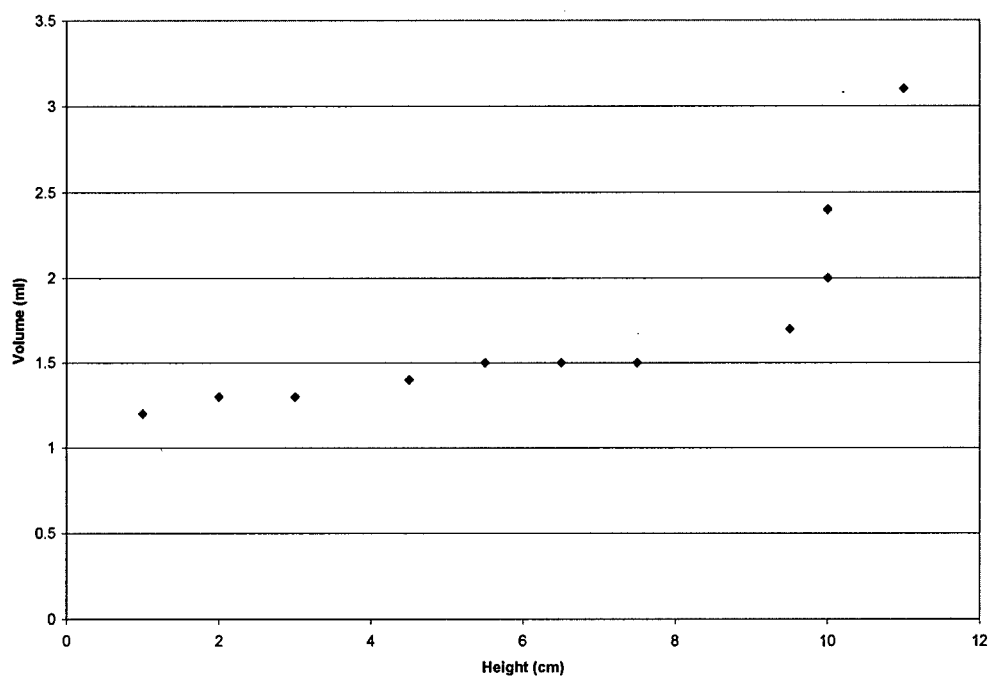
Figure A.6. 75% OTS treated air entry pressure (water saturated)
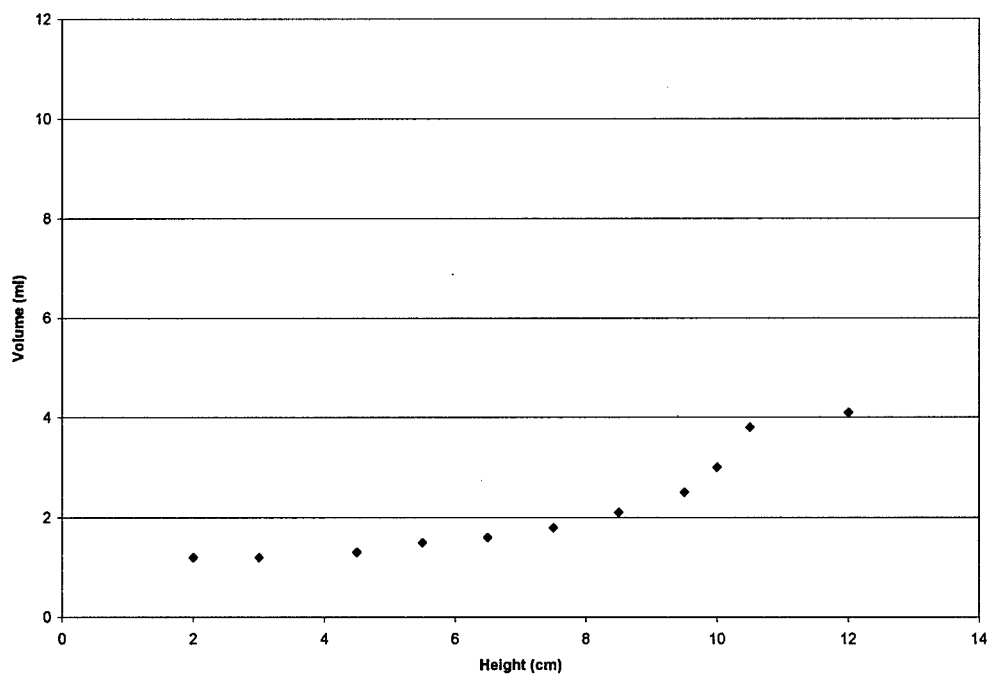
Figure A.7. 100% OTS treated air entry pressure (water saturated)
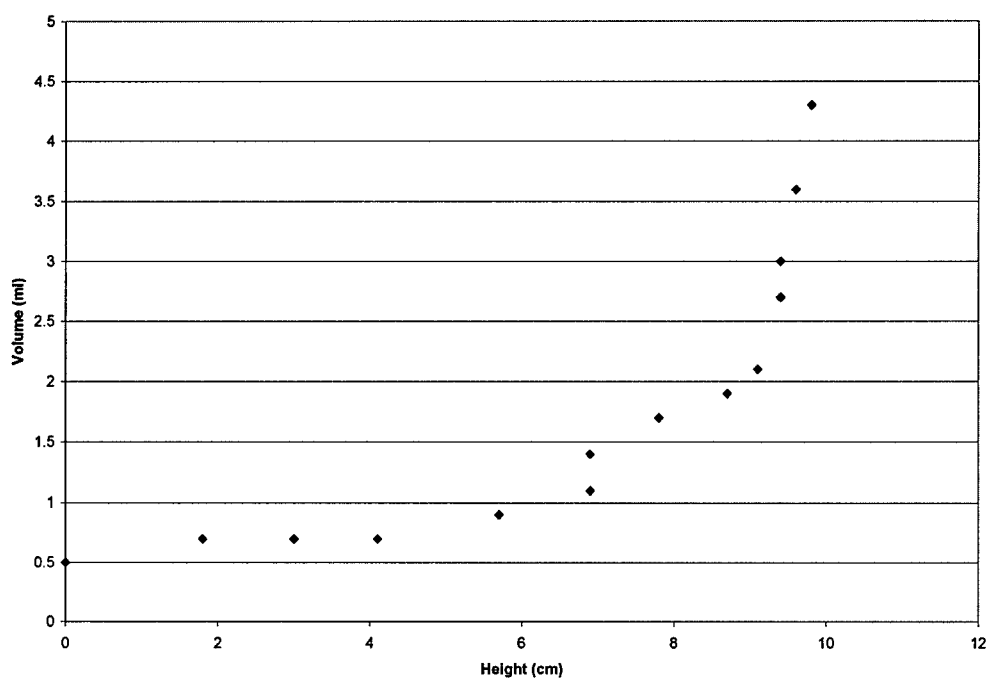
Figure A.8. 100% OTS treated water entry pressure (air saturated)
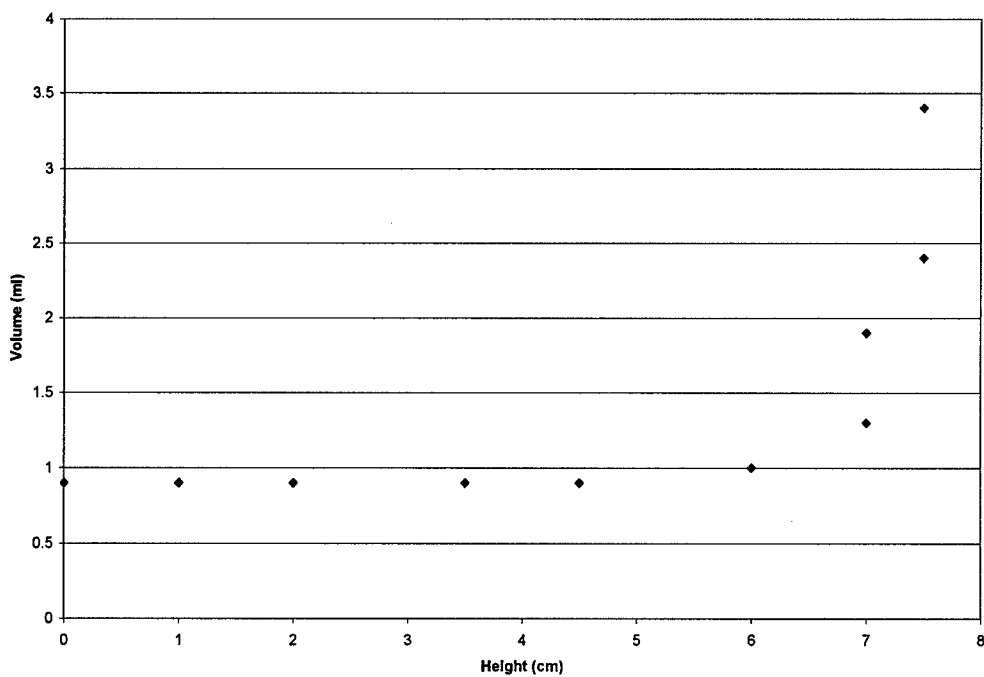
Figure A.9. 75% OTS treated water entry pressure (air saturated)
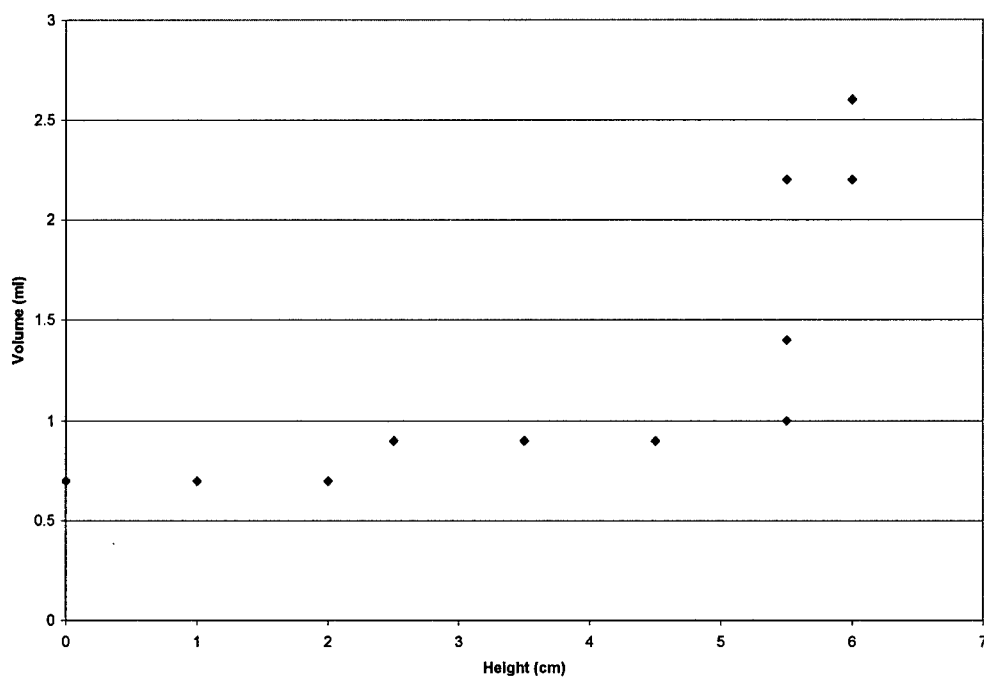
Figure A.10. 60% OTS treated water entry pressure (air saturated)

Figure A.11. 50% OTS treated water entry pressure (air saturated)

Figure A.12. 40% OTS treated water entry pressure (air saturated)

Figure A.13. Untreated oil entry pressure (water saturated)

Figure A.14. 25% OTS treated oil entry pressure (water saturated)

Figure A.15. 50% OTS treated oil entry pressure (water saturated)

Figure A.16. 75% OTS treated oil entry pressure (water saturated)

APPENDIX B
TWO-DIMENSIONAL FLOW CHAMBER DISTRIBUTION CONTOURS FOR GRAIN SIZE AND WETTABILITY EXPERIMENTS

Table B.1. Injection amount and associated sketch number

Injection Amount (ml)	0	0.5	1.0	1.5	2.0	2.5	3.0	3.5	4.0	etc
Sketch Number		1	2	3	4	5	6	7	8	etc
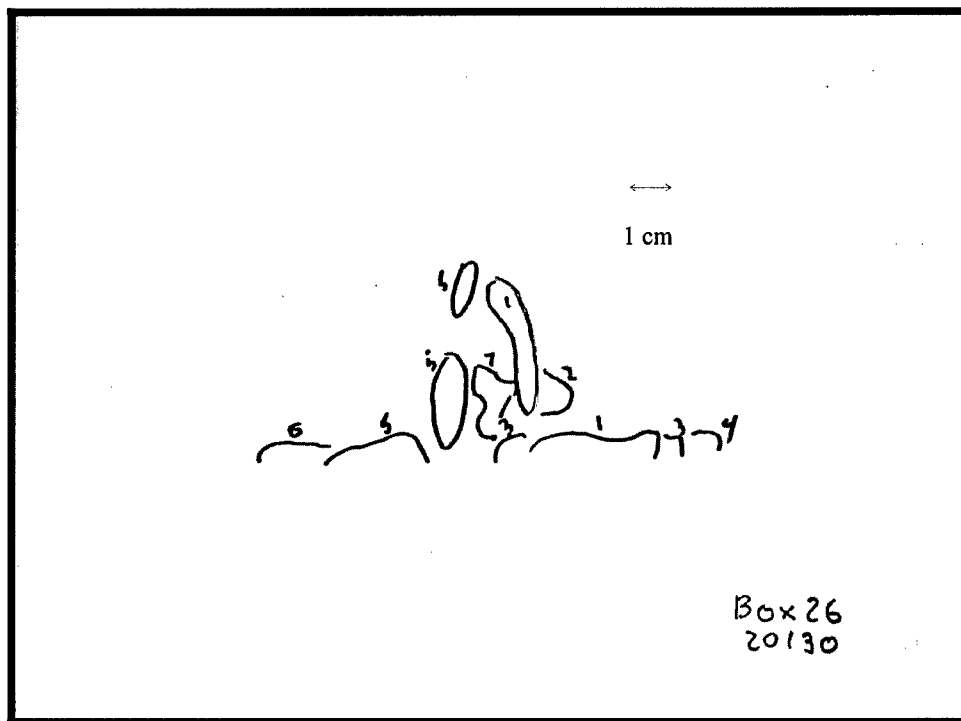
Figure B.1. 20-30 Sieve trace experiment 1
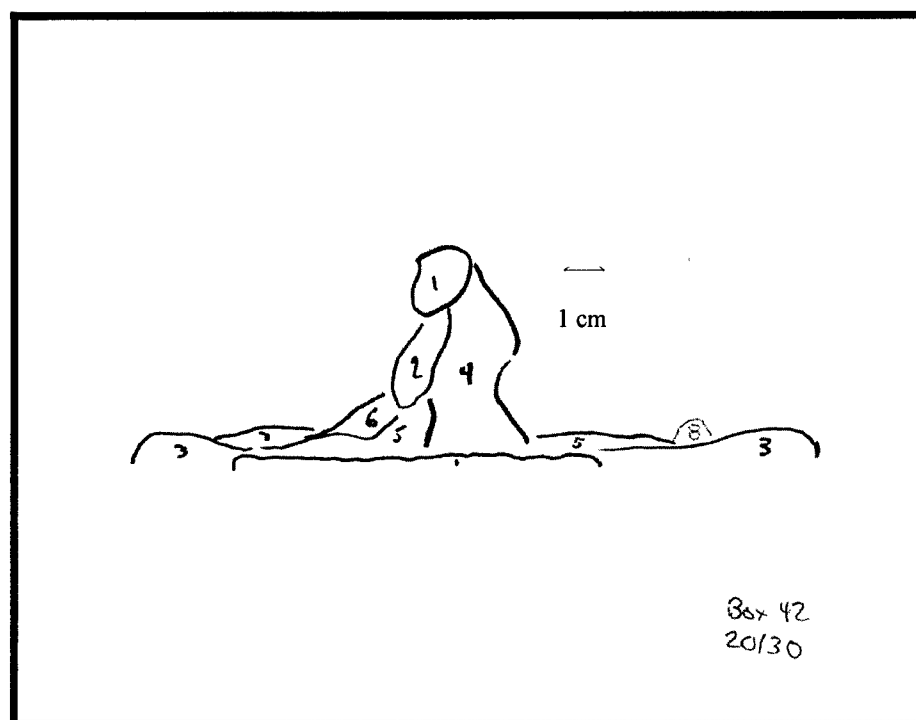
Figure B.2. 20-30 Sieve trace experiment 2
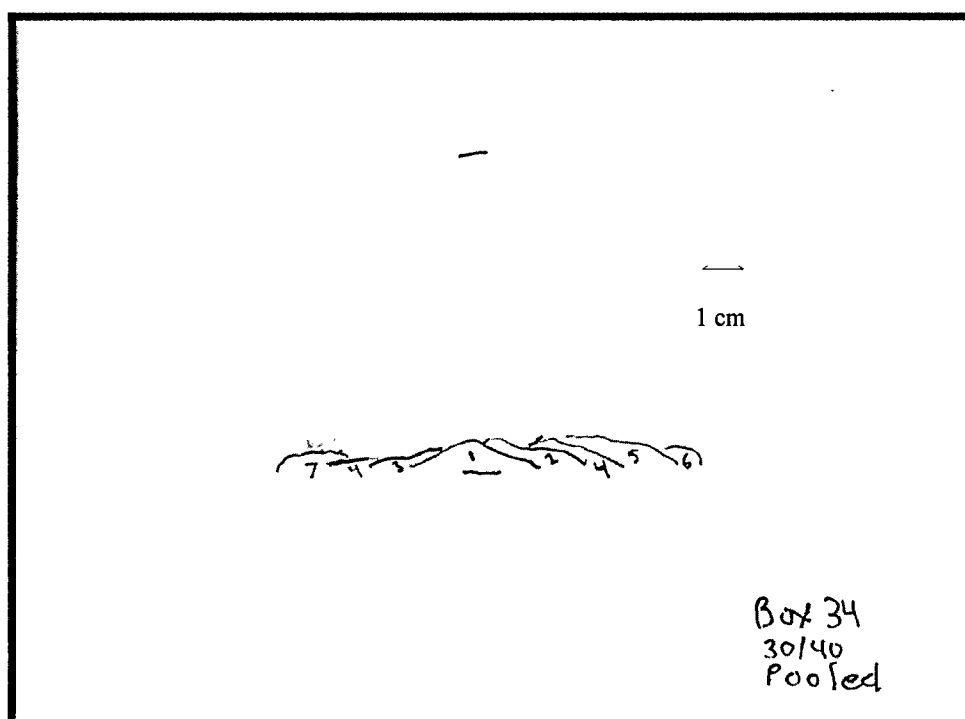
Figure B.3. 30-40 Sieve pooled PCE trace
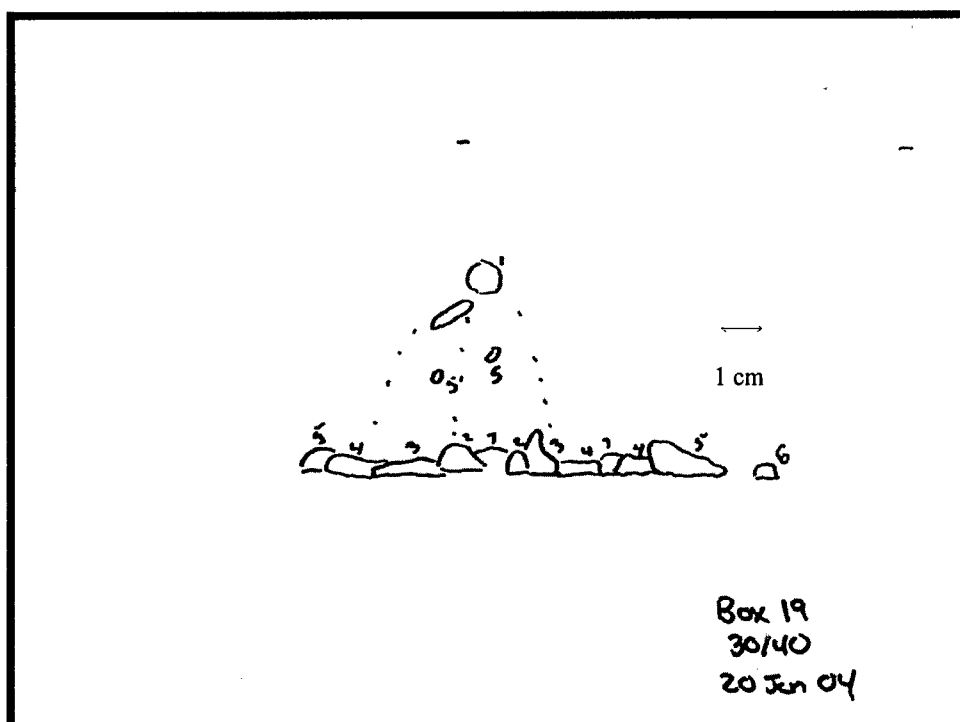
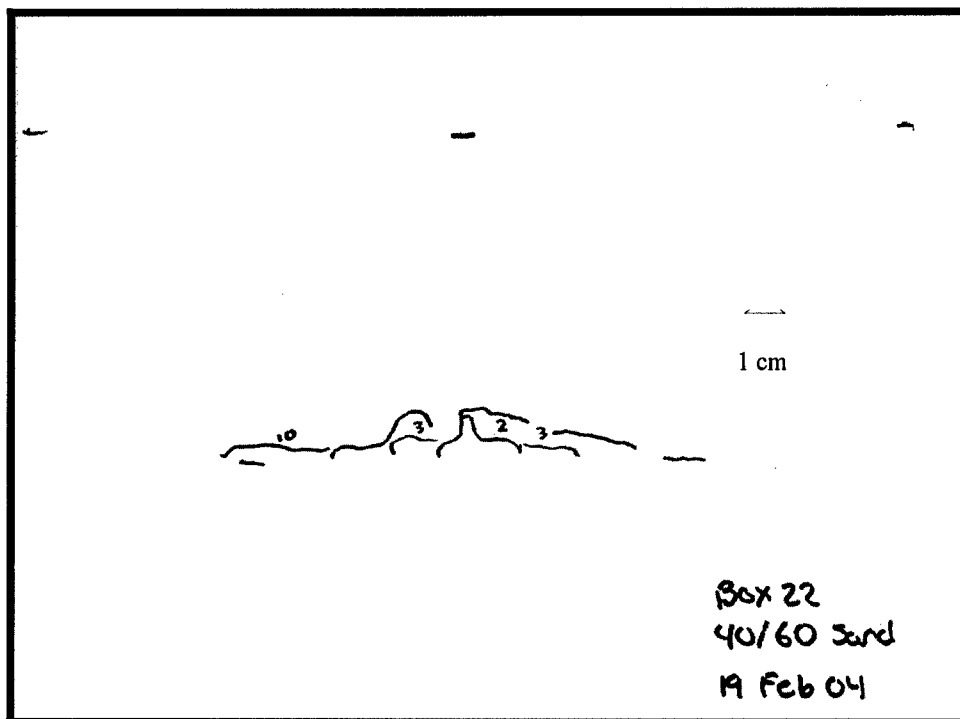Figure B.4. 30/40 Sieve trace
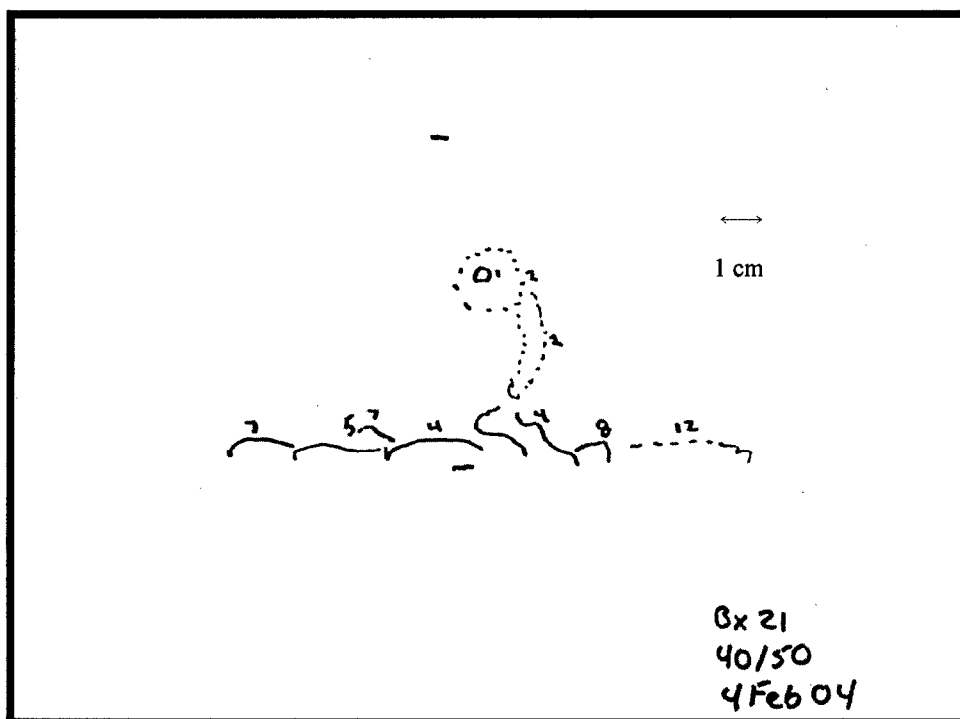
Figure B.5. 40-50 Sieve trace

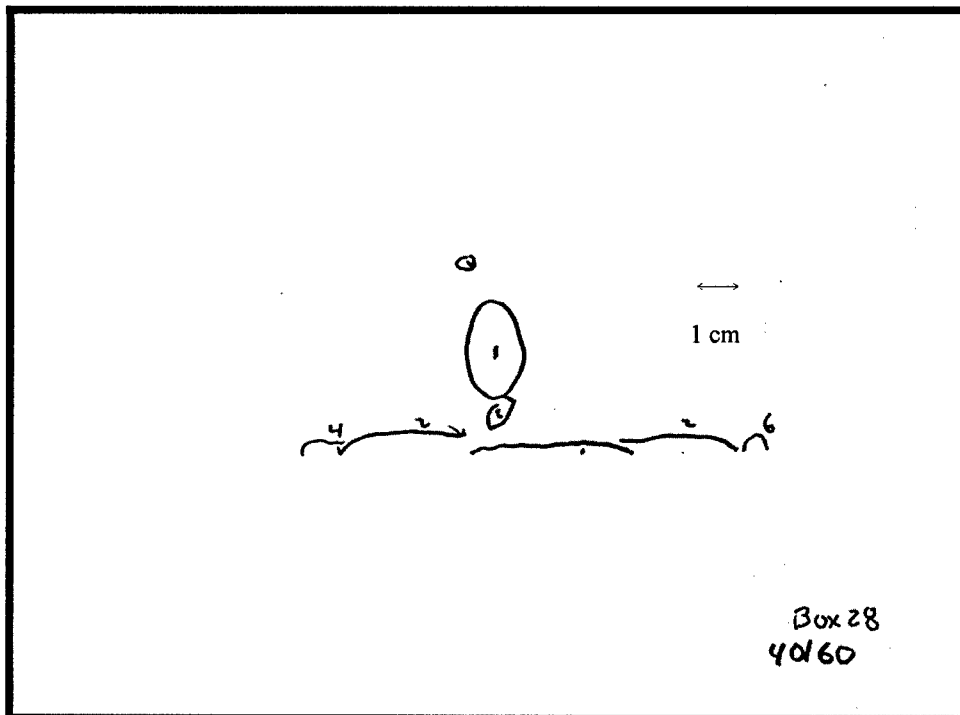Figure B.6. 40-60 Sieve trace experiment 1

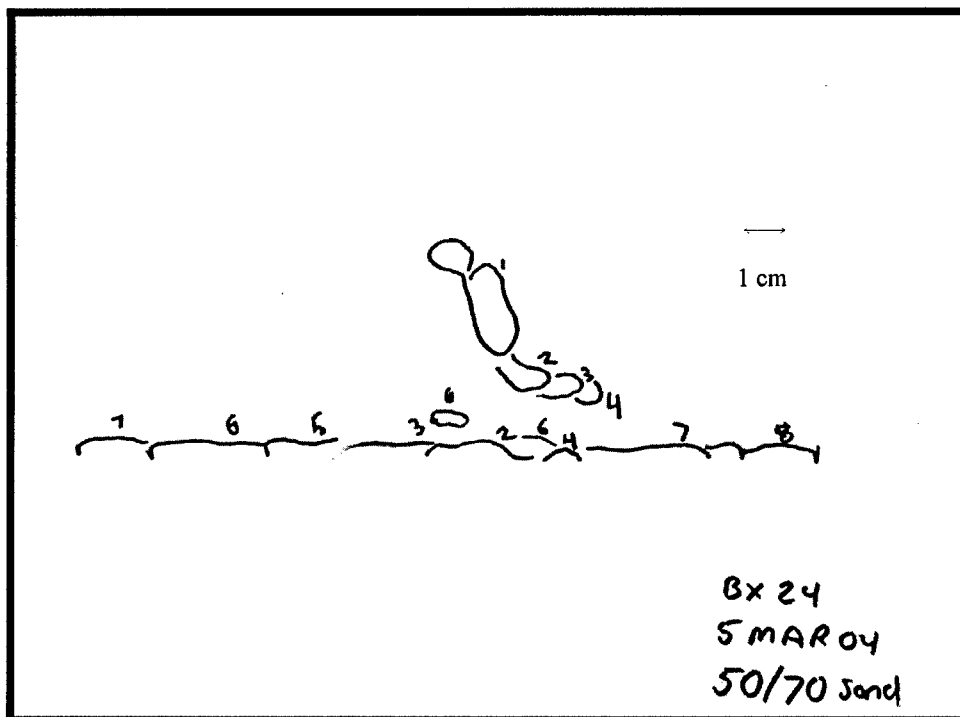Figure B.7. 40-60 Sieve trace experiment 2
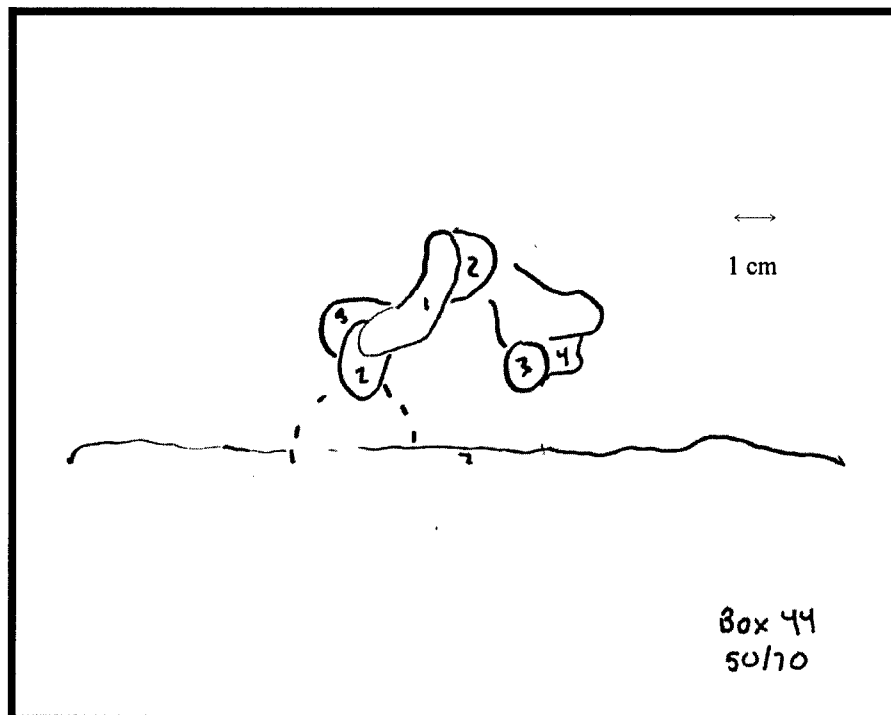
Figure B.8. 50-70 Sieve trace experiment 1

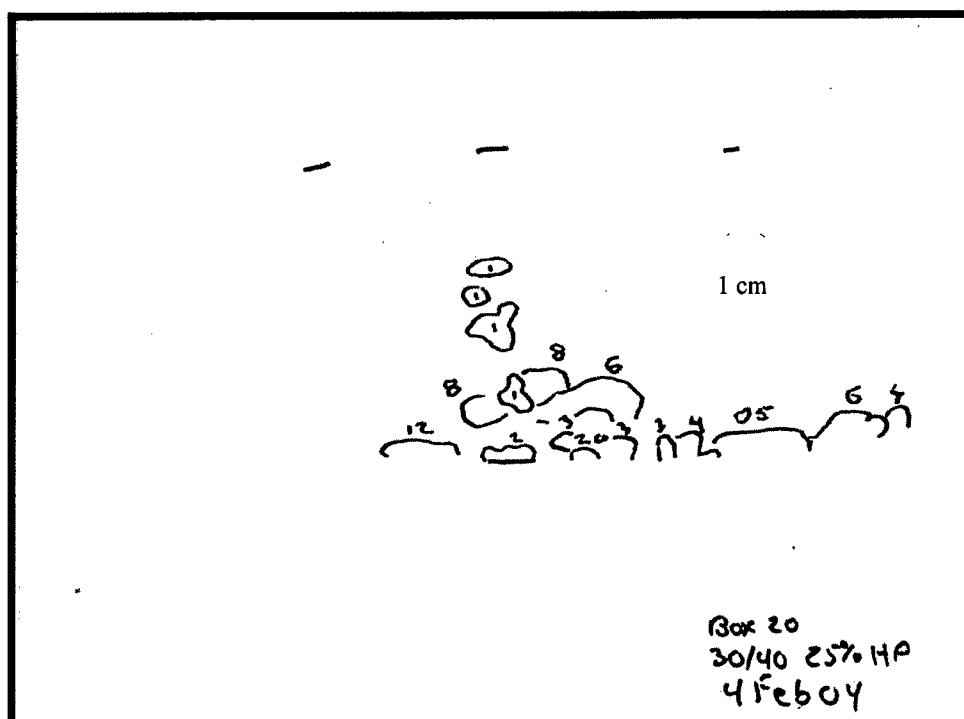Figure B.9. 50-70 Sieve trace experiment 2

Figure B.10. 30/40 Sand 25% OTS mix trace (denatured alcohol (DA))
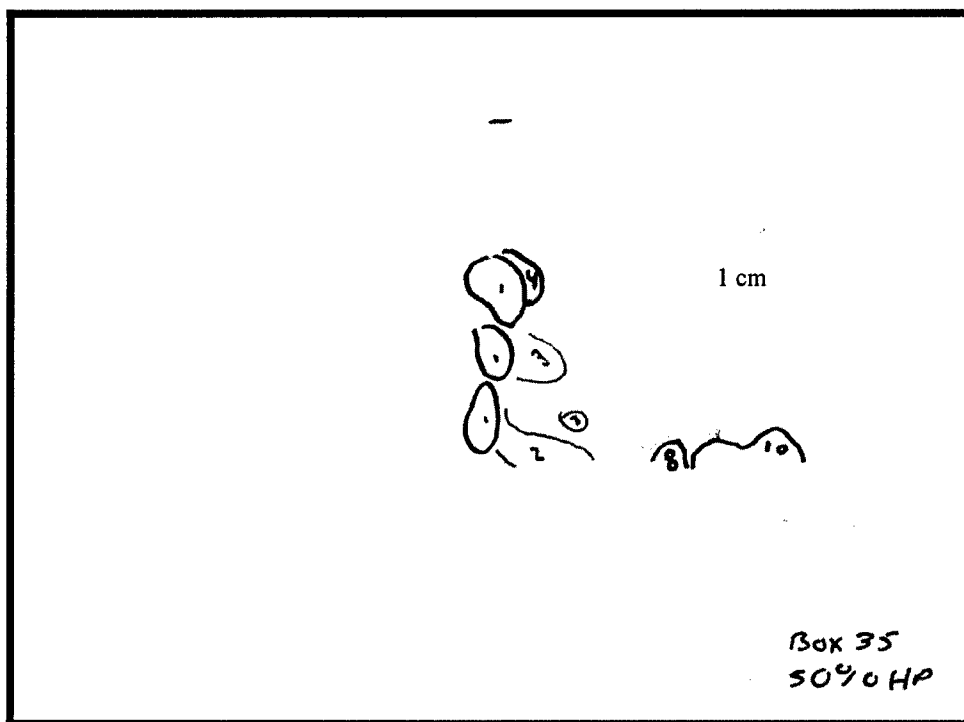

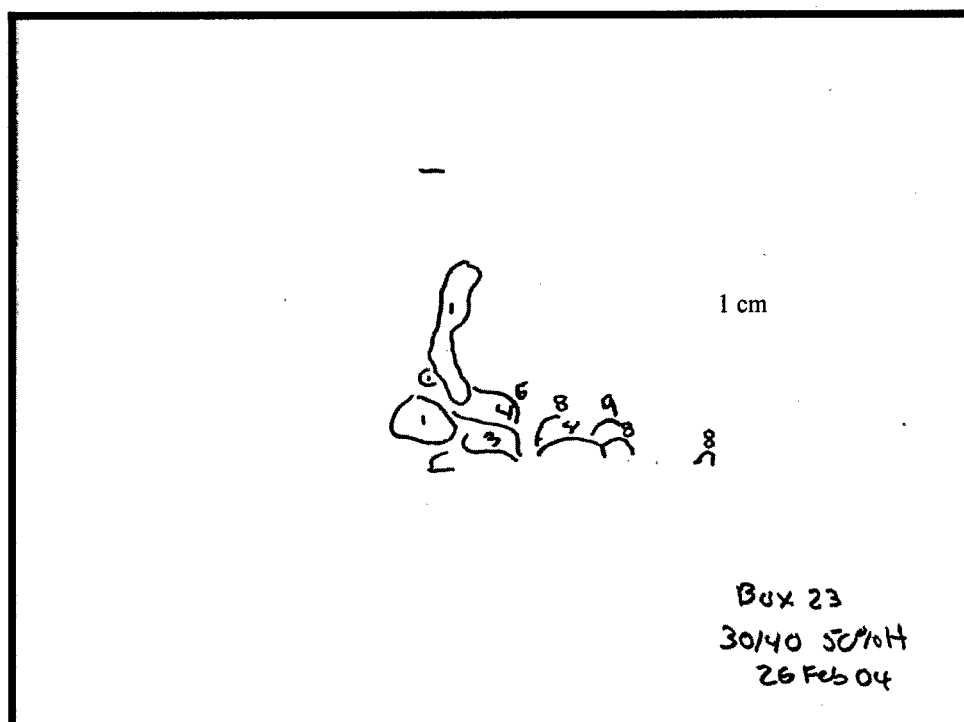Figure B.11. 30/40 Sand 50% hydrophobic mix trace (reagent alcohol (RA))

Figure B.12. 30/40 Sand 50% hydrophobic mix trace (DA)

Figure B.13. 30/40 Sand 75% hydrophobic mix trace (RA)
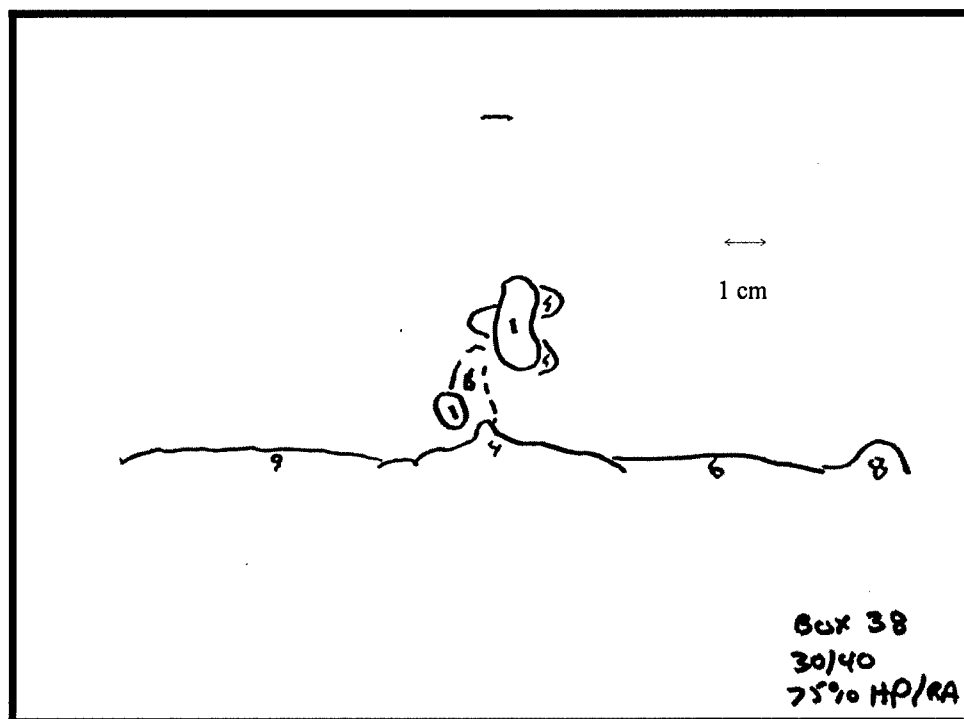
Figure B.14. 30/40 Sand 75% hydrophobic mix trace (DA)
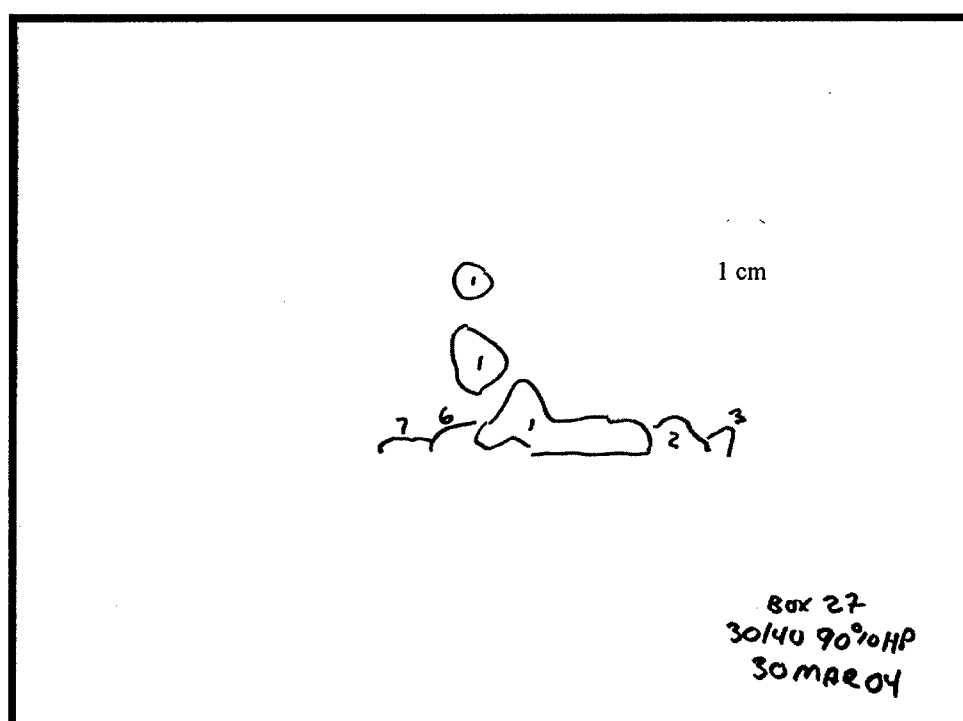
Figure B.15. 30/40 Sand 90% hydrophobic mix trace (DA)
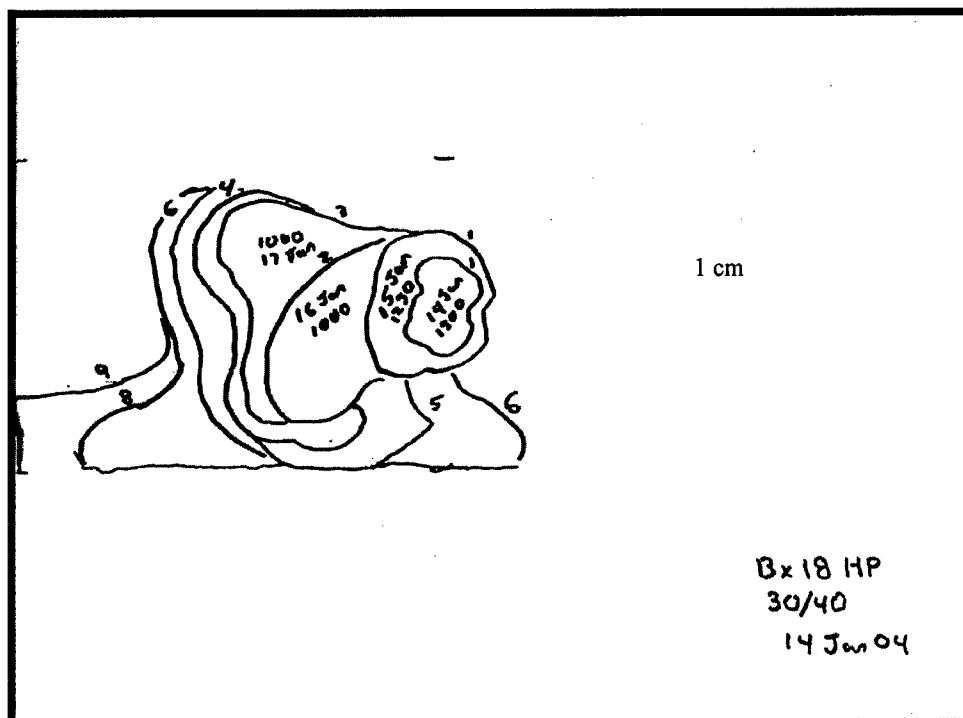
Figure B.16. 30/40 Sand 100% hydrophobic mix trace (RA)
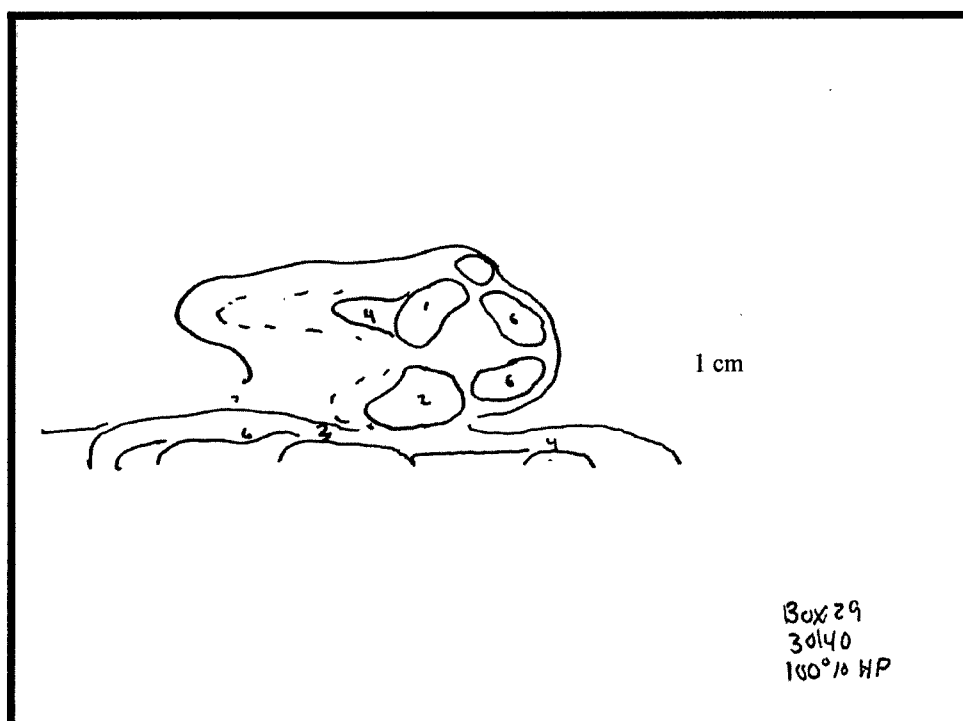
Figure B.17. 30/40 Sand 100% hydrophobic mix trace (DA)

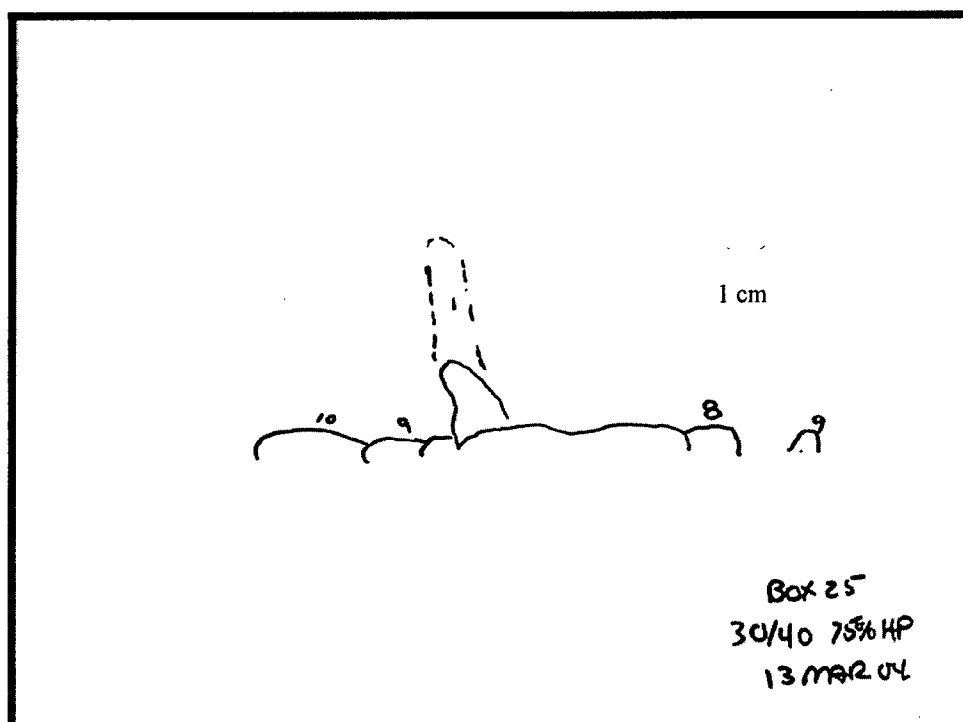TWO-DIMENSIONAL FLOW CHAMBER DISTRIBUTION CONTOURS FOR
INTERFACIAL TENSION AND DENSITY MODIFICATION EXPERIMENTS
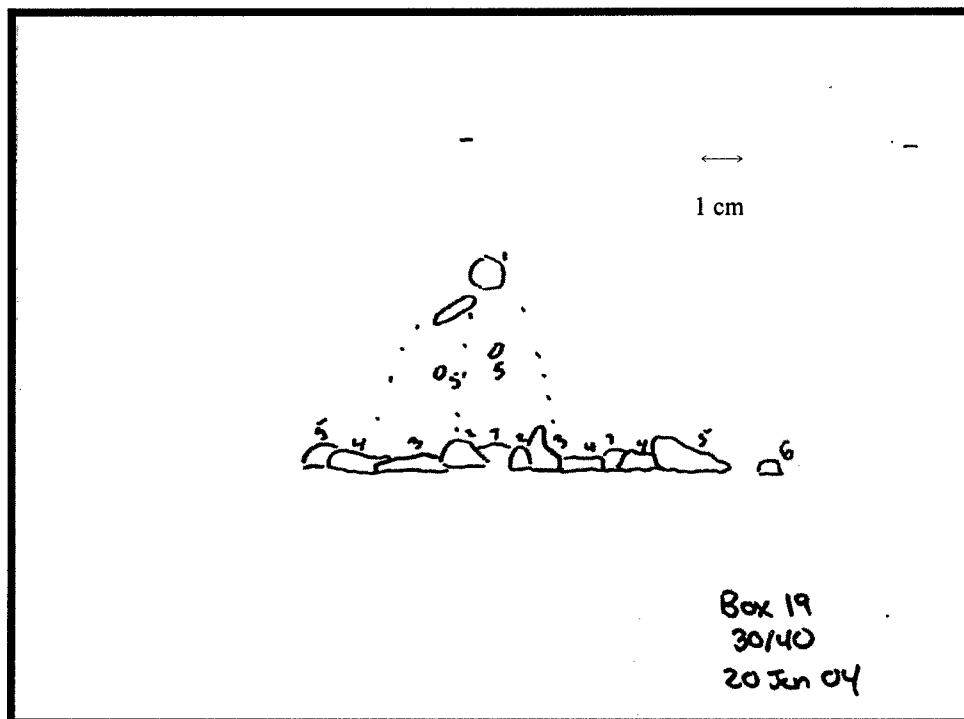
Figure C.1. Untreated (47 dynes/cm) PCE
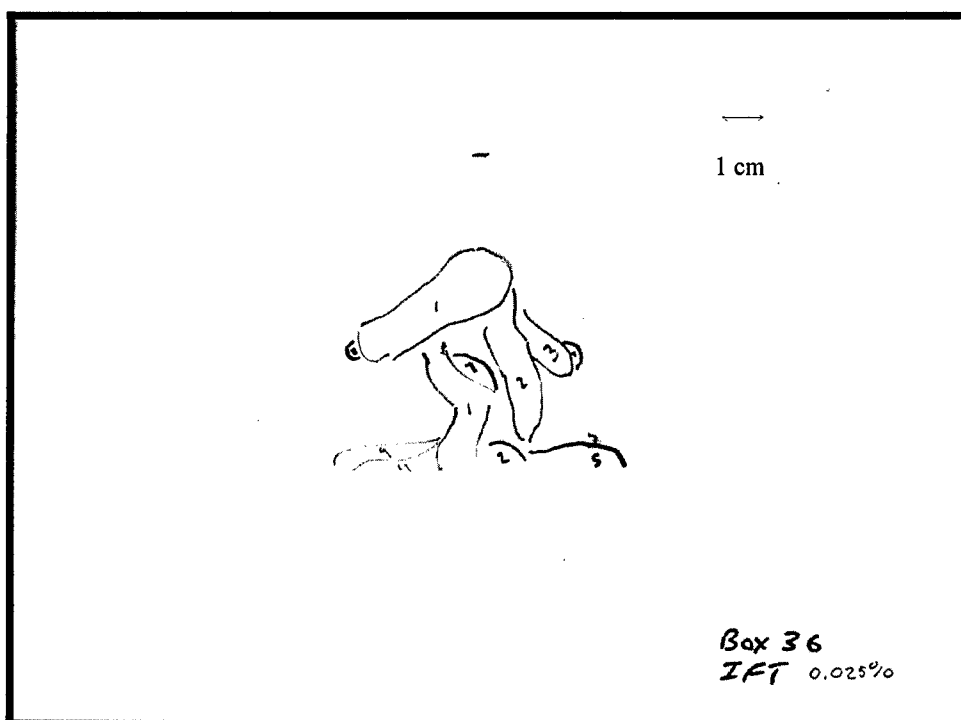
Figure C.2. 0.025% (13 dynes/cm) Span 80 treated PCE
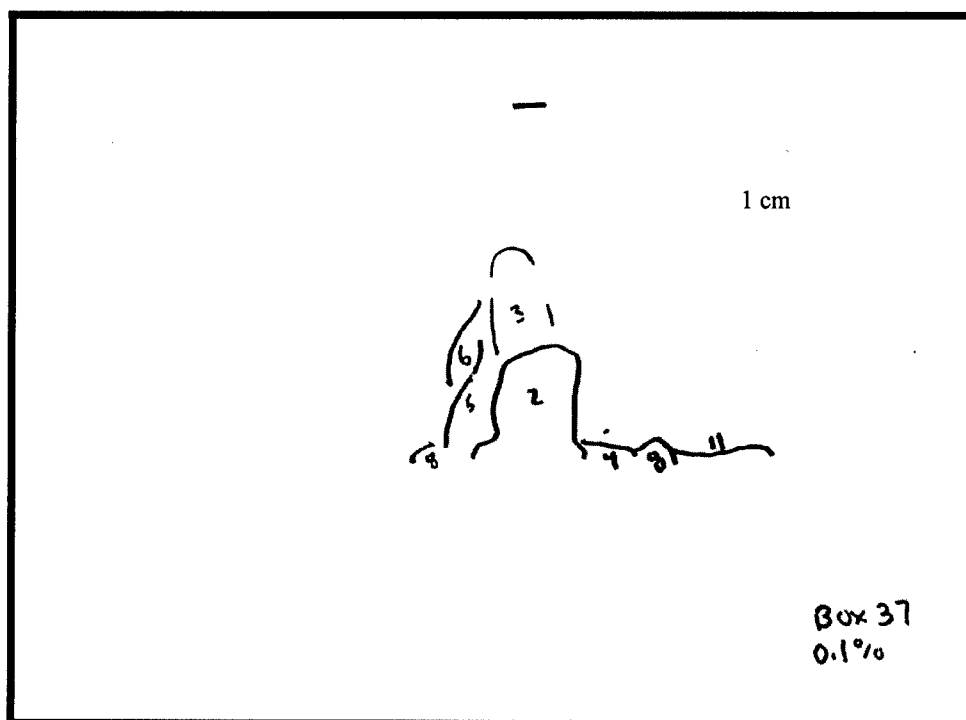
Figure C.3. 0.05% (3 dynes/cm) Span 80 treated PCE
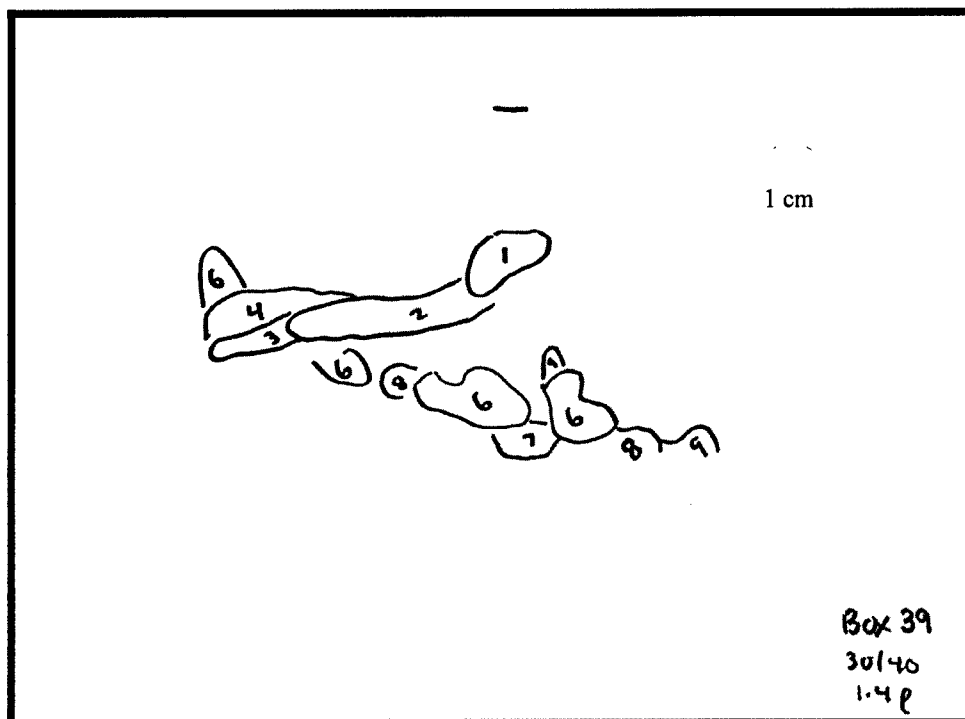
Figure C.4. 1.4 Density PCE in 30/40 sieve sand
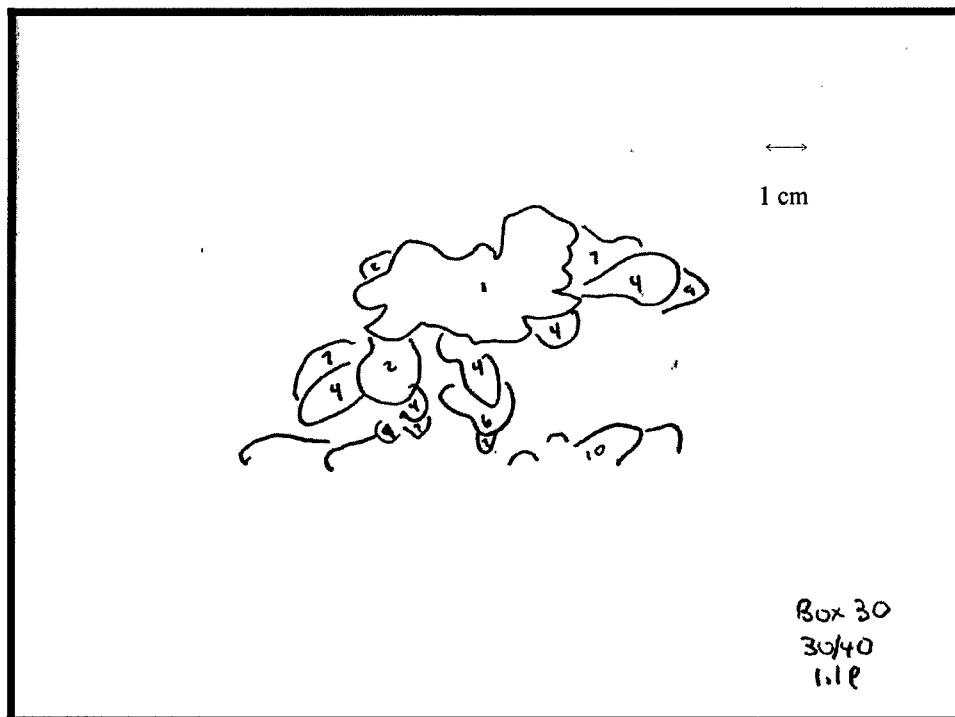
Figure C.5. 1.1 Density PCE in 30/40 sieve sand

Figure C.6. 1.0 Density in 30/40 sieve sand

Figure C.7. Untreated 40/50 sieve sand
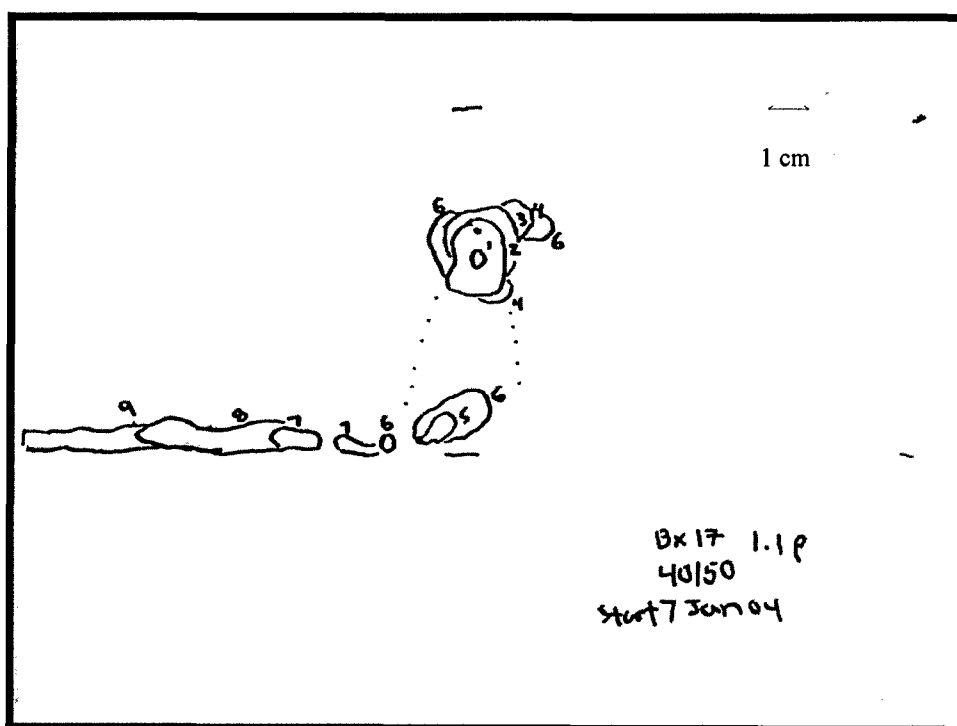
Figure C.8. 1.1 Density PCE in 40/50 sieve sand

LIST OF REFERENCES

Abrams, A. The Influence of Fluid Viscosity, Interfacial Tension, and Flow Velocity on Residual Oil Saturation Left by Waterflood, Society of Petroleum Engineers Journal, 437-447, October, 1975.

Bahrani, B., R.S. Mansell, and L.C. Hammond,. Using Infiltration of Heptane and Water into Soil Columns to Determine Soil-Water Contact Angles, Soil Sci. Soc. Amer. Proc., 37:532-534, 1973.

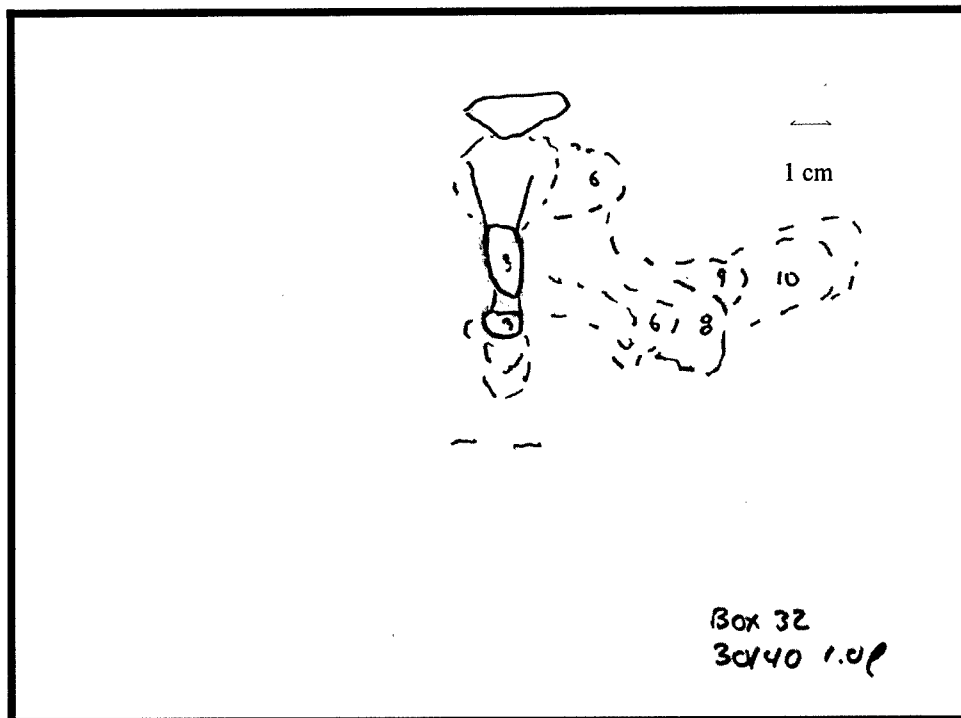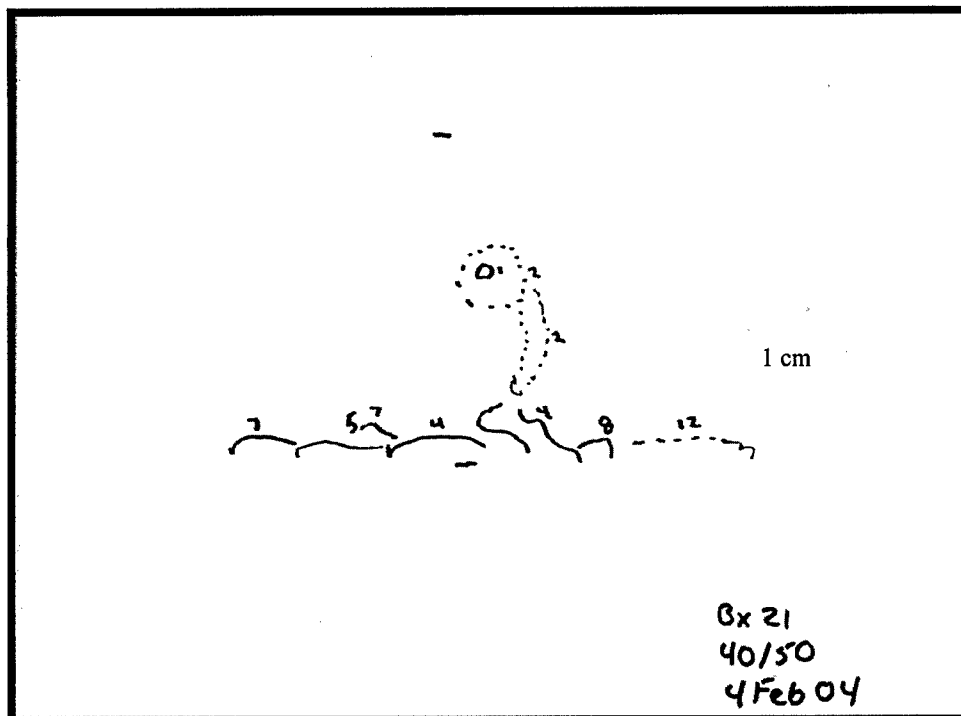Beglund, S. Aquifer Remediation by Pumping: A Model for Stochastic-Advective Transport with Nonaqueous Phase Liquid Dissolution, Water Resources Research, 33:649-661, 1997.

Bradford, S. A., and F.J. Leij. Wettability Effects on Scaling Two and Three Fluid Capillary Pressure – Saturation Relations, Environmental Science and Technology, 29(6):1446-1455, 1995.

Bradford, S. A., T.J. Phelan, and L.M. Abriola. Dissolution of Residual Tetrachloroethylene in Fractional Wettability Porous Media: Correlation Development and Application, Journal of Contaminant Hydrology 45:35-61, 2000.

Brewster, M.L., A.P. Annan, J.P. Greenhouse, B.H. Kueper, J.D. Olhoeft, J.D. Redman,K.A. Sander. Observed Migration of a Controlled DNAPL Release by Geophysical Methods, Ground Water, 33(6):977-988, Nov-Dec 1995.

Brooks, M. C., M. D. Annable, P. S. C. Rao, K. Hatfield, J. W. Jawitz, W. R. Wise, A. L. Wood, and C. G. Enfield. Controlled Release, Blind Tests of DNAPL Characterization using Partitioning Tracers. Journal of Contaminant Hydrology 59:187-210, 2002.

Brusseau, M.B., Complex Mixtures and Groundwater Quality, Environmental Research Brief, EPA 600S93004, 1993.

Chatzis, I., N.R. Morrow and H.T. Lim. Magnitude and Detailed Structure of Residual Oil Saturation, Society of Petroleum Engineering Journal (SPEJ) 23:311-326, 1983.

Chevalier, L.R. and J. Petersen. Literature Review of 2-D Laboratory Experiments in NAPL Flow, Transport, and Remediation, Journal of Soil Contamination, 8(1):149-167, 1999.

Cho, J. Characterization of Spatial NAPL Distribution, Mass Transfer and the Effect of Cosolvent and Surfactant Residuals on Estimating NAPL Saturation using Tracer Techniques, PhD Dissertation, University of Florida, Gainesville FL, 2001.

Conrad, S. H., R.J. Glass, and W.J. Peplinski. Benchscale Visualization of DNAPL Remediation Processes in Analog Heterogeneous Aquifers: Surfactant Floods and In Situ Oxidation using Permanganate, Journal of Contaminant Hydrology, 58(1-2):13-49, September, 2002.

Corey, A. *Mechanics of Immiscible Fluids in Porous Media,* Water Resources Publications, LLC, Highlands Ranch, CO, 2003.

Dawson, H.E. and P.V. Roberts. Influence of Viscous, Gravitational, and Capillary Forces on DNAPL Saturation, Ground Water, 35:261-270, Mar-Apr, 1997.

Donaldson, E.C., R.D. Thomas, and P.B. Lorenz. Wettability Determination and its Effect on Recovery Efficiency, Society of Petroleum Engineers Journal, 13-20, March 1969.

Einarson, M.D. and D.M. Mackay. Predicting Impacts of Groundwater Contamination, Environmental Science and Technology, 35(3):66A-73A, 2001.

Environmental Protection Agency [EPA] Consumer Factsheet on: Tetrachloroethylene, Ground Water and Drinking Water 2003a. http://WWW.epa.gov/safewater/contaminants/dw_contamfs/tetrachl.html Date accessed 12 Mar 03

Environmental Protection Agency [EPA] Consumer Factsheet on: Trichlorothylene, Ground Water and Drinking Water 2003b. http://WWW.epa.gov/safewater/contaminants/dw_contamfs/trichlor.html Date accessed 12 Mar 03

Environmental Protection Agency [EPA] Technology Transfer Network Air Toxics Website: Vinyl Chloride EPA 75-01-4, Date last Updated, 12 Feb2003c. http://www.epa.gov/ttn/atw/hlthef/vinylchl.html Date last accessed 19 Aug 2003

Falta, R. W., S. E. Brame, C. M. Lee, and J. T. Coates. A Field Test of LNAPL Remediation by Tert-butanol Injection, Abstracts of Papers of the American Chemical Society 213:49, 1997.

Fetter, C.W. *Applied Hydrogeology,* 4th edition, Prentice Hall, Inc, Upper Saddle River, NJ, 2001.

Fetter C.W. *Contaminant Hydrology,* 2nd edition, Prentice-Hall, Inc, Upper Saddle River, NJ, 1999.

Fink, D.H. Water Repellency and Infiltration Resistance of Organic-Film-Coated Soils, Soil Science Society of America Proceedings, 34:189-194, 1970.

Fiorenza, S. NAPL Removal: Surfactants, Foams, and Microemulsions, Lewis
Publishers, Boca Raton, FL, 2000.

Fountain, J. C., C. Wadell-Sheets, A. Lagowski, C. Taylor, D. Frazier, and M. M. Byrne.
Enhanced Removal of Dense Nonaqueous-Phase Liquids using Surfactants. *In* D.
A. Sabatini, R. C. Knox, and J. H. Harwell, editors. Surfactant-Enhanced
Subsurface Remediation, ACS Symposium Series Emerging Technologies.
American Chemical Society, Washington, D.C., 1995.

Fountain, J. C., R. C. Starr, T. Middleton, M. Beikirch, C. Taylor, and D. Hodge, A
Controlled Field Test of Surfactant-Enhanced Aquifer Remediation, Ground Water
34:910-916, 1996. Gordon, R. A., CPG, Waging the War Against DNAPLs,
Applied Science and Technology, Inc, January 1996. http://www.asti-
env.com/dnapl.html Date accessed 26 Feb 03

Held, R.J. and T.H. Illangaskare. Fingering of Dense Nonaqueous Phase Liquids in
Porous Media 1. Experimental Investigation, Water Resources Research,
31(5):1213-1222, May, 1995a.

Held, R.J. and T.H. Illangaskare. Fingering of Dense Nonaqueous Phase Liquids in
Porous Media 2. Analysis and Classification, Water Resources Research,
31(5):1223-1231, May, 1995b.

Hofstee, C., R. C. Walker, and J. H. Dane. Infiltration and Redistribution of
Perchloroethylene in Stratified Water-saturated Porous Media. Soil Science Society
of America Journal, 62:13-22, 1998.

Hunt, J.R., N. Sitar, and K.S. Udell, Nonaqueous Phase Liquid Transport and Cleanup, 1,
Anaysis and Mechanisms, Water Resources Research, 24(8):1247-1258, 1988.

Illangasekare, T. H., J. L. Ramsey, K. H. Jensen, and M. B. Butts, Experimental Study of
Movement and Distribution of Dense Organic Contaminants in Heterogeneous
Aquifers, Journal of Contaminant Hydrology 20:1-25, 1995.

Jamison, V.C. Symposium on "Transmission of Water Through Soils in Relation to
Irrigation and Pond Construction" (Joint Program of Sections I and VI), Resistance
to Wetting in the Surface of Sandy Soils Under Citrus Trees in Central Florida and
Its Effect Upon Penetration and the Efficiency of Irrigation, Soil Science Society
Proceedings, 103-109, 1946.

Jawitz, J. W., M. D. Annable, and P.S.C. Rao. Miscible Fluid Displacement Stability in
Unconfined Porous Media; Two Dimensional Flow Experiments and Simulations,
Journal of Contaminant Hydrology 31:211-230, 1998a.

Jawitz, J. W., M. D. Annable, P.S.C. Rao, and R. D. Rhue. Field Implementation of
Winsor Type I Surfactant/Alcohol Mixture for in Situ Solubilization of a Complex
LNAPL as a Single Phase Microemulsion, Environmental Science & Technology
32:523-530. 1998b.

Jawitz, J. W., R. K. Sillan, M. D. Annable, P. S. C. Rao, and K. Warner, In Situ Alcohol Flushing of a DNAPL Source Zone at a Dry Cleaner Site, Environmental Science & Technology 34:3722-3729, 2000.

Jawitz, J. W., M.D. Annable, G.G. Demmy, and P.S.C. Rao. Estimating Nonaqueous Phase Liquid Variability using Partitioning Tracer Higher Temporal Moments, Water Resources Research, 39(7):1192-1209, 2003.

Jeong, S., A.L. Wood, and T.R. Ree. Effects of Pure and Dyed PCE on Physical and Interfacial Properties of Remedial Solutions, Journal of Hazardous Materials, 95(1-2):125-135, 11 Nov 2002.

Johnson, R.L. and J.F. Pankow, Dissolution of Dense Chlorinated Solvents into Groundwater. 2. Source Functions for Pools of Solvent, Environmental Science Technology, 26:896-901, 1992.

Le Grange, J.D. and J.L. Markham. Effects of Surface Hydration on the Deposition of Silane Monolayers on Silica, Langmuir, 9:1749-1753, 1993.

Letey, J., J. Osborn, R.E. and Pelishek. Measurement of Liquid-Solid Contact Angles in Soil and Sand, Soil Science, 93(3):149-153 Mar, 1962.

Lowe, D. F., C. L. Oubre and C. H. Ward. *Surfactants and Cosolvents for NAPL Remediation*, CRC Press, Boca Raton, FL 1999.

Martel, R., P.J. Gelinas, and L. Saumure. Aquifer Washing by Miceller Solutions: 3 Field Test at the Thouin Sand Pit (L'Assomption, Quebec, Canada). Journal of Contaminant Hydrology, 30:33-48, 1998.

Mayer, A. S. and C.T. Miller. The Influence of Porous Medium Characteristics and Measurement Scale on Poor-Scale Distributions of Residual Nonaqueous-Phase Liquids. Journal of Contaminant Hydrology, 11:189-213, 1992.

McCray, J. E. and M. L. Brusseau. Cyclodextrin-Enhanced In-situ flushing of Multiple Component Immiscible Organic Liquid Contamination at the Field Scale: Mass Removal Effectiveness. Environmental Science & Technology 32:1285-1293 1998.

Meinardus, H. W., V. Dwarakanath, J. Ewing, G. J. Hirasaki, R. E. Jackson, M. Jin, J. S. Ginn, J. T. Londergan, C.A. miller, and G. A. Pope. Performance Assessment of NAPL Remediation in Heterogeneous Alluvium, Journal of Contaminant Hydrology 54:173-193, 2002.

Mercer, J. W. and R.M. Cohen. A Review of Immiscible Fluids in the Subsurface: Properties, Models, Characterization and Remediation, Journal of Contaminant Hydrology, 6:107-163, 1990.

Miller, C. T., M.M Poirer-McNeill, and A.S. Mayer. Dissolution of Trapped Nonaqueous Phase Liquids: Mass Transfer Characteristics, Water Resources Research, 26(11):2783-2796, Nov, 1990.

Moore, T. F. and R.L. Slobod. The Effect of Viscosity and Capillarity on the Displacement of Oil by Water, Producers Monthly, 20-30, Aug, 1956.

Morrow, N.R. and J. P. Heller. *Fundamentals of Enhanced Oil recovery, in Enhanced Oil Recovery, 1: Fundamental and Analyses,* Elsevier Publishing Co., New York, 1985.

Morrow, N.R., I. Chatzis, and J.J Taber. Entrapment and Mobilization of Residual Oil in Bead Packs, SPE Reservoir Engineering, 927-934, Aug, 1988.

New Jersey Department of Health and Senior Services [NJDHSS] Hazardous Substance Fact Sheet, Tetrachloroethylene, Mar, 2002.

Newell, C. J. and R.R Ross. EPA Publication 9355.4-07FS, Estimating Potential for Occurrence of DNAPL at Superfund Sites, Jan, 1992.

Ng, K.M., H.T. Davis, and L.E. Scriven. Visualization of Blob Mechanics in Flow Through Porous Media, Chemical Engineering Science, 33:1009-1017, 1978.

Office of Pollution Prevention and Toxics Chemical Fact Sheet [OPPT], Chemicals in the Environment: Perchloroethylene (Cas N. 127-18-4), EPA 749-F-94-020, Aug, 1994.

Parker, J.C. and E. Park. Modeling Filed-Scale Dense Nonaqueous Phase Liquid Dissolution Kinetics in Heterogeneous Aquifers, Water Resources Research, 40, 2004.

Pankow, J. F. and J.A. Cherry. *Dense Chlorinated Solvents and other DNAPLs in Groundwater,* Waterloo Press, Portland, Oregon (IFT), 1996.

Patel, K. and M. Greaves. Role of Capillary and Viscous Forces in Mobilization of Residual Oil, The Canadian Journal of Chemical Engineering, 65:676-679, Aug, 1987.

Pennell, K.D., G.A. Pope, and L.M. Abriola. Influence of Viscous and Bouyancy Forces on the Mobilization of Residual Tetrachlorethylene During Surfactant Flushing, Environmental Science and Technology, 20:1328-1335, 1996.

Perry, P.H. and C.H. Chilton. *Chemical Engineers Handbook,* 5th Edition McGraw-Hill, 1973.

Peters, J.E. and D.L. Flock. The Onset of Instability During Two-Phase Immiscible Displacement in Porous Media, Society of Petroleum Engineers Journal, 249-258, Apr, 1981.

Powers, S. E., W.H. Anckner, and T.F. Seacord. Wettability of NAPL-Contaminated Sands, Journal of Environmental Engineering. 122:889-896. October, 1996.

Powers, S.E. and M.E. Tambin. Wettability of Porous Media after Exposure to Synthetic Gasolines, Journal of Contaminant Hydrology, 19:105-125, 1995.

Powers, S.E., L.M. Abriola, and W.J. Weber, Jr. An Experimental Investigation of Nonaqueous Phase Liquids Dissolution in Saturated Subsurface Systems: Steady State Mass Transfer Rates, Water Resources Research, 28(10): 2691-2705, Oct, 1992.

Rao, P.S.C., M.D. Annable, R. K. Sillan, D.P. Dai, K. Hatfield, W. D. Graham, A. L. Wood, and C. G. Enfield. Field Scale Evaluation of In Situ Cosolvent Flushing for Enhanced Aquifer Remediation, Water Resources Research 33: 2673-2686. 1997.

Rao, P. S. C, J. W. Jawitz, C. G. Enfield, R. W. Falta, M. D. Annable, and A. L. Wood. Technology Integration for Contaminated Site Remediation: Clean-up Goals and Performance Metrics. Ground Water Quality, 410-412, 2001.

Rao, P.S.C and J.W. Jawitz. Comment on "Steady State Mass Transfer from Single-Component Dense Nonaqueous Phase Liquids in Uniform Flow Fields" by T.C Sale and D.B. McWhorter, Water Resources Research, 39(3):1068, 2003.

Ryan, R.G. and V.K. Dhir. The Effect of Soil Particle Size on Hydrocarbon Entrapment Near a Dynamic Water Table, Journal of Soil Contamination, 2(1):59-92, 1993.

Saripalli, K.P., H. Kim, P.S.C. Rao, and M.D. Annable. Measurement of Specific Fluid-Fluid Interfacial Areas of Immiscible Fluids in Porous Media, Journal of Contaminant Hydrology, 30:375-391, 1997.

Sale, T. C. and D.B. McWhorter. Steady State Mass Transfer from Single-Component Dense Nonaqueous Phase Liquids in Uniform Flow Fields, Water Resources Research 37(2):393-404, Feb, 2001.

Schroth, M. H., J.S. Ahearn, J.S. Selker, and J.D. Istok. Characterization of Miller-Similar Silica Sands for Laboratory hydrologic Studies, Soil Science Society American Journal 60: 1331-1339, 1996.

Seo, H. S. and J.E. McCray. Interfacial Tension of Chlorinated Aliphatic DNAPL Mixtures as a Function of Organic Phase Composition, Environmental Science and Technology, 35(6):1292-1298, 2002.

Soerens, T.S., D.A. Sabatini, and J.H. Harwell, Effects of Flow Bypassing and Nonuniform NAPL Distribution on the Mass Transfer Characteristics of NAPL Dissolution, Water Resources Research, 34(7):1657-1673, 1998.

Treiber, L.E., D.L. Archer, and W.W Owens, A Laboratory Evaluation of the Wettability of Fifty Oil Producing Reservoirs, Society of Petroleum Engineers Journal, 12:531-539, 1972.

Verschueren, K. *Handbook of Environmental Data on Organic Chemicals,* 2nd edition, Van Nostrand Reinhold, New York, NY, 1983.

Wang, A., J. Feyen, and D.E. Elrick. Prediction of Fingering in Porous Media, Water Resources Research. 34(9):2183-2190, Sep 1998.

Watson, C.L. and J. Letey. Indices for Characterizing Soil-Water Repellency Based upon Contact Angle-Surface Tension Relationships, Soil Science Society of America Proceedings, 34:841-844, 1970.

Wilson, J.L. The Need for Research: Physical Processes – Land; The Role of Wetting in Environmental Problems, Presented at Proceedings of the Association of Environmental Engineering Professors, Conference on Fundamental Research Directions in Environmental Engineering, Nov 13-15, Arlington, VA 1988.

BIOGRAPHICAL SKETCH

Christian T. Totten was born in New London, CT, ████████████████, the youngest of six children. He graduated from Fitch Senior High School, Groton, CT, in June 1984, and immediately attended Western New England College in Springfield, MA. In May 1988, he was awarded a Bachelor of Science degree in mechanical engineering. Following graduation he worked as an engineer at Portsmouth Naval Shipyard, NH. He remained at the shipyard until September, 1989, when he was commissioned a second lieutenant in the U.S. Air Force as a bioenvironmental engineer. His first duty location was Pope Air Force Base (AFB), Fayetteville, NC, where he held the position of Chief, Bioenvironmental Engineering Services. In May of 1994 he was transferred to Wright-Patterson AFB, where he attended the Air Force Institute of Technology (AFIT) until December 1995. He received a Master of Science degree in engineering and environmental management and was transferred to the Air Force Center for Environmental Excellence (AFCEE) at Brooks AFB, San Antonio, TX. While at the AFCEE, he worked in both the environmental restoration and compliance programs until May 1999. Upon acceptance to an Air Force sponsored fellowship at the Pentagon, Chris was transferred to Washington, D.C. He served at the Pentagon for three years as a fellow, action officer, and executive officer to the Assistant Secretary of the Air Force. Upon selection for an Air Force-sponsored graduate program, Chris transferred to the University of Florida, Gainesville, FL, in August 2002. Chris has a wife, ████████, and two children, ██████████████.